Active Control of the Acoustic Quality in Open-plan Offices Using a Noise Barrier System with Sound Masking

王, 循

https://doi.org/10.15017/1785409

出版情報：九州大学, 2016, 博士（工学）, 課程博士
バージョン：

Kyushu University
Department of Mechanical Engineering

Active Control of the Acoustic Quality in Open-plan Offices Using a Noise Barrier System with Sound Masking

Thesis for the degree of Doctor in Engineering
by

WANG XUN

July, 2016

Abstract

This thesis is concerned with the active control of the acoustic quality in open-plan offices, which is an important aspect affecting the job satisfaction of the employees. Two of the primary complaints about the working environment in open-plan offices are high background noise level and lack of speech privacy. Both of these acoustic problems can be dealt with by active methods: active noise control (ANC) for reducing background noise, and sound masking for improving speech privacy.

In the context of the ANC in offices, this thesis presents an investigation of creating a quiet zone in the private workspace by using a compact active noise barrier (ANB) system. A novel hybrid (HB) control strategy, which controls the diffracting edge of the noise barrier using feedback (FB) control and reduces the noise at the head position of the listener behind the barrier using feedforward (FF) control simultaneously, is proposed. First, the issue of designing a robust adaptive FB controller with limited noise amplification for the HB control system is addressed. Then, a compact ANB system using the proposed HB control strategy is implemented. The noise reduction performance of the ANB has been investigated under different sound field conditions by simulations and experiments in an anechoic chamber. Finally, the effectiveness of the proposed ANB has been examined in a real office room.

As for the sound masking, this thesis aims to find a selection criterion of the maskers used in offices. Using sound masking systems in the workspace has two objectives. One is to prevent the information leakage, and the other is to help the employees concentrate. The first objective requires high masking efficiency and effectiveness, and the latter one requires low annoyance of the maskers. Therefore, two listening experiments are designed and conducted to investigate the efficiency and annoyance of several maskers. According to the experimental results, a selection criterion has been considered.

Based on the above investigations, a sound proof system that integrates the sound masking techniques into the ANB system is finally implemented, and the performance of the proposed system has been confirmed.

Contents

Acknowledgement

The first person I would like to thank is my supervisor Professor Kijimoto Shinya. He has encouraged and motivated me throughout my doctoral period and provided me with the opportunities to attend various academic events, which indeed help me extend my horizon. He has supported me on both the technical and personal aspect. I appreciate him unreservedly.

I would like to give my sincerest thanks to Professor Kondo Takahiro and Professor Omoto Akira for the instructive advice and comments on this thesis, which help me improve the quality of this thesis significantly.

I am grateful to Associate Professor Ishikawa Satoshi for his helpful advice on this thesis, and also for his encouragement and help, especially for his care in the international conferences.

I thank Dr. Takayama Yoshihisa. He provided me with the post of teaching assistant that let me have the opportunity to accumulate educational experience.

I give my thanks to Mr. Koba Yosuke for his help in preparing the experimental equipment. He has helped the work in the thesis directly.

Many thanks to Mr. Fujita and Mr. Ishikawa for their help in performing the listening experiments and collecting the experimental data.

I thank all of the members of Vibration and Acoustics Laboratory and of Dynamics of Mechanical Systems for the unforgettable period we spent together.

At last, I give my thanks to all of my families and friends, and my deepest appreciation goes to my parents. It is your encouragement and unrequited love that help me overcome the difficulties to achieve the goal of my doctoral course.

Chapter 1

Introduction

1.1 Acoustic problems in open-plan offices

The open-plan office layout is widely used nowadays because it provides a flexible and efficient use of space so that the offices can be developed or reconfigured easily and economically to adapt the dynamic requirements of modern organizations [1, 2]. Additionally, the open-plan layout is considered as a working environment that can facilitate communication and teamwork between staff [3, 4]. However, a number of studies, which investigate the working environment from the viewpoint of the workers, indicate that the workspace satisfaction in open-plan offices is lower than that in traditional private office rooms [5–8]. The primary complaints about the open-plan layout involve lack of speech privacy (with the percentage dissatisfied of about 50%) and visual privacy (40%), and unacceptable noise level (30%) [8] – two of the three are associated with the acoustics. The direct negative effect of these acoustic problems is the decreased individual productivity for the cognitively demanding tasks [9–12]. In addition, serious noise and privacy related stress in open-plan offices have been reported [8, 13, 14], which will cause a series of physical and mental symptoms such as irritability, fatigue, headache and impaired concentration [15, 16]. Therefore, the workspace should be carefully designed to guarantee the acoustic quality as it has a significant effect on the health and overall job satisfaction of the workers which influences both of the individual and organizational performance obviously [17].

The unwanted sounds in offices include background noises from the air conditioning system, printers and computers, other people's conversations, and noises from outside the office building. These noises propagate in the workspace by reflection, diffraction, and transmission. Figure 1.1 shows an illustration of the sound propagation paths from a public space to a private workspace in open-plan offices, and sounds propagate in the same way between workstations and private workspaces. The conventional approaches to controlling these noises can be described as the rule of ABC (Absorb, Block, and Cover). Using absorptive materials can attenuate the reflected sound off a hard surface.

Therefore, studies on the workspace design recommend absorptive treatments in open-plan offices in order to reduce the background noise level and improve the speech intelligibility [18–21]. Good speech intelligibility means easy communication, however, it is essentially the opposite of the speech privacy, i.e., to ensure speech privacy, the conversations should not be intelligible to other people [22]. In order to limit the sound propagation within a certain area, the block strategy suggests using inner walls or large screens to alter the acoustic paths. Obviously, this is not the concept of the open-plan layout. To retain the feature of facilitating teamwork and communication, partial height partitions are often installed in open-plan offices which can also provide the visual privacy. However, noises can still transmit and diffract from the partitions to the neighboring workspace. The sound transmission can be reduced by using a heavy partition [23], whereas the diffraction is difficult to be attenuated by a partial height partition, especially at the low frequencies where the wavelength is much longer comparing with the partition size [24]. Therefore, the method using a sound masking system to add artificial and meaningless sounds (masker) in the workspace to cover the unwanted sounds in the private workspace has been introduced [25, 26]. This active method can adjust the acoustic environment dynamically without considering the spatial limitations or the reconfiguration of the office. The control objective of the sound masking system is commonly set as the overheard conversation sounds. This is not only because the information contained in the intelligible conversations should be protected to improve the speech privacy, but also because the overheard conversations can be considered as the most annoying and distracting type of the unwanted sounds in offices [7, 16]. However, adding masker sounds in the workspace will inevitably increase the background noise level, and hence lead to a compromise of the quietness in the workspace. Warnock [27] suggested that the masker sound level should not be set greater than 48 dB(A) or the workers would recognize it as a distraction. However, such

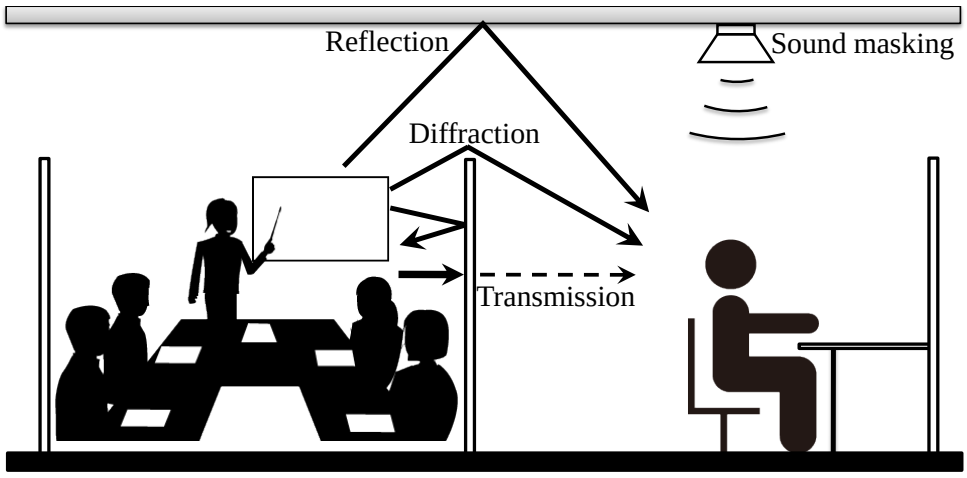

Figure 1.1: An illustration of the acoustic environment in the workspace

small masker sounds cannot guarantee the speech privacy especially in the offices where the sound attenuation in the horizontal direction is insufficient due to the existence of the sound diffraction from low partitions [28].

These facts demonstrate that it is difficult to use the conventional noise control techniques to create an acoustic environment in the workspace that satisfies both of the speech privacy and the noise level requirements. Therefore, it is necessary to develop a new approach to solving the preceding acoustic problems in open-plan offices for improving the individual job satisfaction and the organizational performance.

1.2 Objectives of the thesis

Ease of communication is the distinguishing feature of the open-plan layout that should be preserved in the public workspace. The unwanted sounds propagating into the private workspace from the public space or another workspace cause the problems of speech privacy and distraction. Therefore, the issue of improving the acoustic quality in the private workspace of open-plan offices is addressed in the thesis. According to the background described above, the main problems of the conventional noise control techniques can be concluded as follows:

1. Insufficient attenuation of the sound field especially at low frequencies.

2. Increased background noise level by adding masker sounds.

Active noise control (ANC) is an efficient and effective low frequency noise control technique [29] so it can be applied to cope with the first problem directly. Nevertheless, only reducing the sound pressure level (SPL) is not sufficient for the aim of improving speech privacy. Previous studies indicated that the speech privacy is closely related to the speech intelligibility rather than the SPL [30, 31]. The speech intelligibility can be associated with the signal (target speech) to noise (masker) ratio (SNR) [31–33]. Therefore, it is still necessary to add masker sounds in the workspace to decrease the SNR for improving speech privacy. However, if the target sound is reduced, less masker power is required to achieve the same SNR which can be considered as the same speech privacy level, so that the SPL after sound masking will also become smaller. Consequently, the combination of the ANC and the sound masking techniques will be a prospective method for solving the acoustic problems in the workspace and achieving both of the quietness and the speech privacy.

This thesis focuses on the development of such an acoustic solution that reduces and masks the unwanted sound simultaneously. The objective of the ANC part is to create a quiet zone around the worker in the private workspace, and the sound masking part aims to cover the residual unwanted sounds to improve the speech privacy and reduce the annoyance.

1.3 An overview of the previous works

Actively creating a large quiet zone has been the subject of the ANC-related research for years, and several approaches have been proposed to achieve the overall noise attenuation in the target area. Moreover, the effects of sound masking in offices have also been reported by a number of studies. This section presents a brief overview of the previous works in these two domains with the aim of finding hints for the new acoustic solution in open-plan offices.

1.3.1 Active reduction of noise in a certain area

ANC is based on the principle of the superposition of the primary noise and the synthesized control sound which has the same amplitude but inverted phase to the primary noise [34–36]. Accordingly, the extent of the actively created quiet zone depends on the wavelength at the frequency of interest, and the spatial distribution of the primary noise and the control sound field [37]. The private workspace in open-plan offices can be considered as a large enclosure, in which the acoustic characteristics are different according to the frequency and so is the effect of ANC.

The most desirable result of ANC is the reduction of SPL at all positions in the workspace. However, such global control of noise can only be achieved in some special cases in an enclosure. When the primary sound field is dominated by a few of acoustic modes at low frequencies, the control strategy that minimizes the acoustic potential energy by using a small number of control sources can realize a substantial overall reduction of noise [38]. In order to obtain the optimal reduction in acoustic potential energy, the control sources should be located at maxima of the primary sound field where the major acoustic modes are in the same phase. Nevertheless, this optimized configuration is difficult to be ensured in offices because planning space for the freedom of movement and the comfort of the workers is undoubtedly prior to the configuration of an ANC system. In this control strategy, measurement of the acoustic potential energy which is the cost function of control is another problem. The sum of the squares of the sound pressure at a set of discrete positions can be used as a good approximation of the acoustic potential energy [38, 39]. In practice, however, it is hardly possible to measure the sound pressures at all positions in the workplace because of the cost of using a large number of error sensors and the spatial limitation of wiring and setting the sensors. Above the Schroeder frequency [40, 41], the sound field in the enclosure can be approximated by a diffuse field in which the acoustic energy distributes uniformly. The previous modal control approach does not work in such sound field because obvious acoustic modes do not exist. In this case, the global noise attenuation can only be achieved if the control sources can be located close to the primary noise sources with a distance smaller than the half-wavelength at the frequency of interest [42]. The control

principle here is the reduction of the total acoustic power radiated from the primary noise sources and the control sources. This approach was firstly investigated for a pair of monopole sources in the free field [43]. Then, it was expanded for the problem of minimizing the acoustic power output of multiple noise sources and control sources in the free field and in the enclosure [42, 44, 45]. However, the realization of this control strategy in offices is also difficult because the control sources cannot be set near the people who are talking to reduce the conversation sounds, and there is a too great number of background noise sources to be identified.

When the global control of noise cannot be achieved, local control strategies can still be exploited to reduce the noise in a certain area around the control points. In a diffuse field, the quiet zone with at least 10 dB noise attenuation, which can be created by a remote monopole control source, is an area around the control point with a diameter of about one-tenth of the wavelength at the frequency of interest [46]. For broadband noise, the quiet zone is comparable to that of a tonal sound with a frequency equal to the center frequency of the noise bandwidth [47]. However, the control source cannot be set too distant from the control point as it will increase the SPL at other positions in the enclosure [48]. Therefore, such a local control system can only be effective if the target area of control is small and the control source can be placed near the control point. The active noise canceling headphone [49–52], which creates a quiet zone moving with the ears of the listener, is a successful application of this local control strategy. For the reasons of comfort and communication between the workers, however, the headphones are not appropriate in offices. The active headrest [53–55], in which the control sources and error sensors are fixed around the head position of the listener, is another example of the local control system. The objective of this system is often to reduce the low frequency noise because the larger quiet zone according to the wavelength. However, the quiet zone could become too small if the frequencies of interest are relatively high. In offices, the various noise sources result in a broadband noise, and the head position of the workers would change even when they are working, so the headrest system may not be very useful in such conditions.

Using multiple control sources to minimizing the sound pressures at a set of error sensors located in the target area can be used to enlarge the extent of the quiet zone. However, only a suitable configuration of the control sources and error sensors can achieve less total acoustic power output and larger quiet zones than those of a single control source system [56]. The arrangement for the control sources and error sensors equally located in two parallel lines or in two parallel planes has been investigated on the basis of acoustic power analysis, and a range of optimal spacing for the control sources and error sensors has been obtained for the tonal noise [56] and the broadband noise [57].

Control strategies using different cost functions to extend the quiet zone created by

a limited number of control sources and error sensors have also been investigated. Park and Sommerfeldt [58] proposed an approach to minimizing the total acoustic energy, which is defined as the sum of acoustic potential energy and acoustic kinetic energy, in the target area. This approach was firstly verified in a one-dimensional enclosure [58], and then it was expanded for the noise control problem in a three-dimensional enclosure [59]. This acoustic energy based approach can observe the acoustic modes better than the sound pressures based approaches with the same number of error sensors so that it is capable of creating a larger quiet zone [59, 60]. The investigations also indicated that if only a limited number of control sources is used to reduce the acoustic energy in the target area, there will be a trade-off between the maximum noise attenuation level and the extent of the quiet zone. To tune the balance, Xu and Sommerfeldt [61] proposed an approach in which the generalized acoustic energy is used as the cost function. The generalized acoustic energy is defined by introducing a weighting factor into the sum of acoustic potential energy and acoustic kinetic energy [62]. By adjusting the weighting factor, the system users can find the desired trade-off between the maximum noise attenuation level in the target area and the extent of the quiet zone. Comparing with these total acoustic energy based approaches, in which special error sensors must be used to obtain the particle velocity to calculate the acoustic kinetic energy, Li and Hodgson [63] presented an approach that minimizes the acoustic potential energy in a certain area, which is only associated with the sound pressures, inside a large room by controlling a few number of locally distributed positions. However, the locations of the control sources and control points must also be optimized to ensure that the acoustic potential energy can be correctly estimated by the measured sound pressures at the local positions. This optimization process was realized by genetic algorithms in Ref. [63]. Besides the acoustic energy based cost functions, a method that directly maximizes the area of the quiet zone with at least 10 dB noise attenuation was proposed in Ref. [64]. However, this is an off-line design method for the tonal noise based on the ideal free space acoustic transfer function. In the sound field where the acoustic paths are complex and time-variant such as in offices, this method is difficult to be implemented.

In Ref. [65], an approach to overall noise attenuation in the case where the primary noise source is embedded in an infinite baffle was considered. This approach is based on the concept of creating an image source located close to the primary source by the reflection of the infinite baffle to realize the global control strategy described in Ref. [44]. A parametric array loudspeaker [66] was applied as the control source since the super directivity of it can focus the control sound waves to create an equivalent point control source on the position of the primary noise source. Therefore, a large quiet zone can be created in the downstream of the reflected sound. Obviously, however, this is an approach for a very special case that cannot be expected to work well under the other

sound field conditions.

In the above control strategies, error sensors must be placed in the target area to obtain the acoustic quantities such as the sound pressures or particle velocities. However, in offices, it is not desirable to locate sensors around the head of an worker. There are two possible solutions to this problem.

The first solution is the virtual sensing technique [67]. This technique estimates the acoustic quantities in the target area according to those observed by the sensors located distant from the target area. The estimation process can be done by using the transfer functions from the locations of the sensors to the target area [68, 69] or the interpolation methods [70]. An analytical method to obtain a stochastically optimal virtual sensor in a diffuse field has also been developed [71]. However, if the sound field is complex and time-variant, it is difficult to precisely predict the acoustic quantities by using whichever type of the virtual sensing techniques. Therefore, the practical application of the virtual sensing techniques can only be found in the active headphone systems [52] and headrest systems [55, 69] where the acoustic paths from the error sensors to the ears of the listener are time-invariant and the path length is much shorter than the wavelength of interest that allows more accurate estimation.

The second solution is the acoustic boundary control [72–74]. The Kirchhoff-Helmholtz integral equation

$$\int_S \left[G(\boldsymbol{r}|\boldsymbol{r_s}) \frac{\partial p(\boldsymbol{r_s})}{\partial \boldsymbol{n}} - p(\boldsymbol{r_s}) \frac{\partial G(\boldsymbol{r}|\boldsymbol{r_s}))}{\partial \boldsymbol{n}} \right] dS = \boldsymbol{p(r)} \quad \boldsymbol{r} \in \boldsymbol{V}, \tag{1.1}$$

indicates that the sound pressure distribution $\boldsymbol{p(r)}$ in a region $\boldsymbol{V}$ is determined by the sound pressures $p(\boldsymbol{r_s})$ and the particle velocities $\partial p(\boldsymbol{r_s})/\partial \boldsymbol{n}$ on its boundary S, where $G(\boldsymbol{r}|\boldsymbol{r_s})$ is the Green's function from the position on the boundary $\boldsymbol{r_s}$ to the position in the region $\boldsymbol{r}$, and $\boldsymbol{n}$ is the normal vector of the boundary surface. Accordingly, one can produce an anti-noise field in the target area to cancel the primary noise by controlling the points on the boundary surface without placing any control devices inside the area, or in other words, one can actively create an acoustic boundary which noise cannot pass through [74]. However, if the target area is large, a great number of control sources and error sensors have to be used to control the acoustic boundary. Therefore, the application of the acoustic boundary control often combines passive noise insulation methods, in which the boundary needed to be controlled is small. For instance, the active noise shielding window developed in Refs. [75–77] can achieve an overall noise attenuation in a large room by only controlling the sound pressures at the surface of the window because the other parts of the boundary, i.e. the exterior walls of the room, can block most of the incident noise. Active noise barrier (ANB) is another application based on the concept of acoustic boundary control. The acoustic boundary on the top edge of a noise barrier significantly affects the noise attenuation performance of it [78–80]. Therefore, actively controlling the acoustic boundary on the top edge of a

barrier is an effective way to improve the insertion loss to create a quiet zone behind the barrier. The partial height office partition is a noise barrier of which the insertion loss at low frequencies is insufficient. Therefore, the concepts and approaches of the ANBs will be useful to the realization of quietness in a private workspace enclosed by partitions.

The ANB was firstly proposed in the early 1990s [81, 82]. From then on, a large body of literature has reported the advances in the ANB. In order to investigate the noise attenuation mechanism, Ise et al. [81] measured the acoustic intensities around the ANB and found that the control sources absorb noise at some frequencies and reflect it at others. A further theoretical investigation of the mechanism of the ANB [83] also demonstrated that sound absorption or reflection occurs at low frequencies according to the relation between the wavelength and the distance from the primary noise source to the control sources, and sound absorption is the dominant mechanism at high frequencies. In a non-reflective sound field, the active control can provide an extra noise attenuation of more than 10 dB behind the noise barrier [82]. In practice, however, the reflection from the ground will reduce the effectiveness of the ANB. In such a sound field, the system performance can be improved by adding additional control sources to cancel the reflected sound or by using passive acoustic materials to reduce the ground reflection [84, 85]. Another practical aspect for the ANB applications is the moving noise source which has been investigated in Ref. [86]. In an outdoor real-time experiment [87], the ANB was used to reduce the noise radiated from a fan blower, and the experimental result demonstrated that the ANB can provide about 5 dB extra attenuation. This may be the first experiment validated the effectiveness of the ANB in practical application. After that, a product-typed highway ANB was developed and proved to be capable of providing about 4 dB extra reduction of the traffic noise [88, 89]. This ANB has been commercialized [90].

All the above ANBs exploit the control strategy that minimizes the sound pressures at the control points located on the top edge of a noise barrier. Other control strategies for the ANBs have also been proposed, of which the majority is to improve the noise attenuation at the positions far from the ANB. Controlling the sound pressures at the far-field points is the direct method for improving the far-field noise attenuation performance. However, for the sake of the compactness of the ANB system, it is more desirable to locate error sensors near the barrier. A control strategy using near-field located error sensors to predict far-field sound pressures based on the virtual sensing technique was proposed to solve this problem and improve the far-field performance of an ANB [91]. Another study revealed that simply amplifying the control sound can also be an effective approach to improve the reduction in far-field [92]. Hart and Lau [93] demonstrated that minimizing the sound pressure gradient perpendicular to the diffracting edge can not only improve the performance of an ANB but also weaken

the dependence of the performance on the primary noise source position. Besides these sound pressure based approaches, Han and Qiu [94] presented a control strategy in which the near-field sound intensity is used as the cost function to obtain better far-field performance.

In an ANB, the configuration of the control sources and error sensors at the top edge is another aspect that influences its performance. Niu et al. [95] compared three locations of the error sensors – above, before and behind the barrier, and indicated that the error sensors should be placed above the top edge of a barrier to reduce the diffraction better. This study also indicated that there is an optimal distance between the error sensor and the control source which depends on the frequency of interest and the primary noise source position. Liu and Niu [96] investigated the influence of the control source density on the ANB performance. The result demonstrated that larger control source density can improve the noise attenuation performance, and the improvement is more obviously by increasing the control source density along the top edge of a barrier than along the noise incident direction. As for the hardware, Chen et al. [97] demonstrated that using unidirectional control sources in an ANB can achieve larger noise attenuation than using omni-directional control sources because the anti-noise field can be reproduced better by tuning the directivity of the control sources.

However, the majority of the previous studies are concerned with the large ANBs aiming to reduce outdoor noises such as the traffic noise. Only a few works focus on the indoor ANB. Based on the concept of the ANB in Ref. [88], a small-typed indoor ANB was developed [98]. The numerical and experimental investigations showed that about 2 dB extra noise attenuation within the frequency band up to 1 kHz can be obtained behind the ANB. This number is smaller than the large outdoor ANBs because the sound diffraction from the side of the small barrier, which is not included in the control objective, contribute much to the primary noise field behind the ANB. In another work [99], a numerical investigation of the noise attenuation performance of a full-length ANB, in which the side diffraction does not exist, was conducted. The result indicated that 6–8 dB extra noise attenuation can be obtained, which implied the indoor ANB performs better if the side diffraction can be reduced. However, a full-length noise barrier is often not available in open-plan offices so that it is challenging to improve the noise attenuation performance of a compact indoor ANB in the workspace.

1.3.2 Sound masking in offices

There are two different sound masking phenomena – energetic and informational masking [100–105]. Energetic masking is the phenomenon that the target sound cannot be heard as it is covered by the masker sound of larger power. The effect of energetic masking relies on the masker level (or the SNR). Informational masking refers that the target sound and the masker are audible, but the listeners cannot separate the target

sound from the masker to understand the meaning of it. The effect of informational masking depends on the target-masker similarity and uncertainty [103]. The target-masker similarity means to what extent the spectrum of the masker resemble that of the target sound [106], and the uncertainty means the sound is unstructured and unfamiliar for people [107]. Higher the similarity and uncertainty are, better the sound masking effect is [108]. Lutfi [109] indicated that every sound masking phenomenon actually contains both of energetic and informational effects, but the amount of each effect is different. Usually, a stationary random noise such as the pink noise [110, 111], of which the sound masking effect stems from the noise power, is considered as the most typical energetic masker, and the informational masker refers to a speech-like meaningless sound [112–114].

Energetic maskers are used more frequently in the workspace because the stationary noises are more acceptable for the workers. Haapakangas et al. [115] assessed the effects of five different maskers including the stationary pink noise and the non-stationary maskers such as the vocal and instrumental music on the acoustic satisfaction of the workers in open-plan offices. The result revealed that using pink noise to mask overheard conversations can be a more effective and practical method to decrease the annoyance and to improve the cognitive work performance of the workers. Ebissou et al. [116] linked the individual performance to the Speech Transmission Index (STI) that is a quantity to evaluate the speech intelligibility in a room. This work also showed that reducing STI by adding stationary noise in the workspace can relieve the acoustic distractions. There are also other studies confirmed the effectiveness of the sound masking system to improve the workers' performance in open-plan offices [117–119]. Virjonen et al. [28] addressed another objective of the sound masking in offices – speech privacy. Their work indicated that sound masking can improve the speech privacy, but it is still insufficient unless the approaches to attenuate the overheard conversation is used simultaneously because the masker level cannot be set to be too large as indicated in Ref. [27].

Using smaller masker power to improve the speech privacy is another subject of the sound masking related research. In the stationary random noise maskers, the pink noise with limited bandwidth from 177 Hz to 5656 Hz ([177, 5656] Hz) has the better masking efficiency than the broadband white noise and pink noise [110]. It is possible to achieve higher masking efficiency by using the informational maskers because of its masking mechanism which does not rely on the masker level only. However, the annoyance of the non-stationary maskers could be a problem. Time-reversed masker that is a representative of the informational maskers was investigated thoroughly in Ref. [113]. The result demonstrated that this masker can achieve good speech privacy more efficiently even than the band-limited pink noise, whereas it is more annoying than the stationary pink noise at the same masker level. However, the annoyance of

the maskers under the same speech privacy has not been assessed yet, which might be more important for the sound masking in offices. Therefore, a further investigation of the comprehensive evaluation of maskers should be conducted.

1.4 Acoustic solution in the thesis

Based on the aforementioned background, this thesis proposes an acoustic solution as shown in Fig. 1.2, which combines a compact indoor ANB system with sound masking techniques, in order to actively create a private workspace of good acoustic quality in open-plan offices. This system consists of a partial height partition and a set of loudspeakers and microphones used as the control sources and error sensors.

The noise attenuation effects of the proposed system are provided by three mechanisms. At high frequencies, the passive sound insulation effect of the partition can work well, i.e., the unwanted sounds are blocked by the partition. The low frequency sound diffraction is reduced by the control units located on the top of the partition to control the acoustic boundary at the diffracting edge. However, only controlling the diffracting edge cannot provide sufficient noise attenuation for such a compact ANB used in open-plan offices [98, 99]. Therefore, another control unit is placed on the back of the partition to reduce the sound pressure of the noise at the head position of the worker in the private workspace. This sound pressure reduction mechanism works at low and mid-frequencies. The question here is the effect of the acoustic boundary control and the sound pressure control can superpose or not. The investigations in the thesis give a positive answer. By exploiting these three mechanisms, the proposed system is able to achieve good noise attenuation performance in a wide frequency band.

There are two available choices, feedforward (FF) and feedback (FB) control [34, 35] as shown in Fig. 1.3, which can be used to implement the proposed control system. An

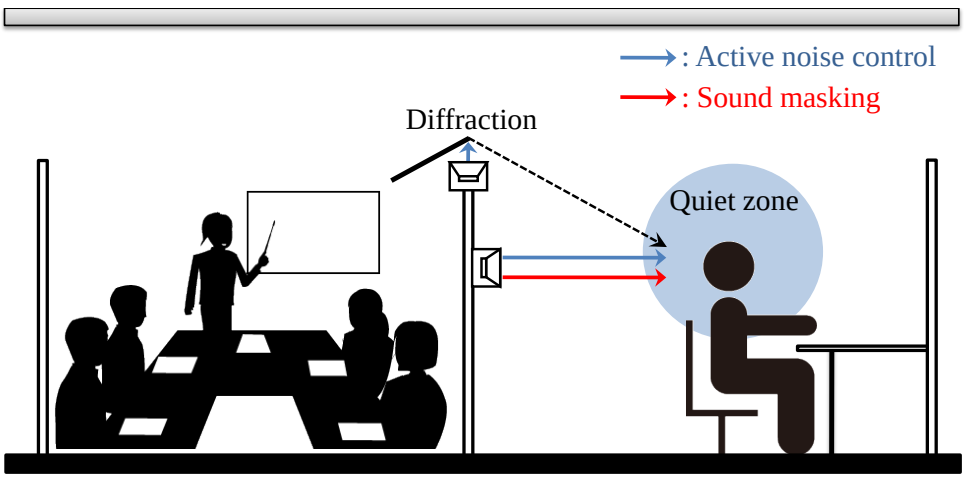

Figure 1.2: Concept of the proposed system

adaptive FF-ANC system uses a reference sensor placed in the upstream of the primary noise to detect the time-advanced noise signal to predict the noise at the control point where an error sensor is located to monitor the control result. In comparison with the FF system structure, the FB-ANC system dose not require a reference sensor. Therefore, the FB-ANC system is preferred for the applications in which available space for setting reference sensors is restricted [49–53], or the number of noise sources and propagation paths is too great to be effectively observed [120]. However, the performance of the FB control is influenced by the time delay in the system [121] so that the FB control should be used in the occasion where a short system delay is allowed. In the acoustic boundary control part of the proposed system, the error sensors can be located in a very small distance from the control sources, which is also for satisfying the requirement of the compactness of such an indoor ANB system. Therefore, FB control is used to realize the active control of the diffracting edge in the proposed system. On the other hand, the distance between the worker and the ANB may be relatively remote, which yields a large time delay due to the propagation time of the control sound. Therefore, the sound pressure control part of the proposed system is implemented by the FF control. In the thesis, simultaneously controlling the acoustic boundary at the diffracting edge by FB controller and the sound pressure at the head position of the worker by FF controller is termed as hybrid (HB) control strategy. The issues in the system implementation are the robust stability of the FB control and the efficient system realization of the combination of the FB and FF control.

The sound masking effect is achieved by outputting the masker sound from the control source located on the back of the partition. This control source is set towards the head position of the worker, and can be seen as a private sound source. Therefore, the masker level can be adjusted individually according to the activities of the worker in the private workspace as suggested in Ref. [27]. As the unwanted sounds have been reduced by the ANC part, the required masker level becomes smaller. In the implementation of the sound masking part, careful selection of an appropriate masker is important for achieving speech privacy and avoiding extra annoyance.

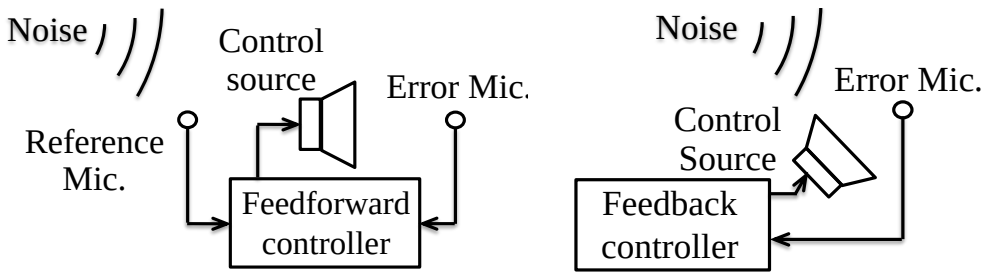

(a) FF control (b) FB control

Figure 1.3: FF and FB active noise control systems

An acoustic environment of lower noise level and less acoustic distractions can be created for the worker in the private workspace behind the proposed ANB system. Additionally, speech privacy between workspaces can also be improved by introducing the proposed system into open-plan offices.

1.5 Thesis structure and contributions

This chapter introduces the background and objectives of this work, and the following chapters present the approaches, investigations, and results in the development of the proposed system. The remainder of the thesis is organized as follows:

Chapter 2 focuses on the design process of the FB controller which will be applied in the acoustic boundary control part of the HB control strategy. A practical FB controller should be with robust stability, limited noise amplification outside the control bandwidth, and adaptability to the time-variant noise. According to this philosophy, two methods for designing a robust adaptive FB controller are proposed in this chapter. The first one is a frequency domain method based on the direct formulation of the FB controller. By considering the easiness of real-time realization, the second method finds a constraint of the control filter coefficients by converting the frequency domain robust stability condition and noise amplification constraint into the time domain. The effectiveness of the proposed methods is verified by simulations and experiments.

Chapter 3 investigates the noise attenuation performance of the proposed ANB system. Based on the HB control structure, a technique for canceling the noise amplification of the FB control propagating into the control area behind the ANB is also proposed in this chapter. First, the proposed control strategies are described, and an efficient system implementation of the control strategies is presented. Then, the noise attenuation performance of the ANB under different sound field conditions is investigated by simulations and experiments. Finally, an experiment is conducted to verify the effectiveness of the proposed ANB in a real office room.

In Chapter 4, selection of the maskers for the sound masking part of the proposed system is considered. Two listening experiments are conducted to investigate the masking efficiency and annoyance of several representative energetic and informational maskers. According to the experimental results, the features of the energetic and informational maskers are discussed, and a criterion of selecting an appropriate masker for the sound masking system in offices is concluded.

In Chapter 5, the whole proposed system combining the ANB system with sound masking is implemented based on the investigations in the preceding chapters. The performance of the proposed system is validated by simulations.

Chapter 6 presents an approach to achieving overall noise attenuation in a certain area based on the concept of wavefront synthesis, which can be applied to the sound

pressure control part of the HB control strategy. The basic idea of this approach is to divide a global ANC system into two sub-systems according to the different control objectives. One sub-system is to reproduce the wavefront of the incident noise into the target area, and the other one is to tune the amplitude and phase of the reproduced control sound wavefront. By using this approach, the control algorithm and the hardware configuration of a global ANC system can be significantly simplified. The effectiveness of the approach is verified by numerical simulations.

Chapter 7 presents a summary of the work in this thesis.

The primary contributions of the thesis are concluded as follows:

- Two adaptive methods for designing a robust FB controller have been proposed. By applying the proposed methods, it is possible to guarantee the robust stability of the FB controller and limit the noise amplification to within a given value in the real-time FB control process.

- A modified frequency domain least mean squares algorithm, which has the reduced computational complexity and the guaranteed optimal steady-state performance, has been proposed.

- A novel HB control strategy has been proposed to improve the noise attenuation performance of a compact indoor ANB, and an efficient system implementation, in which no control device is needed to be placed around the listener, has been developed.

- A technique to suppress the noise amplification caused by the FB control in the target area of control has been proposed. By using this technique, the classic trade-off between reducing noise and limiting noise amplification becomes less important in the FB controller design process.

- The noise attenuation performance of the ANB system in a real office room has been investigated.

- The masking efficiency and annoyance of several typical energetic and informational maskers have been investigated.

- A sound proof system, which reduces and masks the unwanted sounds in offices simultaneously, has been developed.

- A global noise control approach based on the concept of wavefront synthesis has been proposed. By using this approach, the software and hardware of a global ANC system can be simplified.

Part of this work has been reported in the following publications:

1. X. Wang, Y. Koba, S. Ishikawa, and S. Kijimoto, "Hybrid active noise barrier with sound masking in open-plan offices," *Noise Control Engineering Journal*, vol. 64, no. 3, pp. 403–415, 2016.

2. X. Wang, Y. Koba, S. Ishikawa, and S. Kijimoto, "Noise barrier using hybrid ANC system (Proposal and application of an adaptive robust feedback ANC system)," *Transactions of the JSME (in Japanese)*, vol. 82, no. 835, pp. 1-15, 2016.

3. X. Wang, Y. Koba, S. Ishikawa, and S. Kijimoto, "An adaptive method for designing a robust IMC structured feedback active noise controller," *Noise Control Engineering Journal*, vol. 63, no. 6, pp. 496–507, 2015.

4. X. Wang, Y. Koba, S. Ishikawa, and S. Kijimoto, "Noise barrier using hybrid ANC system (Suppression of the noise enhancement caused by the waterbed effect and investigation of the noise attenuation performance under various sound field configurations)," *Transactions of the JSME (in Japanese)*, vol. 81, no. 827, pp. 1-15, 2015.

5. X. Wang, Y. Koba, S. Ishikawa, and S. Kijimoto, "A noise barrier using hybrid ANC system," *Transactions of the JSME (in Japanese)*, vol. 80, no. 814, pp. 1-10, 2014.

6. X. Wang, T. Satake, Y. Koba, S. Ishikawa, and S. Kijimoto, "Active reduction of the two-way diffraction from a noise barrier by using feedforward control," in *Inter-Noise 2016*, 2016.

7. X. Wang, Y. Koba, S. Ishikawa, and S. Kijimoto, "Locally global active noise control based on wavefront synthesis," in *The 23th International Congress on Sound and Vibration*, 2016.

8. X. Wang, Y. Koba, S. Ishikawa, and S. Kijimoto, "Hybrid active noise barrier with sound masking (Experiment for verifying the noise attenuation performance in an office room and evaluation of maskers by listening experiments)," in *Inter-Noise 2015*, 2015.

9. X. Wang, Y. Koba, S. Ishikawa, and S. Kijimoto, "Development of indoor hybrid active noise," in *The 22th International Congress on Sound and Vibration*, 2015.

10. X. Wang, Y. Koba, S. Ishikawa, and S. Kijimoto, "Hybrid active noise barrier with sound masking," in *Inter-Noise 2014*, 2014.

Chapter 2

Robust Adaptive Feedback Controller Design Methods

2.1 Introduction

FB control is often used in the ANC applications where there is the spatial limitation for setting reference sensors or the coherent reference signal cannot be obtained. In the FB-ANC systems, the internal model control (IMC) structure [122] is usually employed owing to two of its outstanding features. One is that an adaptive algorithm, such as the filtered-x least mean squares (FX-LMS) algorithm [123, 124], can be applied in the feedback controller because a reference signal is synthesized internally. The second feature is that the stability can be easily ensured if the secondary path (the acoustic path from the control source to the control point) model is accurate and the inverse system of the time-delayed secondary path, which is the optimum properties of the controller [122], is approximated by an inherently stable finite impulse response (FIR) filter. In practice, however, uncertainties exist in the secondary path model so that the robust stability of the FB controller must be considered during the design process. Moreover, in the feedback control of a time-delayed system, if the system sensitivity is reduced at some frequencies, it must grow larger over some other frequencies, a phenomenon known as the waterbed effect [125, 126]. The waterbed effect will cause noise amplification (NA) at some frequencies outside the target band of control. Therefore, in order to improve the practicality of the acoustic boundary control part in the HB control strategy, this chapter focuses on the issue of designing a robust adaptive FB controller with constrained waterbed effect induced noise amplification.

Regarding the robustness problem of the FB-ANC system, the stability and convergence condition of the adaptive IMC structured FB-ANC system have been analyzed [127], and a similar convergence condition with the adaptive FF-ANC system [128, 129], i.e., the phase difference between the physical secondary path and the model should be smaller than $\pi/2$, has been found. In Refs. [130, 131], the convergence behavior of the IMC structured FB-ANC system with an imperfect secondary

path model has been modeled, and the maximum step-size parameter condition to guarantee the convergence has been derived. In addition to the IMC structure, another adaptive FB-ANC system with the simplified structure, which applies the error signal directly as the reference signal, has been proposed [132]. Simplification of the system structure reduces the computational complexity, but it weakens the stability of the system. Therefore, a leaky FX-LMS algorithm [133], which can limit the gain of the control filter, has been used in the simplified FB-ANC system to improve the stability [132]. However, a specific constraint of the control filter gain to guarantee the stability is not given. Additionally, little quantitative work has been conducted to evaluate the noise amplification caused by the waterbed effect for an adaptive FB-ANC system.

For the non-adaptive FB-ANC systems, several approaches to designing a fixed controller with robust stability based on the H_∞ criterion [134] have been presented in Refs. [49, 53, 135–138]. In these approaches, a weighting function must be carefully selected to determine the target band of control, which also determines the frequency band where the waterbed effect exists. To simplify the design process, an approach, which does not require complicated weighting function selections and numerical optimizations, has been proposed [139]. This approach can suppress the waterbed effect induced noise amplification by flattening the noise amplification in the whole frequency band. Although these robust fixed controllers can achieve the pre-designed noise attenuation performance even several secondary path model uncertainties exist, they may become less effective if the primary noise is time-variant.

In this chapter, two adaptive methods for designing a robust FB controller are proposed. The first one is a frequency domain method based on the direct formulation of the IMC structured FB controller. A modified frequency domain block least mean squares (Modified FDB-LMS, MFDB-LMS) algorithm, which has the reduced computation complexity and the guaranteed steady-state performance comparing with the conventional FDB-LMS algorithm [140], is developed, and used to update the FB controller because of the easiness to verify the robust stability and the noise amplification constraint in the frequency domain adaptive process. Even though the computation of the MFDB-LMS algorithm has been reduced, it is also more complex than the time domain LMS algorithm ("LMS" in the following context refers to the time domain LMS algorithm). Therefore, the second method determines a time domain constraint for the FIR control filter coefficients, which can be easily implemented in a real-time system using time domain algorithms. This time domain method divides the controller design process into two dependent procedures. In the first procedure, the robust stability condition and the noise amplification constraint in the frequency domain are converted to the filter coefficient constraint. Then, a robust controller solution can be obtained by employing a time domain adaptive algorithm to update the filter coefficients accord-

ing to the constraint. By using both of the proposed methods, the robust controller can keep adaptive to the primary noise in the online design stage so that better noise attenuation performance can be realized in comparison with the offline-designed fixed controllers. Simulations and experiments are performed to validate the effectiveness of the proposed methods.

2.2 Internal model control

The block diagram of the IMC structured FB-ANC system is shown in Fig. 2.1, where $\boldsymbol{G}(z)$ and $\hat{\boldsymbol{G}}(z)$ stand for the physical secondary path and secondary path model, respectively. The primary noise $d(n)$ can be seen as the system disturbance, and the residual noise $e(n)$ is the error signal of the system. The estimate of the primary noise signal $\hat{d}(n)$ is calculated by using the internal secondary path model $\hat{\boldsymbol{G}}(z)$ and the control output signal $u(n)$, and is applied as the reference signal of the control filter $\boldsymbol{C}(z)$. $u(n)$ is output from the control source to cancel the primary noise.

2.2.1 Robust stability condition

The sensitivity function of the IMC structured FB-ANC system is defined as follows:

$$\boldsymbol{S}(z) = \frac{\boldsymbol{E}(z)}{\boldsymbol{D}(z)} = \frac{1 + \boldsymbol{C}(z)\hat{\boldsymbol{G}}(z)}{1 - \boldsymbol{C}(z)[\boldsymbol{G}(z) - \hat{\boldsymbol{G}}(z)]}, \tag{2.1}$$

where $\boldsymbol{D}(z)$ and $\boldsymbol{E}(z)$ are the z-transform of primary noise $d(n)$ and error signal $e(n)$, respectively. The primary noise is reduced at the frequencies where $|\boldsymbol{S}(z)| < 1$, in which $|\ |$ denotes the amplitude. If the uncertainties between $\hat{\boldsymbol{G}}(z)$ and $\boldsymbol{G}(z)$ are small enough to be ignored ($\boldsymbol{G}(z) \approx \hat{\boldsymbol{G}}(z)$), Eq. (2.1) can be rewritten as

$$\boldsymbol{S}(z) = 1 + \boldsymbol{C}(z)\boldsymbol{G}(z), \tag{2.2}$$

and the optimal controller to cancel the primary noise entirely is given by

$$\boldsymbol{C}_{opt}(z) = -\frac{1}{\boldsymbol{G}(z)}. \tag{2.3}$$

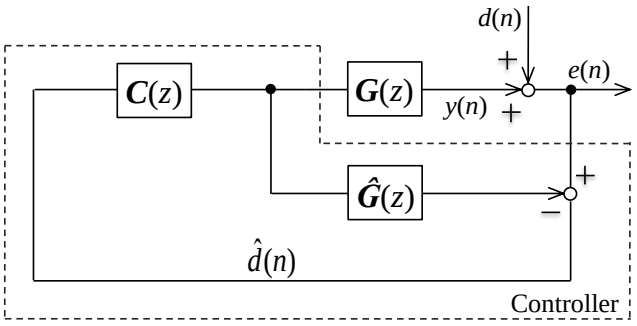

Figure 2.1: IMC structured FB-ANC system

In this case, the IMC structured FB-ANC system has the inherently stable open loop sensitivity function so that an adaptive algorithm can be used to implement the FB control.

In practice, however, secondary path model uncertainties, which may be caused by modeling error, measurement error, or physical secondary path changes, exist so that the feedback loop gain cannot be ignored and the robust stability of the sensitivity function should be considered. To consider the influence of the uncertainties $\triangle \boldsymbol{G}(z)$ contained in the secondary path model, it is assumed that the frequency response of the physical secondary path $\boldsymbol{G}(z)$ is given by the multiplicative form as

$$\boldsymbol{G}(j\omega) = \hat{\boldsymbol{G}}(j\omega)[1 + \triangle \boldsymbol{G}(j\omega)], \tag{2.4}$$

such that the H_∞ robust stability condition can be expressed by using the complementary sensitivity function $\boldsymbol{T}(j\omega)$ and the boundary function for the model uncertainties $\boldsymbol{B}(\omega)$ as follows [35, 122]:

$$\|\boldsymbol{T}(j\omega)\boldsymbol{B}(\omega)\|_\infty < 1, \tag{2.5}$$

where $z = \mathrm{e}^{j\omega}$, j is the imaginary unit, $\| \ \|_\infty$ denotes the H_∞ norm, $\boldsymbol{T}(j\omega)$ and $\boldsymbol{B}(\omega)$ are defined as

$$\boldsymbol{T}(j\omega) = 1 - \boldsymbol{S}(j\omega) = \boldsymbol{C}(j\omega)\hat{\boldsymbol{G}}(j\omega), \tag{2.6}$$

$$\boldsymbol{B}(\omega) \geq |\triangle \boldsymbol{G}(j\omega)|, \tag{2.7}$$

respectively. Equation (2.5) and Equation (2.6) establishes that

$$\max(\boldsymbol{C}(j\omega)\hat{\boldsymbol{G}}(j\omega)\boldsymbol{B}(\omega)) < 1, \tag{2.8}$$

which means the gain of $\boldsymbol{C}(j\omega)\hat{\boldsymbol{G}}(j\omega)\boldsymbol{B}(\omega)$ should be smaller than 1 at each frequency so that the robust stability condition can be rewritten as

$$|\boldsymbol{C}(j\omega)| < \frac{1}{|\hat{\boldsymbol{G}}(j\omega)\boldsymbol{B}(\omega)|}. \tag{2.9}$$

The notation max( ) denotes the maximum of a set of values.

2.2.2 Noise amplification constraint

The noise amplification caused by the waterbed effect can be evaluated by the gain of the sensitivity function defined in Eq. (2.1) or Eq. (2.2). The constraint that the maximum noise amplification should be limited within a (or A in dB) can be expressed as

$$|\boldsymbol{S}(j\omega)| < a, \quad a = 10^{\frac{A}{20}}. \tag{2.10}$$

According to Eq. (2.1), Eq. (2.4), and Eq. (2.7), Eq. (2.10) can be rewritten as

$$\left| \frac{1 + \boldsymbol{C}(j\omega)\hat{\boldsymbol{G}}(j\omega)}{1 - \boldsymbol{C}(j\omega)\hat{\boldsymbol{G}}(j\omega)\boldsymbol{B}(\omega)} \right| < a. \tag{2.11}$$

Equation (2.10) can also be expressed according to Eq. (2.2) as follows:

$$\left|1 + \boldsymbol{C}(j\omega)\hat{\boldsymbol{G}}(j\omega)\right| < a. \tag{2.12}$$

By expressing the $\boldsymbol{C}(j\omega)$ and $\hat{\boldsymbol{G}}(j\omega)$ in the polar form of the complex as

$$\boldsymbol{C}(j\omega) = |\boldsymbol{C}(j\omega)|\mathrm{e}^{j\boldsymbol{\theta}_{\boldsymbol{C}}}, \tag{2.13}$$

$$\hat{\boldsymbol{G}}(j\omega) = |\hat{\boldsymbol{G}}(j\omega)|\mathrm{e}^{j\boldsymbol{\theta}_{\hat{\boldsymbol{G}}}}, \tag{2.14}$$

$$\mathrm{e}^{j\boldsymbol{\theta}} = \cos\boldsymbol{\theta} + j\sin\boldsymbol{\theta}, \tag{2.15}$$

Equation (2.11) can be rewritten as

$$\frac{\sqrt{1 + |\boldsymbol{C}(j\omega)\hat{\boldsymbol{G}}(j\omega)|^2 + 2|\boldsymbol{C}(j\omega)\hat{\boldsymbol{G}}(j\omega)|\cos\boldsymbol{\theta}}}{\sqrt{1 + |\boldsymbol{C}(j\omega)\hat{\boldsymbol{G}}(j\omega)\boldsymbol{B}(\omega)|^2 - 2|\boldsymbol{C}(j\omega)\hat{\boldsymbol{G}}(j\omega)\boldsymbol{B}(\omega)|\cos\boldsymbol{\theta}}} < a, \tag{2.16}$$

$$\boldsymbol{\theta} = \boldsymbol{\theta}_{\boldsymbol{C}} + \boldsymbol{\theta}_{\hat{\boldsymbol{G}}}. \tag{2.17}$$

Equation (2.16) can be rewritten in the form of a quadratic equation form with the unknown $|\boldsymbol{C}(j\omega)|$ as

$$(1 - a^2\boldsymbol{B}(\omega)^2)|\hat{\boldsymbol{G}}(j\omega)|^2|\boldsymbol{C}(j\omega)|^2 + 2\cos\boldsymbol{\theta}(1 + a^2\boldsymbol{B}(\omega))|\hat{\boldsymbol{G}}(j\omega)||\boldsymbol{C}(j\omega)| + (1 - a^2) < 0, \tag{2.18}$$

so that the solution of $|\boldsymbol{C}(j\omega)|$ can be expressed as

$$|\boldsymbol{C}(j\omega)| < \frac{-(1 + a^2\boldsymbol{B}(\omega))\cos\boldsymbol{\theta} + \sqrt{\cos^2\boldsymbol{\theta}(1 + a^2\boldsymbol{B}(\omega))^2 - (1 - a^2\boldsymbol{B}(\omega)^2)(1 - a^2)}}{|\hat{\boldsymbol{G}}(j\omega)|(1 - a^2\boldsymbol{B}(\omega)^2)}. \tag{2.19}$$

If Eq. (2.12) is used to calculate the solution of $|\boldsymbol{C}(j\omega)|$, a simpler form of Eq. (2.19) can be obtained as

$$|\boldsymbol{C}(j\omega)| < \frac{-\cos\boldsymbol{\theta} + \sqrt{\cos^2\boldsymbol{\theta} - (1 - a^2)}}{|\hat{\boldsymbol{G}}(j\omega)|}. \tag{2.20}$$

2.3 Frequency domain method

This section presents an FB controller design method which applies an MFDB-LMS algorithm and verifies the robust stability condition and the noise amplification constraint in the frequency domain adaptation directly. The FDB-LMS algorithm is an efficient realization of the time domain block LMS by using fast Fourier transform (FFT) so that it has the improved convergence rate than the LMS algorithm [141, 142]. There are two types of FDB-LMS algorithms – with and without causal constraint [140]. The FDB-LMS algorithm without the causal constraint is more computationally efficient, whereas it suffers from the problem of poorer convergence behavior than the constrained one

because of the circular convolution effects in the signal filtering computation [143, 144]. Therefore, this section investigates the FDB-LMS algorithm with causal constraint. By considering the easiness of the real-time implementation, an MFDB-LMS algorithm with the reduced computational complexity is proposed in this section. Firstly, the proposed MFDB-LMS algorithm is proved to be capable of converging to the Wiener solution [145] with the guaranteed optimal steady-state performance. Then, the proposed MFDB-LMS algorithm is introduced into the IMC structured FB-ANC system in which the online verification of the robust stability condition and the noise amplification constraint are performed. The effectiveness of the proposed system is validated by simulations.

2.3.1 Modified frequency domain least mean squares algorithm

Figure 2.2(a) shows the block diagram of the conventional FDB-LMS algorithm. In order to correctly calculate the L-point linear convolution output, the length of the signal vectors should be set as $2L$. Therefore, for the control filter coefficients $\boldsymbol{c}(n)$ with the effective length of L, the reference signal vector $\boldsymbol{x}(n)$ and the error signal vector $\boldsymbol{e}(n)$ are defined as

$$\boldsymbol{c}(n) = [c_1(n), c_2(n), \ldots, c_L(n), \boldsymbol{0}_{1\times L}]^{\mathrm{T}}, \tag{2.21}$$

$$\boldsymbol{x}(n) = [x(n-2L+1), x(n-2L+2), \ldots, x(n)]^{\mathrm{T}}, \tag{2.22}$$

$$\boldsymbol{e}(n) = [\boldsymbol{0}_{1\times L}, e(n-L+1), \ldots, e(n)]^{\mathrm{T}}, \tag{2.23}$$

where n is the discrete time. To avoid the circular effects, a L-point zero vector $\boldsymbol{0}_{1\times L}$ is inserted into the error signal vector $\boldsymbol{e}(n)$ [140]. By using these defined signal vectors, the FDB-LMS algorithm can be written as follows [140, 142]:

$$\boldsymbol{C}(n+1) = \boldsymbol{C}(n) - \mu \left\{ \boldsymbol{X}^{\mathrm{H}}(n)\boldsymbol{E}(n) \right\}_{+}, \tag{2.24}$$

in which

$$\boldsymbol{C}(n) = \boldsymbol{F}\boldsymbol{c}(n), \tag{2.25}$$

$$\boldsymbol{X}(n) = \mathrm{diag}[\boldsymbol{F}\boldsymbol{x}(n)], \tag{2.26}$$

$$\boldsymbol{E}(n) = \boldsymbol{F}\boldsymbol{e}(n). \tag{2.27}$$

The superscript $^{\mathrm{H}}$ denotes the Hermitian transpose, and the notation $\{\ \}_+$ is the causality operator [127, 142] which is explicitly defined in Appendix A. μ is the step-size parameter that is a small positive real number. $\boldsymbol{F}$ is the $2L \times 2L$ discrete Fourier transform matrix. $\boldsymbol{C}(n)$, $\boldsymbol{X}(n)$ and $\boldsymbol{E}(n)$ are the FFT result of $\boldsymbol{c}(n)$, $\boldsymbol{x}(n)$ and $\boldsymbol{e}(n)$, respectively. $\boldsymbol{X}(n)$ is diagonalized for the calculation of matrices. Equation (2.24) can be written by the matrix form as

$$\boldsymbol{C}(n+1) = \boldsymbol{C}(n) - \mu \boldsymbol{F}\boldsymbol{Z}_{L,0}\boldsymbol{F}^{-1}\boldsymbol{X}^{\mathrm{H}}(n)\boldsymbol{E}(n). \tag{2.28}$$

where $\boldsymbol{Z}_{L,0}$ is defined as

$$\boldsymbol{Z}_{L,0} = \begin{bmatrix} \boldsymbol{I}_{L\times L} & \boldsymbol{0}_{L\times L} \\ \boldsymbol{0}_{L\times L} & \boldsymbol{0}_{L\times L} \end{bmatrix}, \tag{2.29}$$

and $\boldsymbol{I}_{L\times L}$ is a $L \times L$ unit matrix. It has been proved that a causal filter obtained by the update equation with the causality constraint in Eq. (2.28) can accurately converge to the Wiener solution [142, 146]. The unconstrained FDB-LMS algorithm saves the calculation enclosed by the dashed line in Fig. 2.2(a), whereas the converge behavior deteriorates.

In order to guarantee the algorithm performance and reduce the computation complexity simultaneously, the FDB-LMS algorithm is modified as shown in Fig. 2.2(b).

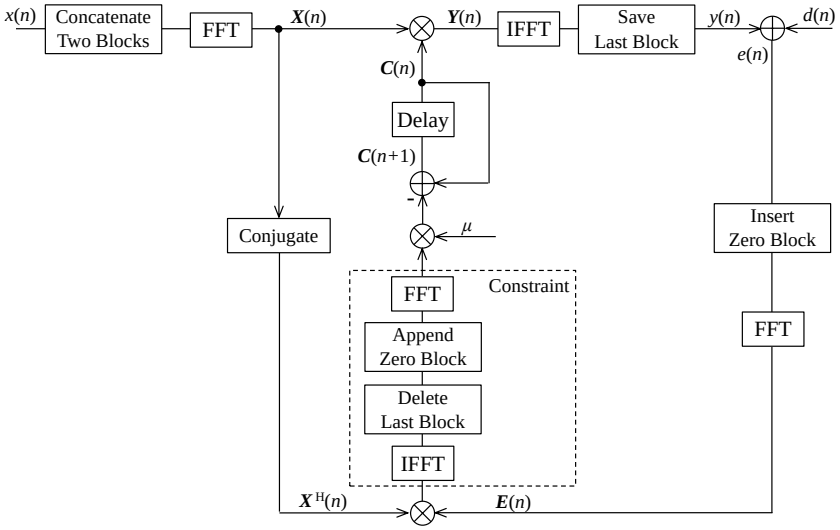

(a) Conventional FDB-LMS

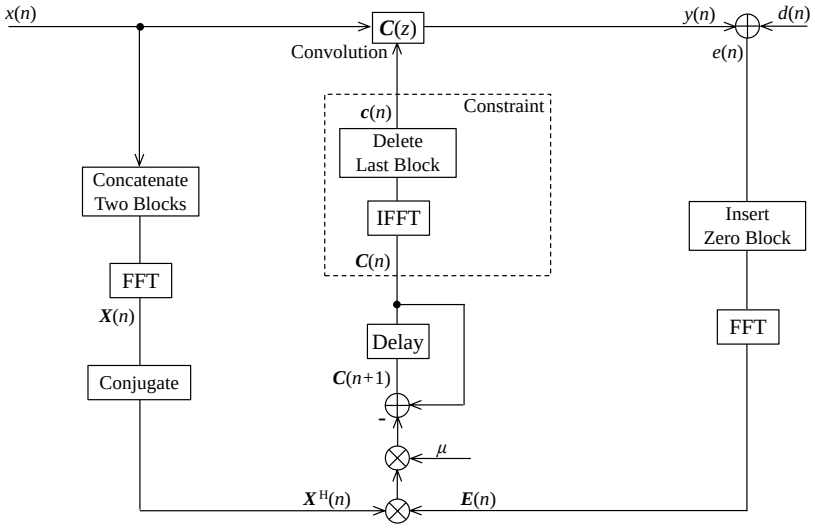

(b) Proposed MFDB-LMS

Figure 2.2: Block diagrams of the FDB-LMS algorithms

The proposed MFDB-LMS algorithm can be written as

$$\boldsymbol{c}(n) = \boldsymbol{F}^{-1}\left\{\boldsymbol{C}(n)\right\}_{+}, \tag{2.30}$$

$$\boldsymbol{C}(n+1) = \boldsymbol{C}(n) - \mu\boldsymbol{X}^{\mathrm{H}}(n)\boldsymbol{E}(n). \tag{2.31}$$

The causality constraint for the filter coefficients is performed in prior to the calculation of the filter output. The matrix form of Eq. (2.30) can be written as

$$\boldsymbol{c}(n) = \boldsymbol{F}^{-1}\boldsymbol{F}\boldsymbol{Z}_{L,0}\boldsymbol{F}^{-1}\boldsymbol{C}(n) = \boldsymbol{Z}_{L,0}\boldsymbol{F}^{-1}\boldsymbol{C}(n). \tag{2.32}$$

In the computation of the causality constraint in Eq. (2.32), FFT and IFFT are canceled. Consequently, the MFDB-LMS algorithm can save one FFT and one IFFT computation.

Steady-state performance

The steady-state performance of the proposed MFDB-LMS algorithm is investigated by using the analysis framework in Ref. [146]. By substituting Eq. (2.31) into Eq. (2.32), the control filter coefficients can be written as

$$\boldsymbol{c}(n+1) = \boldsymbol{Z}_{L,0}\boldsymbol{F}^{-1}\left[\boldsymbol{C}(n) - \mu\boldsymbol{X}^{\mathrm{H}}(n)\boldsymbol{E}(n)\right], \tag{2.33}$$

which can be rearranged as

$$\boldsymbol{c}(n+1) = \boldsymbol{Z}_{L,0}\left[\boldsymbol{c}(n) - \mu\boldsymbol{X}_x(n)\boldsymbol{e}(n)\right]. \tag{2.34}$$

$\boldsymbol{X}_x(n)$ is a circulant matrix formed by the reference signal vector $\boldsymbol{x}(n)$, which can be written as

$$\begin{aligned}\boldsymbol{X}_x(n) = \boldsymbol{F}^{-1}\boldsymbol{X}^{\mathrm{H}}(n)\boldsymbol{F} \quad &= \begin{bmatrix} x(n-2L+1) & x(n) & \dots & x(n-2L+2) \\ x(n-2L+2) & x(n-2L+1) & \dots & x(nL-2L+3) \\ \vdots & \vdots & \ddots & \vdots \\ x(n) & x(n-1) & \dots & x(n-2L+1) \end{bmatrix} \\ &= \begin{bmatrix} \boldsymbol{X}_{1,L\times L} & \boldsymbol{X}_{2,L\times L} \\ \boldsymbol{X}_{2,L\times L} & \boldsymbol{X}_{1,L\times L} \end{bmatrix}, \end{aligned} \tag{2.35}$$

From Eq. (2.29), Eq. (2.34) and Eq. (2.35), the update equation of the filter coefficients becomes

$$\boldsymbol{c}(n+1) = \boldsymbol{Z}_{L,0}\left(\begin{bmatrix} \boldsymbol{c}_{L\times 1}(n) \\ \boldsymbol{c}_{nc,L\times 1}(n) \end{bmatrix} - \mu\begin{bmatrix} \boldsymbol{X}_{2,L\times L}\boldsymbol{e}_{L\times 1(n)} \\ \boldsymbol{X}_{1,L\times L}\boldsymbol{e}_{L\times 1(n)} \end{bmatrix}\right), \tag{2.36}$$

where $\boldsymbol{c}_{nc,L\times 1}(n)$ is the non-causal part of $\boldsymbol{c}(n)$ that does not influence the control output because of the multiplication by $\boldsymbol{Z}_{L,0}$. Equation (2.36) can be expressed by the non-zero part of the vectors $\boldsymbol{c}(n+1)_{L\times 1}$, $\boldsymbol{c}(n)_{L\times 1}$ and $\boldsymbol{e}(n)_{L\times 1}$ as

$$\boldsymbol{c}(n+1) = \boldsymbol{c}(n) - \mu\boldsymbol{X}_2\boldsymbol{e}(n), \tag{2.37}$$

where the subscripts $L \times 1$ and $L \times L$ are omitted for convenience. This is exactly the update equation of the time domain block LMS algorithm which proves that the MFDB-LMS algorithm can realize the time domain block LMS algorithm by using less computation. Moreover, the error signal vector can be written as

$$\boldsymbol{e}(n) = \boldsymbol{d}(n) + \boldsymbol{X}_2^{\mathrm{T}}\boldsymbol{c}(n). \tag{2.38}$$

Substitute Eq. (2.38) into Eq. (2.37) such that

$$\boldsymbol{c}(n+1) = \boldsymbol{c}(n) - \mu[\boldsymbol{X}_2\boldsymbol{d}(n) + \boldsymbol{X}_2\boldsymbol{X}_2^{\mathrm{T}}\boldsymbol{c}(n)], \tag{2.39}$$

where $\boldsymbol{d}(n)$ is the desired signal vector. $\boldsymbol{X}_2\boldsymbol{d}(n)$ is the cross-correlation vector $\boldsymbol{p}$ between the reference signal and the desired signal, and $\boldsymbol{X}_2\boldsymbol{X}_2^{\mathrm{T}}$ is the auto-correlation matrix $\boldsymbol{R}$ of the reference signal, which are defined as

$$\boldsymbol{p} = E[\boldsymbol{X}_2\boldsymbol{d}(n)], \tag{2.40}$$

$$\boldsymbol{R} = E[\boldsymbol{X}_2\boldsymbol{X}_2^{\mathrm{T}}]. \tag{2.41}$$

$E[\ ]$ is the expectation operator. Assuming when $n \to \infty$,

$$\boldsymbol{c}(n+1) \approx \boldsymbol{c}(n) \approx \boldsymbol{c}_{opt}, \tag{2.42}$$

then, from Eq. (2.39) – Eq. (2.42), the optimal filter coefficients $\boldsymbol{c}_{opt}$ can be written as

$$\boldsymbol{c}_{opt} = -\boldsymbol{R}^{-1}\boldsymbol{p}. \tag{2.43}$$

Accordingly, an adaptive filter using the proposed MFDB-LMS algorithm can converge to the Wiener solution correctly.

Improvement of the convergence rate

Equation (2.31) uses the same step-size parameter μ for the filter coefficient adaptation at each frequency. In such case, μ is determined by the minimum value of the step-size parameters that can ensure the stability of the adaptive process. Actually, $\boldsymbol{C}(n)$ is updated independently at each frequency so that using a set of step-size parameters with respect to the frequency can improve the overall convergence rate [140, 147].

The frequency related step-size parameter matrix $\boldsymbol{\mu}_M(n)$ can be obtained by normalizing the a small positive number α by the power spectral density $\hat{\boldsymbol{P}}_{xx}$ of the reference signal at each discrete frequency as follows [140]:

$$\begin{aligned}\boldsymbol{\mu}_M(n) &= \alpha[\hat{\boldsymbol{P}}_{xx}(n) + \epsilon\boldsymbol{I}_{2L\times 2L}]^{-1} \\ &= \mathrm{diag}\left[\frac{\alpha}{\hat{P}_{xx,1}(n)+\epsilon}, \frac{\alpha}{\hat{P}_{xx,2}(n)+\epsilon}, \ldots, \frac{\alpha}{\hat{P}_{xx,2L}(n)+\epsilon}\right].\end{aligned} \tag{2.44}$$

The power spectral density $\hat{\boldsymbol{P}}_{xx}$ can be estimated by the following exponential averaging calculation:

$$\hat{\boldsymbol{P}}_{xx}(n) = (1-\lambda)\hat{\boldsymbol{P}}_{xx}(n-1) + \lambda|\boldsymbol{X}(n)|^2, \tag{2.45}$$

where

$$|\boldsymbol{X}(n)|^2 = \boldsymbol{X}(n)^{\mathrm{H}}\boldsymbol{X}(n), \tag{2.46}$$

ϵ is a small positive number to avoid division by zero, and λ is the forgetting factor with the value between 0 and 1. By introducing $\boldsymbol{\mu}_M(n)$ into the filter adaptation, Eq. (2.31) can be rewritten as

$$\boldsymbol{C}(n+1) = \boldsymbol{C}(n) - \boldsymbol{\mu}_M(n)\boldsymbol{X}^{\mathrm{H}}(n)\boldsymbol{E}(n). \tag{2.47}$$

2.3.2 Feedback active noise control system using the modified frequency domain least mean squares algorithm

Figure 2.3(a) shows the block diagram of the IMC structured FB-ANC system applying a FX-typed algorithm [123], in which the reference signal $\hat{d}(n)$ is filtered by the

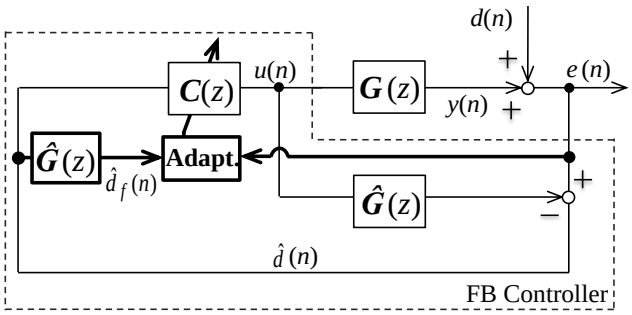

(a) Adaptive IMC structured FB-ANC system

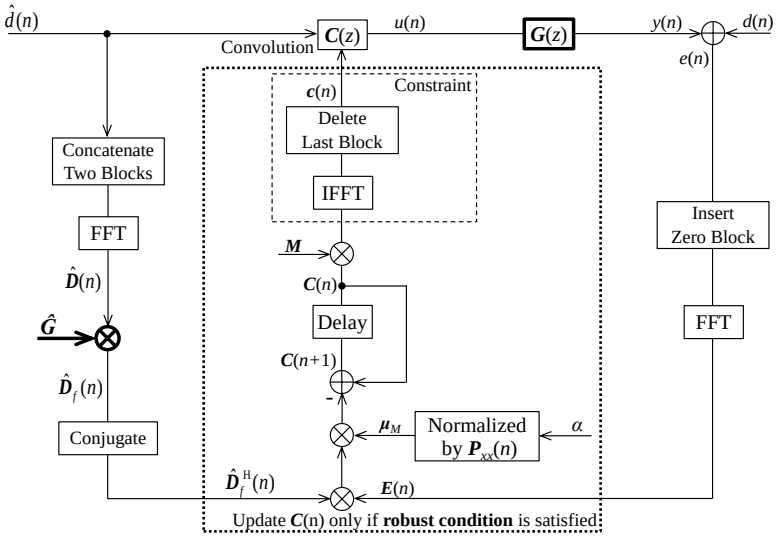

(b) MFDB-FXLMS applied to the IMC structured FB-ANC system

Figure 2.3: Block diagrams of the adaptive IMC structured FB-ANC system

secondary path model $\hat{\boldsymbol{G}}(z)$ to take the influence of the secondary path into the adaptation of $\boldsymbol{C}(z)$. The FX-typed MFDB-LMS (MFDB-FXLMS) algorithm is introduced into the FB-ANC system, and the detailed adaptive process is shown in Fig. 2.3(b).

The control filter $\boldsymbol{C}(z)$ applies the estimated primary noise signal $\hat{d}(n)$ as the reference signal. $\hat{d}(n)$ is calculated according to the block diagram in Fig. 2.3(a) as

$$u(n) = \boldsymbol{c}(n)^{\mathrm{T}} \hat{\boldsymbol{d}}(n), \tag{2.48}$$

$$\hat{d}(n) = e(n) - \hat{\boldsymbol{g}}^{\mathrm{T}} \boldsymbol{u}(n), \tag{2.49}$$

$$\hat{\boldsymbol{d}}(n) = [\hat{d}(n),\ \hat{d}(n-1),\ \ldots,\ \hat{d}(n-2L+1)]^{\mathrm{T}}, \tag{2.50}$$

$$\boldsymbol{u}(n) = [u(n),\ u(n-1),\ \ldots,\ u(n-2L+1)]^{\mathrm{T}}, \tag{2.51}$$

where $\hat{\boldsymbol{g}}$ is a FIR filter expressing the impulse response of the secondary path model. In the MFDB-FXLMS algorithm, the secondary path model filtered signal $\hat{\boldsymbol{D}}_f(z)$ is used as the input of the adaptive process. This filtering computation is conducted in the frequency domain.

The robust stability condition and the noise amplification constraint are verified in the adaptive process of the MFDB-FXLMS algorithm. Equation (2.9) can be rewritten by the matrix form as

$$|\boldsymbol{C}(n)| < |\hat{\boldsymbol{G}}\boldsymbol{B}|^{-1}, \tag{2.52}$$

and used to verify the robust stability condition. If $\hat{\boldsymbol{G}}(z)$ and $\boldsymbol{B}$ are time-invariant, the right-hand of Eq. (2.52) can be prepared in the initialization stage of the algorithm to save the computation in the real-time control stage. The noise amplification constraint verification can be performed according to Eqs. (2.11, 2.12) or Eqs. (2.19, 2.20). The right-hand of Eqs. (2.19, 2.20) cannot be accurately obtained in advance as it requires the phase of $\boldsymbol{C}(z)$ in the calculation. Although it is possible to find an estimate of the controller phase based on Eq. (2.3) to calculate the right-hand of Eqs. (2.19, 2.20) in the system initialization in order to save the real-time computation burden, the accuracy of the estimation will affect that of the noise amplification constraint. Therefore, the proposed method calculates the noise amplification constraint based on Eqs. (2.11, 2.12) in the adaptive process. Both of Eqs. (2.11, 2.12) are accurate enough if the model uncertainties are small, otherwise Eq. (2.12) becomes a loose constraint but it consumes less computation. With a light compromise of the accuracy, the computationally efficient Eq. (2.12) is used in the noise amplification verification, of which the matrix form can be written as

$$|\boldsymbol{I}_{2L\times 2L} + \boldsymbol{C}(n)\hat{\boldsymbol{G}}| \ < \ a\boldsymbol{I}_{2L\times 2L}. \tag{2.53}$$

Only when both of Eq. (2.52) and Eq. (2.53) are satisfied, the adaptation of $\boldsymbol{C}(z)$ is conducted.

Additionally, in order to control the primary noise selectively in the frequency domain, a filter $\boldsymbol{M}$ is used to adjust the properties of the control filter $\boldsymbol{C}(n)$. Therefore, Eq. (2.32) becomes

$$\boldsymbol{c}(n) = \boldsymbol{Z}_{L,0}\boldsymbol{F}^{-1}\boldsymbol{M}\boldsymbol{C}(n). \tag{2.54}$$

Table 2.1 concludes the proposed MFDB-FXLMS algorithm applied to the IMC structured FB-ANC system.

Table 2.1: MFDB-FXLMS algorithm applied to the IMC structured FB-ANC system

Initialization:

$\boldsymbol{C}(0), \boldsymbol{c}(0),\ \hat{\boldsymbol{d}}(0),\ \boldsymbol{e}(0),\ \boldsymbol{u}(0) = \boldsymbol{0}_{2L\times 1}$;
$\hat{\boldsymbol{P}}_{xx}(0) = \boldsymbol{0}_{2L\times 2L}$;
$\hat{\boldsymbol{g}}$ =impulse response FIR filter of the secondary path model;
$\hat{\boldsymbol{G}} = \text{diag}[\boldsymbol{F}\hat{\boldsymbol{g}}]$;
$\boldsymbol{B}$ = estimated uncertainty boundary;
$\boldsymbol{A}_R = |\hat{\boldsymbol{G}}\boldsymbol{B}|^{-1}$;
$\boldsymbol{M}$ = a filter to modify $\boldsymbol{C}(n)$;
$\boldsymbol{Z}_{L,0} = \begin{bmatrix} \boldsymbol{I}_{L\times L} & \boldsymbol{0}_{L\times L} \\ \boldsymbol{0}_{L\times L} & \boldsymbol{0}_{L\times L} \end{bmatrix}$;
$\boldsymbol{F}$ = discrete Fourier transform matrix;
L = effective filter length;
λ = forgetting factor;
α = step-size parameter;
ϵ = a small positive number to avoid division by zero;
A = maximum noise amplification in dB;
$a = 10^{A/20}$;

Real-time control for each $n > 0$:

$u(n) = \boldsymbol{c}(n)^{\mathrm{T}}\hat{\boldsymbol{d}}(n)$;
$\boldsymbol{u}(n) = [u(n), \ldots, u(n-2L+1)]^{\mathrm{T}}$;
Sensing error signal $e(n)$;
$\boldsymbol{e}(n) = [\boldsymbol{0}_{L\times 1}, e(n-L+1), \ldots, e(n)]^{\mathrm{T}}$;
$\hat{d}(n) = e(n) - \hat{\boldsymbol{g}}^{\mathrm{T}}\boldsymbol{u}(n)$;
$\hat{\boldsymbol{d}}(n) = [\hat{d}(n), \ldots, \hat{d}(n-2L+1)]^{\mathrm{T}}$;

Filter coefficients update for each new signal block:

$\boldsymbol{E}(n) = \boldsymbol{F}\boldsymbol{e}(n)$;
$\hat{\boldsymbol{d}}'(n)$ = reversed $\hat{\boldsymbol{d}}(n)$;
$\hat{\boldsymbol{D}}(n) = \text{diag}[\boldsymbol{F}\hat{\boldsymbol{d}}'(n)]$;
$\hat{\boldsymbol{D}}_f(n) = \hat{\boldsymbol{G}}\hat{\boldsymbol{D}}(n)$;
$\hat{\boldsymbol{P}}_{xx}(n) = (1-\lambda)\hat{\boldsymbol{P}}_{xx}(n-1) + \lambda|\hat{\boldsymbol{D}}_f(n)|^2$;
$\boldsymbol{\mu}_M(n) = \alpha[\hat{\boldsymbol{P}}_{xx}(n) + \epsilon\boldsymbol{I}_{2L\times 2L}]^{-1}$;
If $|\boldsymbol{C}(n)| < \boldsymbol{A}_R$ and $|\boldsymbol{I}_{2L\times 2L} + \boldsymbol{C}(n)\hat{\boldsymbol{G}}| < a\boldsymbol{I}_{2L\times 2L}$ **// Robust condition check**
  $\boldsymbol{C}(n+1) = \boldsymbol{C}(n) - \boldsymbol{\mu}_M(n)\hat{\boldsymbol{D}}_f^{\mathrm{H}}(n)\boldsymbol{E}(n)$;
  $\boldsymbol{c}(n+1) = \boldsymbol{Z}_{L,0}\boldsymbol{F}^{-1}\boldsymbol{M}\boldsymbol{C}(n+1)$.
End

2.3.3 Verification

Computer simulations are conducted to verify the effectiveness of the proposed frequency domain method in this section. The simulation configuration is depicted in Fig. 2.4, in which the FB-ANC system is supposed to be used to reduce the sound diffraction at the loudspeaker surface as the use of it in the proposed ANB system. In the simulations, the acoustic paths are expressed as 2048-tap FIR filters, which are measured in the anechoic chamber in advance. The FB controller applies a 512-tap FIR filter, and the sampling frequency of the control system is set as 20 kHz. The target band of the FB control is set as [178, 708] Hz (from 200 Hz to 630 Hz 1/3 octave band) by using the filter $\boldsymbol{M}$ shown in Fig. 2.5. $\boldsymbol{M}$ is equivalent to a band-pass filter of which the passband is the target band of the FB control. The small number α for calculating the step-size parameter is set by trial and error to obtain the optimal noise attenuation in the control bandwidth.

Secondary model uncertainty

The uncertainties of the secondary path model must be estimated prior to the controller design process. In the simulations, the uncertainties between the physical secondary

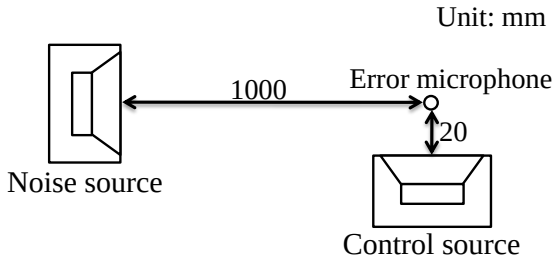

Figure 2.4: Simulation configuration

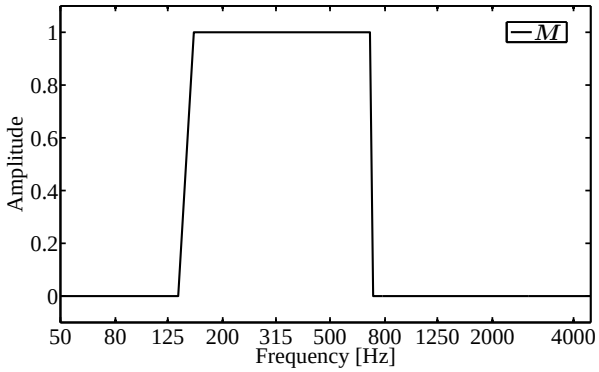

Figure 2.5: Filter $\boldsymbol{M}$ to set the target band of the FB control that is from 200 Hz to 630 Hz 1/3 octave band

path and the model are respectively defined as

$$\triangle|\boldsymbol{G}(z)| = \frac{|\boldsymbol{G}(z)| - |\hat{\boldsymbol{G}}(z)|}{|\hat{\boldsymbol{G}}(z)|} \times 100\%, \tag{2.55}$$

$$\boldsymbol{\theta}_{\triangle \boldsymbol{G}} = \frac{\boldsymbol{\theta}_{\boldsymbol{G}} - \boldsymbol{\theta}_{\hat{\boldsymbol{G}}}}{\pi/2} \times 100\%. \tag{2.56}$$

The phase uncertainties are modeled as a percentage between the phase difference and $\pi/2$ by considering the $\pi/2$ convergence condition for the adaptive IMC typed FB-ANC system [127]. The uncertainties are assumed to be small at low frequencies and to increase linearly along with increasing frequency. In the simulations, the physical secondary path $\boldsymbol{G}(z)$ is calculated from the measured secondary path model $\hat{\boldsymbol{G}}(z)$ according to Eq. (2.55) and Eq. (2.56) where the signs of $\triangle|\boldsymbol{G}(z)|$ and $\boldsymbol{\theta}_{\triangle \boldsymbol{G}}$ are set randomly. The uncertainty boundary function $\boldsymbol{B}$ is determined by Eq. (2.7).

Simulation results

The first simulation is to confirm the effectiveness of the proposed method for limiting the waterbed effect induced noise amplification to within a given value. In this simulation, it is assumed that the secondary model uncertainty is 5% at 1 Hz and 25% at 4 kHz (5% – 25%). Figure 2.6 shows the secondary path $\boldsymbol{G}(z)$, secondary path model $\hat{\boldsymbol{G}}(z)$ and uncertainty boundary $\boldsymbol{B}$ used in the simulation. Three noise amplification conditions including 5 dB maximum noise amplification, 10 dB maximum noise amplification, and only robust stability without noise amplification constraint, are compared in the simulation.

The SPL at the error microphone before and after control is shown in Fig. 2.7(a), and the noise attenuation that is the difference of SPL is shown in Fig. 2.7(b). The result indicates that the primary noise is reduced within the FB control bandwidth, whereas

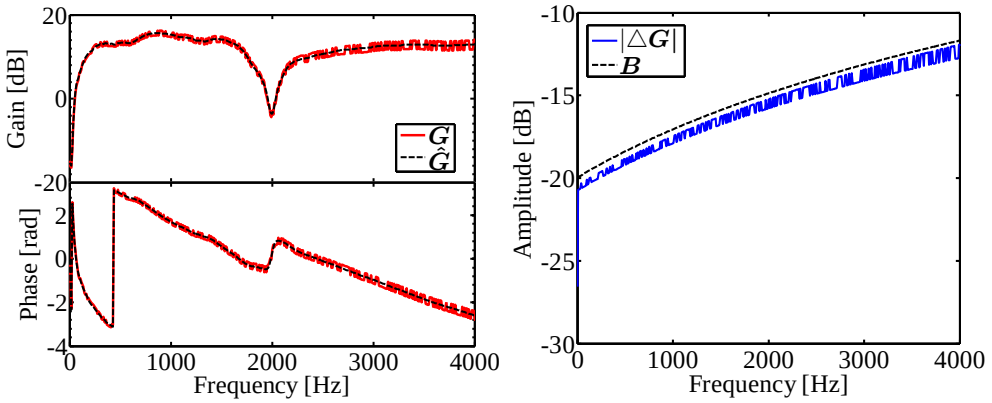

(a) Frequency properties

(b) Boundary of the uncertainty

Figure 2.6: Secondary path $\boldsymbol{G}(z)$, secondary path model $\hat{\boldsymbol{G}}(z)$, and the boundary function $\boldsymbol{B}$ of the uncertainty $\triangle \boldsymbol{G}(z)$

the noise amplification caused by the waterbed effect exists at the other frequencies. The classic trade-off of the FB control between reducing the primary noise and limiting the noise amplification can also be confirmed from the results. When the maximum noise amplification is set as 10 dB, about 5 dB noise attenuation can be obtained within the control bandwidth; however, if the noise amplification is limited to within 5 dB, the noise attenuation decreases to 2 – 3 dB. In addition, the same results are obtained on the condition that the maximum noise amplification is set as 10 dB, and on the condition that only the robust stability is verified online. This demonstrates that the robust FB control with 10 dB noise amplification, which also means the possibility to obtain larger noise attenuation within the target band, cannot be realized for the given secondary path uncertainties, and the upper bound of the noise amplification is determined by the robust stability condition. These simulation results confirm that the FB-ANC system using the proposed MFDB-FXLMS algorithm can effectively limit the noise amplification to within the given value.

The second simulation investigates the robust stability of the FB-ANC system using the MFDB-FXLMS algorithm. Three secondary model uncertainties are set as 2% – 10%, 5% – 25%, 10% – 50% in this simulation, and the performance of the FB control with and without the online robust stability verification is compared.

First, the occasion in which the secondary path and the model uncertainty are time-invariant so that the uncertainty boundary $\boldsymbol{B}$ can be correctly set is investigated. Figure 2.8(a) shows the noise attenuation performance of the FB-ANC system without online robust stability verification. The FB control does not diverge even under the largest 10% – 50% uncertainty condition. This is because the stability of the system using the MFDB-FXLMS algorithm is equivalent to the $\pi/2$ stability condition of the adaptive FB-ANC system if the secondary path and the model uncertainty are time-invariant. However, it can be found from the result that the noise amplification existing around 800 Hz becomes large as the uncertainty increases. Under the uncertainty

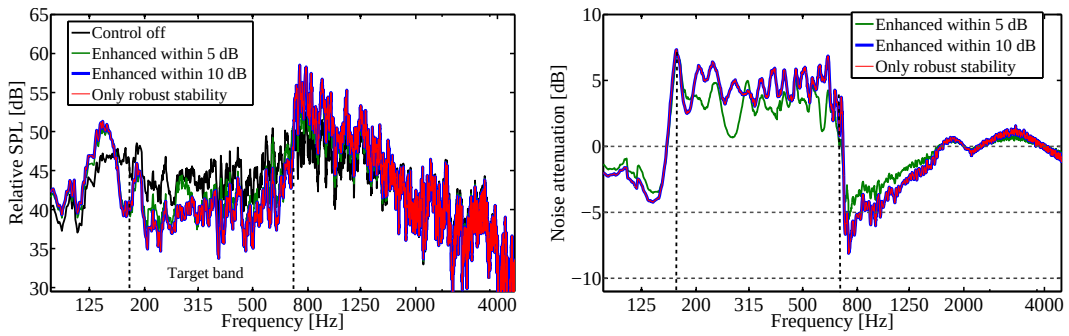

(a) SPL before and after control

(b) Noise attenuation

Figure 2.7: A comparison of the control results for the different noise amplification conditions at the center FB control point

condition of 10% – 50%, the noise amplification is as large as 25 dB, which implies that it is also necessary to limit the noise amplification to within an acceptable range even in the time-invariant secondary path case. Figure 2.8(b) shows the noise attenuation performance of the FB-ANC system with online robust stability verification. As the model uncertainty increases, larger boundary function $\boldsymbol{B}$ has to be used in order to guarantee the robust stability so that the achievable noise attenuation becomes small.

Then, the robust stability of the FB control in the case where the secondary path changes with time is investigated. The control filter is obtained under the uncertainty of 5% – 25% and applied as fixed filter during control. The simulation considers the occasions that the uncertainties change from 5% – 25% to 2% – 10% and 10% – 50% in the real-time control stage because of the changes in the secondary path. Figure 2.9(a) shows noise attenuation performance of the system without online robust stability condition verification. For the smaller 2% – 10% uncertainty, a similar noise attenuation result with the 5% – 25% case is obtained. For the 10% – 50% uncertainty, however, the FB control becomes unstable. On the other hand, if the online robust stability

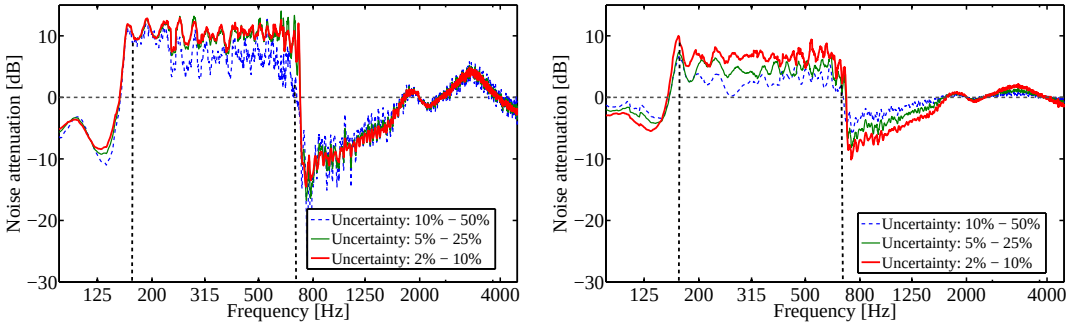

(a) Without robust stability verification (b) With robust stability verification

Figure 2.8: A comparison of the noise attenuation at the center FB control point for the time-invariant uncertainties

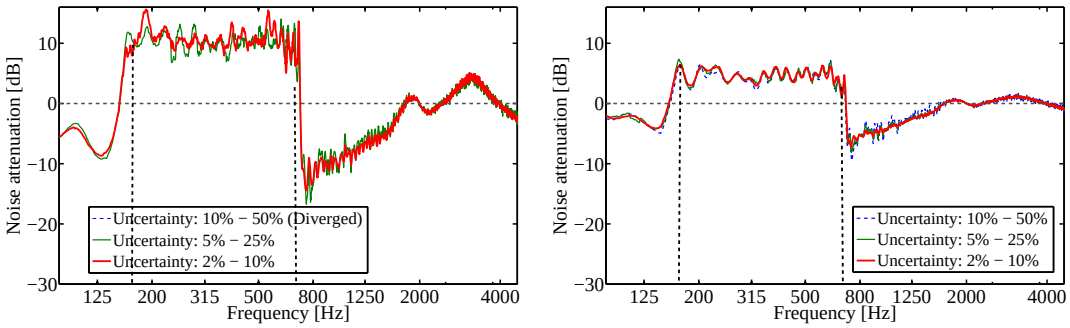

(a) Without robust stability verification (b) With robust stability verification

Figure 2.9: A comparison of the noise attenuation at the center FB control point for the time-variant uncertainties

verification is conducted, the system does not diverge, and similar noise attenuation performance can be obtained for the three uncertainties conditions, which indicates that the FB-ANC system using the proposed MFDB-LMS algorithm has better robust stability than the conventional FB-ANC system.

The above simulations demonstrate that the robust stability condition and the noise amplification constraint of the FB-ANC system can be guaranteed by using the proposed frequency domain design method.

2.4 Time domain method

This section presents a method in which the frequency domain robust stability condition and the noise amplification constraint are converted to the control filter coefficient constraint. Therefore, a robust FB controller with constrained noise amplification can be obtained by exploiting any time domain adaptive algorithm, such as the ordinary FX-LMS algorithm, to update the filter coefficients according to the constraint. Comparing with the MFDB-FXLMS algorithm, the time domain FX-LMS algorithm is more computational efficient so that it is easier to be implemented in the real-time control.

2.4.1 Procedures and application

The method can be described according to the following steps:

Step 1: Identify the secondary path model $\hat{\boldsymbol{G}}(j\omega)$ and determine the uncertainties boundary function $\boldsymbol{B}(\omega)$. $\hat{\boldsymbol{G}}(j\omega)$ can be obtained by an adaptive system identification technique or other modeling techniques. To determine $\boldsymbol{B}(\omega)$, the model uncertainties $\triangle\boldsymbol{G}(j\omega)$ in the frequency domain are estimated firstly, and then the upper bound of the uncertainties amplitude can be used as $\boldsymbol{B}(\omega)$.

Step 2: Estimate the controller phase. Within the target bandwidth of control, the phase of $-\hat{\boldsymbol{G}}^{-1}(j\omega)$, which is the optimum phase for the controller, is used as the estimation. The target band of control should be located within the low frequencies, where the ANC is more effective, and the target bandwidth should be set narrow enough comparing with the sampling frequency to achieve an acceptable potential noise attenuation. A numerical method to simulate the potential noise attenuation of the FB-ANC systems is presented in Appendix B. For the frequency band beyond a certain range, which is set as three times of the target bandwidth in this study, from the target band, it is assumed that the controller has a zero-phase filter property. This range of three times of the target bandwidth is decided according to the observation of the frequency responses of several control filters obtained by computer simulations. For the transition band between the target bandwidth and a bandwidth three times the target bandwidth, the phase approaches 0 linearly. Therefore, by defining ω_S as the start of the target band, ω_E as the end of the target band, ω_B as the target bandwidth and

ω_N as the Nyquist frequency that is half of the sampling frequency, the estimate of the controller phase $\hat{\boldsymbol{\theta}}_{\boldsymbol{C}}(\omega)$ can be described as

$$\hat{\boldsymbol{\theta}}_{\boldsymbol{C}}(\omega) = \begin{cases} 0, & \text{if } \omega \in [0,\ \max(0,\ \omega_S - 2\omega_B)] \\ \boldsymbol{\theta}_{\boldsymbol{C}_{opt}}(\omega_S)\left(1 - \frac{\omega_S - \omega}{2\omega_B}\right), & \text{if } \omega \in (\max(0,\ \omega_S - 2\omega_B), \omega_S) \\ \boldsymbol{\theta}_{\boldsymbol{C}_{opt}}(\omega), & \text{if } \omega \in [\omega_S,\ \omega_E] \\ \boldsymbol{\theta}_{\boldsymbol{C}_{opt}}(\omega_E)\left(1 - \frac{\omega - \omega_E}{2\omega_B}\right), & \text{if } \omega \in (\omega_E,\ \omega_E + 2\omega_B) \\ 0, & \text{if } \omega \in [\omega_E + 2\omega_B,\ \omega_N] \end{cases}, \tag{2.57}$$

$$\omega_B = \omega_E - \omega_S. \tag{2.58}$$

Step 3: Determine the constraints of the controller gain. The robust stability condition and the maximum noise amplification constraint can be calculated by Eq. (2.9) and Eq. (2.19), respectively. In Eq. (2.19), the controller phase $\boldsymbol{\theta}_{\boldsymbol{C}}$ is substituted by the controller phase estimated in Step 2. The controller gain constraint $\boldsymbol{A}(\omega)$ can be determined by

$$A(\omega) = \min(A_r(\omega),\ A_{NA}(\omega)), \quad \text{at each } \omega, \tag{2.59}$$

where $\boldsymbol{A}_r(\omega)$ and $\boldsymbol{A}_{NA}(\omega)$ are the robust condition and the maximum noise amplification constraint calculated by the right hand of Eq. (2.9) and Eq. (2.19), respectively, and min( ) denotes the minimum value.

Step 4: Estimate the robust controller gain. Within a frequency band three times of the target bandwidth, the mean robust controller gain is set as the minimum value of the gain constraint determined in Step 3. Over a frequency band three times of the target bandwidth, the controller is expected to have no output, and the gain should be a small positive number ε. ε is set as one third of estimated mean gain in this study, which is determined by trial and error. Therefore, the estimate of the controller gain $\hat{\boldsymbol{K}}_{\boldsymbol{C}}(\omega)$ can be described as

$$\hat{\boldsymbol{K}}_{\boldsymbol{C}}(\omega) = \begin{cases} \varepsilon, & \text{if } \omega \in [0,\ \max(0,\ \omega_S - 2\omega_B)] \\ \min(\boldsymbol{A}(\omega)), & \text{if } \omega \in (\max(0,\ \omega_S - 2\omega_B),\ \omega_E + 2\omega_B) \\ \varepsilon, & \text{if } \omega \in [\omega_E + 2\omega_B,\ \omega_N] \end{cases}, \tag{2.60}$$

$$\varepsilon = \min(\boldsymbol{A}(\omega))/3. \tag{2.61}$$

Step 5: Determine the time domain constraint. The frequency domain constraint that the mean controller gain is smaller than the minimum value of the gain constraint determined in Step 3:

$$\frac{1}{\omega_N}\int_0^{\omega_N} |\boldsymbol{C}(j\omega)| d\omega < \min(\boldsymbol{A}(\omega)), \tag{2.62}$$

is converted into the time domain by using the inverse discrete Fourier transform (IDFT). It can be proven that the filter will satisfy the constraint in the frequency

domain shown in Eq. (2.62), if the absolute value of the first control filter coefficient c_1 is no larger than a constraint c_{Lim}, which is the first absolute value of the impulse response calculated by IDFT according to the controller phase and gain estimated in Step 2 and Step 4. c_1 and c_{Lim} can be calculated as

$$c_1 = \frac{1}{N}\sum_{k=1}^{N} |\boldsymbol{C}|(k)\cos\boldsymbol{\theta_C}(k), \tag{2.63}$$

$$c_{Lim} = \frac{1}{N}\left|\sum_{k=1}^{N} \hat{\boldsymbol{K}}_{\boldsymbol{C}}(k)\cos\hat{\boldsymbol{\theta}}_{\boldsymbol{C}}(k)\right|, \tag{2.64}$$

where $\hat{\boldsymbol{K}}_{\boldsymbol{C}}(k)$ and $\hat{\boldsymbol{\theta}}_{\boldsymbol{C}}(k)$ stand for the kth element of $\hat{\boldsymbol{K}}_{\boldsymbol{C}}(\omega)$ and $\hat{\boldsymbol{\theta}}_{\boldsymbol{C}}(\omega)$ in the discrete frequency domain, $|\boldsymbol{C}|(k)$ and $\boldsymbol{\theta_C}(k)$ are the gain and phase vector of the designed controller in the discrete frequency domain, and N is the number of DFT points. The constraint that $|c_1| \leq c_{Lim}$ establishes

$$\frac{1}{N}\left|\sum_{k=1}^{N} |\boldsymbol{C}|(k)\cos\boldsymbol{\theta_C}(k)\right| \leq \frac{1}{N}\left|\sum_{k=1}^{N} \hat{\boldsymbol{K}}_{\boldsymbol{C}}(k)\cos\hat{\boldsymbol{\theta}}_{\boldsymbol{C}}(k)\right|. \tag{2.65}$$

By considering

$$\left|\sum_{k=1}^{N} |\boldsymbol{C}|(k)\cos\boldsymbol{\theta_C}(k)\right| = r_1\sum_{k=1}^{N} |\boldsymbol{C}|(k), \tag{2.66}$$

$$\left|\sum_{k=1}^{N} \hat{\boldsymbol{K}}_{\boldsymbol{C}}(k)\cos\hat{\boldsymbol{\theta}}_{\boldsymbol{C}}(k)\right| = r_2\sum_{k=1}^{N} \hat{\boldsymbol{K}}_{\boldsymbol{C}}(k), \tag{2.67}$$

where r_1 and r_2 are two numbers between 0 and 1, which are defined as

$$r_1 = \left|\sum_{k=1}^{N} |\boldsymbol{C}|(k)\cos\boldsymbol{\theta_C}(k)\right| / \sum_{k=1}^{N} |\boldsymbol{C}|(k), \tag{2.68}$$

$$r_2 = \left|\sum_{k=1}^{N} \hat{\boldsymbol{K}}_{\boldsymbol{C}}(k)\cos\hat{\boldsymbol{\theta}}_{\boldsymbol{C}}(k)\right| / \sum_{k=1}^{N} \hat{\boldsymbol{K}}_{\boldsymbol{C}}(k), \tag{2.69}$$

Equation (2.65) can be rewritten as

$$\frac{1}{N}\sum_{k=1}^{N} |\boldsymbol{C}|(k) \leq \frac{r_2}{r_1 N}\sum_{k=1}^{N} \hat{\boldsymbol{K}}_{\boldsymbol{C}}(k). \tag{2.70}$$

According to Eq. (2.60), the value of $\frac{1}{N}\sum_{k=1}^{N} \hat{\boldsymbol{K}}_{\boldsymbol{C}}(k)$ is between that of $\min(\boldsymbol{A}(k))$ and ε, and relates to ε, so $\frac{1}{N}\sum_{k=1}^{N} \hat{\boldsymbol{K}}_{\boldsymbol{C}}(k)$ can be described as

$$\frac{1}{N}\sum_{k=1}^{N} \hat{\boldsymbol{K}}_{\boldsymbol{C}}(k) = r_3(\varepsilon)\min(\boldsymbol{A}(k)), \tag{2.71}$$

where $r_3(\varepsilon)$ is a function of ε, of which the value is between 0 and 1. Thus, Eq. (2.70) becomes

$$\frac{1}{N}\sum_{k=1}^{N}|\boldsymbol{C}|(k) \leq \frac{r_2 r_3(\varepsilon)}{r_1}\min\left(\boldsymbol{A}(k)\right). \tag{2.72}$$

Equation (2.72) implies if $|c_1|$ is no larger than the constraint c_{Lim} and ε is determined appropriately, the designed controller can be expected to satisfy the constraint shown in Eq. (2.62).

Step 6: Obtain a solution of the robust controller. An FIR filter is used as the controller, and the filter coefficients are updated by an adaptive algorithm according to the time domain constraint determined in Step 5. In this study, the FX-LMS algorithm is used to obtain the control filter coefficients $\boldsymbol{c}(n)$. The adaptation of $\boldsymbol{c}(n)$ exploiting the constraint c_{Lim} can be described as

$$\boldsymbol{c}(n+1) = \boldsymbol{c}(n) - \mu e(n)\boldsymbol{f}(n), \quad \text{for } n > 0 \text{ and } |c_1(n)| \leq c_{Lim}, \tag{2.73}$$

where μ is the step-size parameter, and $\boldsymbol{f}(n)$ is the secondary path model filtered reference signal. When the first absolute value of the control filter coefficients c_1 becomes larger than c_{Lim}, the adaptation will be terminated, and the control filter can be used as a fixed filter.

The proposed method described above can be applied in the online or offline controller design process.

Online controller design can tune the controller to trace the properties of the primary noise in real time. However, the potential noise attenuation will become quite small if the bandwidth of the primary noise is too broad. Therefore, application of the online controller design is suitable for occasions that the expected primary noise is band-limited. In the online controller design process, the constraint for the filter coefficients is calculated by using the steps 1 – 5 of the method given previously, firstly. This can be implemented in the system initialization stage. Then, an adaptive control system updates the filter coefficients online according to the constraint, and controls the noise in real time.

The offline-designed controller reduces the primary noise at the frequencies that have been decided upon in advance, so that, if the properties of the noise changed, the controller may become less effective. However, a controller with fixed properties can achieve the designed noise attenuation within the target band even against a broad-band noise. The controller is often designed so as to be able to attenuate noise equally within the target band if the properties of the primary noise are unknown. In the offline controller design process, the properties of the controller are obtained according to the method given previously. The filter coefficients can be calculated based on the block diagram shown in Fig. 2.3(a). The primary noise used in the calculation is the band-limited white noise for which the bandwidth is determined by the target band of

control. Then, the controller can be implemented in a real time ANC system as a fixed filter.

2.4.2 Verification

Simulations

The proposed method is validated by simulations, firstly. The configuration considered in the simulations, where the FB-ANC system is used to reduce the sound diffraction at the loudspeaker surface, is shown in Fig. 2.10. The acoustic properties are expressed as 512-tap FIR filters. The FB controller is a 128-tap FIR filter, and the sampling frequency of the control system is set as 20 kHz. The uncertainties of the secondary path model are also considered according to the definitions in Eq. (2.55) and Eq. (2.56). Supposing the gain and phase uncertainties are 2% at 1 Hz and 20% at 4 kHz, the properties of $\hat{\boldsymbol{G}}(z)$ and $\boldsymbol{G}(z)$ are shown in Fig. 2.11(a). Figure 2.11(b) shows the uncertainty boundary function $\boldsymbol{B}(\omega)$ determined by Eq. (2.7).

The first simulation is to verify the effectiveness of the method in the online con-

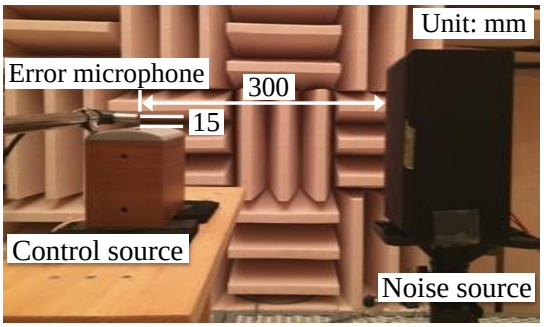

Figure 2.10: Configuration for simulations

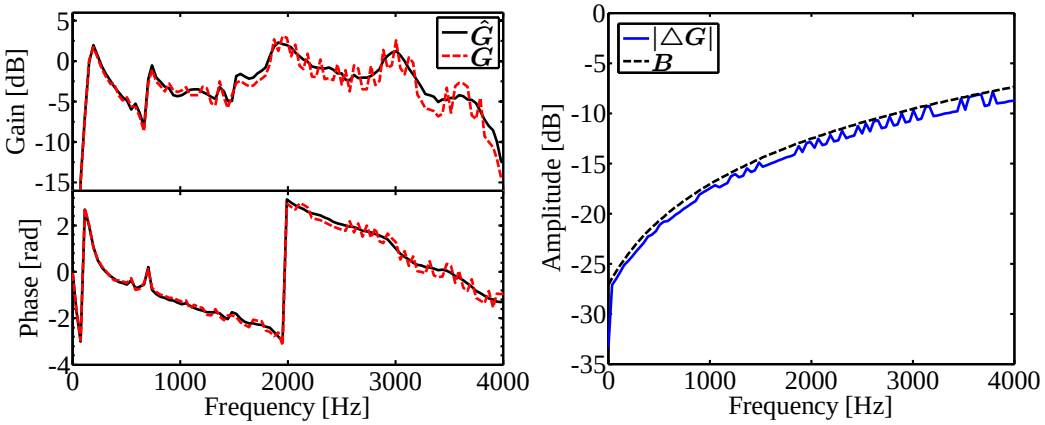

(a) Frequency properties

(b) Boundary of the uncertainty

Figure 2.11: Secondary path $\boldsymbol{G}(z)$, secondary path model $\hat{\boldsymbol{G}}(z)$, and the boundary function $\boldsymbol{B}$ of the uncertainty $\triangle\boldsymbol{G}(z)$

troller design process. The primary noise is assumed to be a white noise filtered by a low-pass filter with a cut-off frequency of 1 kHz. The FX-LMS algorithm is used to update the filter coefficients of the controller, where the step-size parameter is set as 0.00016. The maximum noise amplification is set as 5 dB, 10 dB, so that the time domain constraint c_{Lim} should be 0.21, 0.48, respectively, according to the method given in Section 2.4.1. In addition, as indicated in Ref. [132], the leaky FX-LMS algorithm can limit the controller gain in the online adaptation process by introducing a leak parameter γ into the filter coefficients update equation to improve the stability of the FB-ANC system. Therefore, a comparison of the performance of the controller designed by the proposed method and the one updated by the leaky FX-LMS algorithm is conducted in the simulation.

Figure 2.12 shows simulation results. Figure 2.12(a) and (b) compares the perfor-

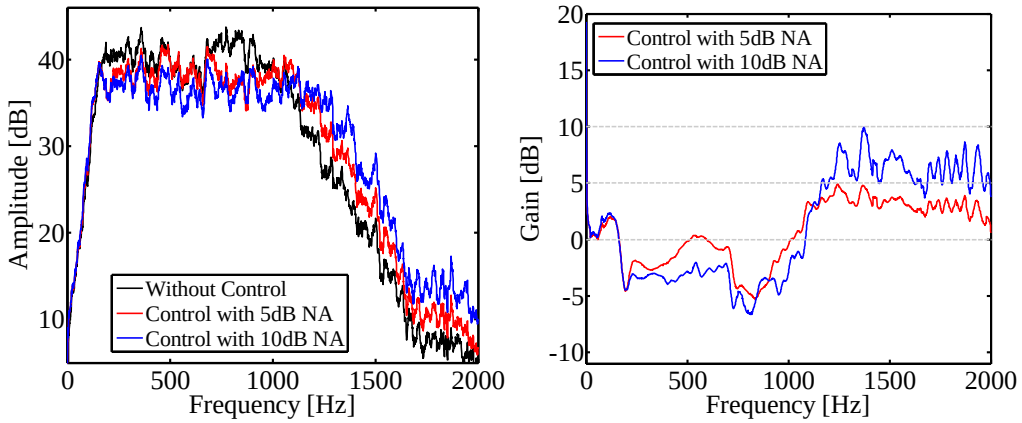

(a) SPL before and after control

(b) the sensitivity $|\boldsymbol{E}(z)|/|\boldsymbol{D}(z)|$

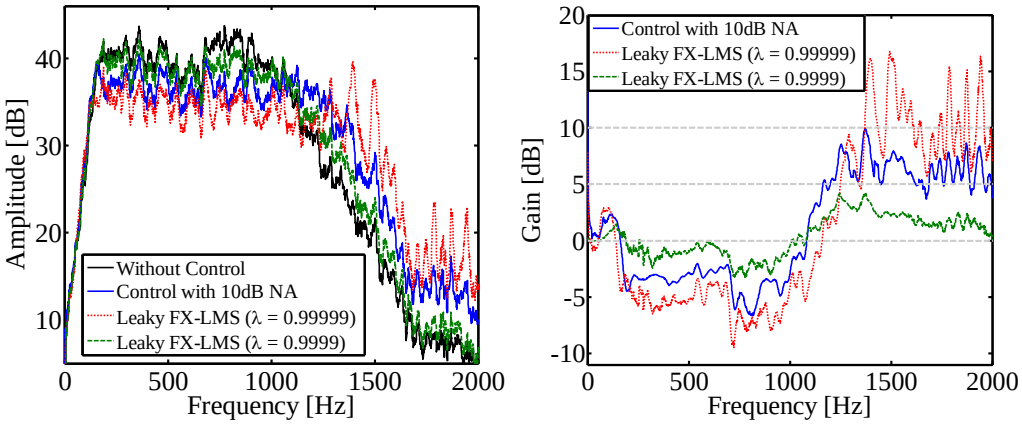

(c) SPL before and after control

(d) the sensitivity $|\boldsymbol{E}(z)|/|\boldsymbol{D}(z)|$

Figure 2.12: Performance of the online-designed controller in the simulation. (a), (b) compares the performance of the proposed method under different maximum noise amplification conditions. (c), (d) compares the performance of the proposed method and the leaky FX-LMS algorithm using different leak parameter λ.

mance of the controller designed by the proposed method under different maximum noise amplification conditions. The results show that the maximum noise amplification has been successfully limited to within the given 5 dB and 10 dB. The classic trade-off between reducing noise and limiting noise amplification in the feedback control can also be found in the results, where about 5 dB noise attenuation is obtained for the maximum 10 dB noise amplification case, whereas only about 2–3 dB noise attenuation is obtained for the maximum 5 dB noise amplification case. Figure 2.12(c) and (d) compares the performance of the proposed method and the leaky FX-LMS algorithm. Two different leak parameters, 0.9999 and 0.99999, are used in this simulation. The results imply that the controller gain can be confined effectively if an appropriate γ is used. However, it can be also confirmed from the results that a too small γ leads to an unacceptable noise reduction performance, and a too large γ can neither limit the noise amplification nor guarantee the stability. It is difficult to relate the leak parameter γ to the noise amplification quantitatively. On the other hand, the proposed method can obtain a specific coefficient constraint to limit the noise amplification within a given value.

Figure 2.13 compares the properties of the calculated controller and the constraints for the 5 dB maximum noise amplification case. The results indicate that the method given in Section 2.4.1 is able to design a controller satisfying both the robust stability condition and the maximum noise amplification constraint. According to Fig. 2.13, the gain of the controller is closest to the noise amplification constraint at a frequency of around 2 kHz, where the maximum noise amplification should appear, but the maximum noise amplification appears at around 1.3 kHz in Fig. 2.12. This mismatch is because of the existence of the estimation errors due to several assumptions used in the

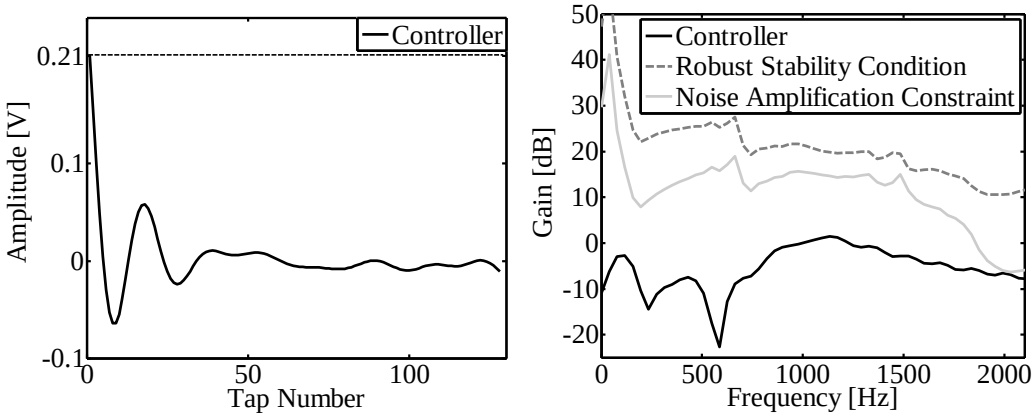

(a) Impulse response

(b) Controller gain, robust stability condition, and maximum noise amplification constraint

Figure 2.13: Properties of the controller for the 5 dB maximum noise amplification case

determination process of the frequency domain constraints described in Section 2.4.1. However, the simulation results demonstrate that the maximum noise amplification can be effectively limited within the designed noise amplification, though the frequency domain constraints cannot be accurate at each frequency.

Another simulation is conducted to confirm the performance of the controller designed offline by the proposed method. In this simulation, the primary noise is white noise. The target band of control is designed to be 100 Hz to 500 Hz. The FX-LMS algorithm is used to obtain the filter coefficients. The maximum noise amplification is set as 5 dB, 10 dB, so that the time domain constraint c_{Lim} should be 0.17, 0.39, respectively, according to the method given in Section 2.4.1.

The properties of the noise used to update the filter coefficients of the controller are shown in Fig. 2.14. Figure 2.15 compares the properties of the obtained controller and the constraints for the 10 dB maximum noise amplification case. Once the controller is designed, the sensitivity function can be calculated so that the performance of the FB-ANC system can be predicted. The noise attenuation performance of the obtained controller and the gain of the designed sensitive function are shown in Fig. 2.16. The sensitivity functions imply that a noise attenuation of about 8 dB can be achieved within the target band for the 5 dB maximum noise amplification case, and an attenuation of about 15 dB can be achieved for the 10 dB maximum noise amplification case, which accords with the achieved noise attenuation. Out of the target band, the noise amplification has been successfully limited within the designed 5 dB and 10dB maximum noise amplification. Moreover, by comparing the results of the two simulations, it can be confirmed that the achievable noise attenuation becomes less for a wider control bandwidth. This is another trade-off that should be taken into consideration for the application of FB-ANC systems.

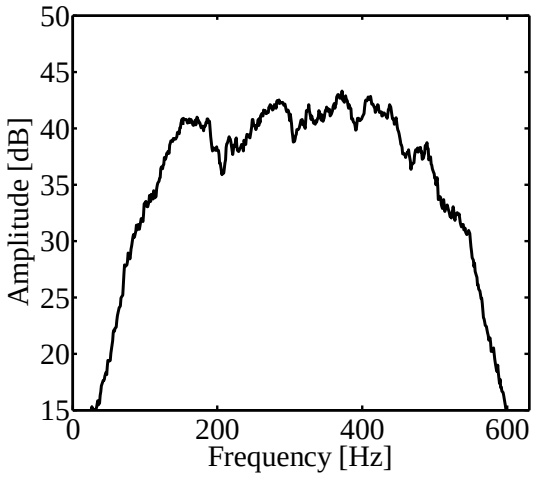

Figure 2.14: Properties of the noise used in the offline controller design process

Experiments

Experiments are conducted to further verify the effectiveness of the proposed method. The experiment configurations are shown in Fig. 2.17, where four different cases are considered to investigate the uncertainties possibly exist in practice. For some large scale ANC applications, such as the active expressway noise barrier [89] and the virtual sound barrier for transformer noise [148], it is difficult to measure the secondary path or design the controller for each control unit. However, the frequency response variance of the electronic devices must exist even the same product model is used to construct the whole system. Therefore, in comparison with the default configuration 1, a different microphone is used as the error sensor in configuration 2 to consider the uncertainties

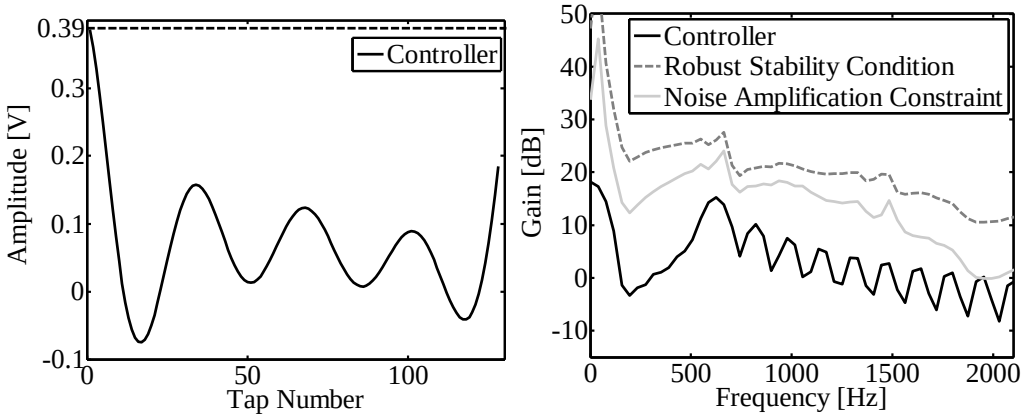

(a) Impulse response

(b) Controller gain, robust stability condition, and maximum noise amplification constraint

Figure 2.15: Properties of the controller for the 10 dB maximum noise amplification case

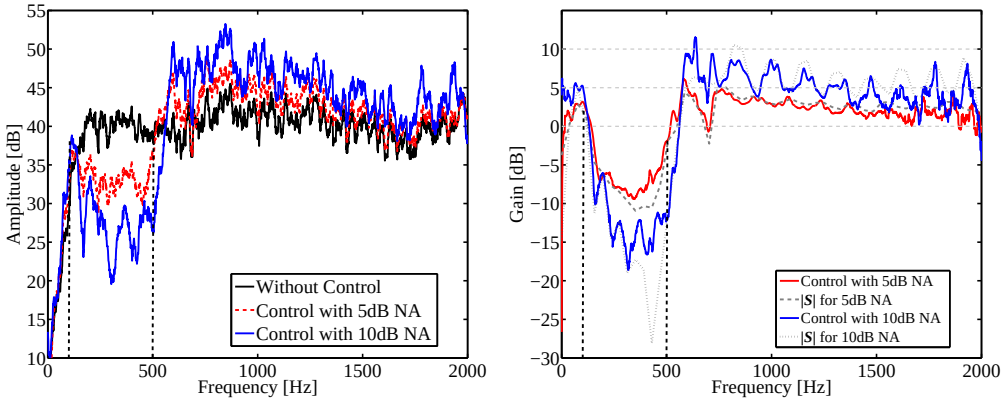

(a) SPL before and after control

(b) Sensitivity $|\boldsymbol{E}(z)|/|\boldsymbol{D}(z)|$ and gain of the designed sensitive function $|\boldsymbol{S}(z)|$

Figure 2.16: Performance of the offline-designed controller in the simulation

due to the electronic devices. There are also some applications that tend to be influenced by the sound field changes, such as people that can be seen as reflection surfaces passing through a low active noise office partition considered in this thesis. Therefore,

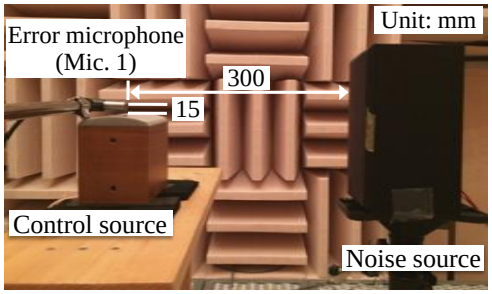

(a) Configuration 1: original configuration to measure the secondary path model $\hat{\boldsymbol{G}}(z)$

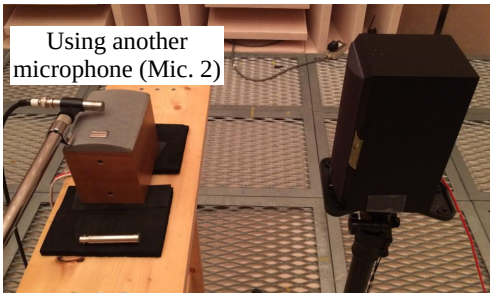

(b) Configuration 2: another microphone is used to consider the uncertainties between different electronic devices

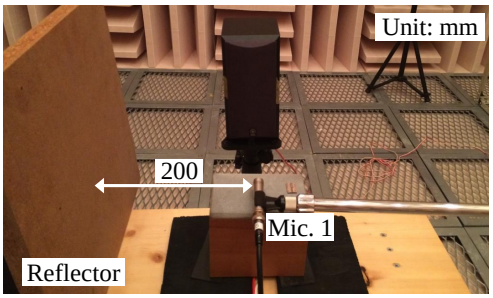

(c) Configuration 3: a reflector is placed near to the control source to investigate uncertainties caused by the change of sound field

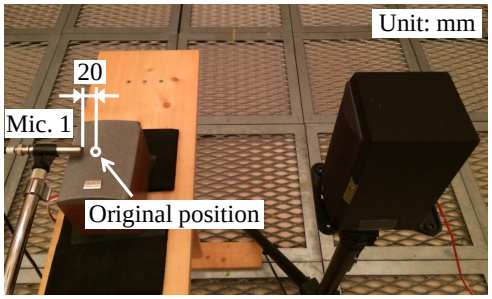

(d) Configuration 4: the error microphone is placed 20 mm off from its original position to consider the uncertainties due to the position error

Figure 2.17: Experiment Configurations

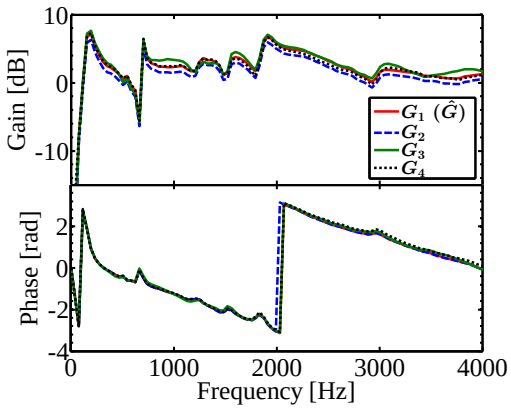

(a) Frequency properties

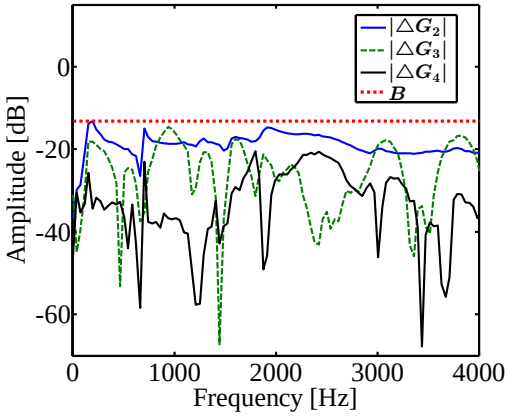

(b) $|\triangle \boldsymbol{G}(z)|$s in configuration 2–4 and the uncertainty boundary function $\boldsymbol{B}$

Figure 2.18: Secondary paths in the experiment configuration 1–4

configuration 3 considers the uncertainties due to the sound field changes by placing a reflector aside the control unit. In configuration 4, the error microphone is moved 20 mm away from its original position to consider the uncertainties due to the position error in assembly of the control unit.

In the experiments, the controller, which is implemented on a DSP with a TMS 320C6713 DSK chip, applies a 128-tap FIR filter, and the sampling frequency is set as 20 kHz. The frequency properties of the secondary paths for the four experiment configurations, which are measured as 512-tap FIR filters, are shown in Fig. 2.18(a). The secondary path in the default configuration 1 $\boldsymbol{G}_1(z)$ is used as the model $\hat{\boldsymbol{G}}(z)$. The uncertainties, which are the differences between the secondary paths in configuration 2–4 and the model $\hat{\boldsymbol{G}}(z)$, are depicted in Fig. 2.18(b). In comparison with the uncertainties caused by reflection and position error of the microphone, of which the amplitude depends on the frequency, using a different error microphone causes the similarly large uncertainties over the whole frequency band. Therefore, a flat uncertainty bound is selected as shown in Fig. 2.18(b).

The first experiment is to verify the performance of the offline-designed controller. In this experiment, white noise is used as the primary noise. The target band of control is designed to be 100 Hz to 500 Hz. The maximum noise amplification is set as 5 dB, so that the calculated time domain constraint c_{Lim} is 0.06. The controller is designed offline according to the same procedures of the offline control simulation, and the obtained control filter is implemented in a real time ANC system as a fixed filter.

From Fig. 2.19(a), which shows the amplitude of the primary noise and the residual noise under the default configuration 1 as a representative of the results of the four configurations, it can be confirmed that the primary noise can be reduced effectively within the target band of control when the uncertainties are small. Figure. 2.19(b)

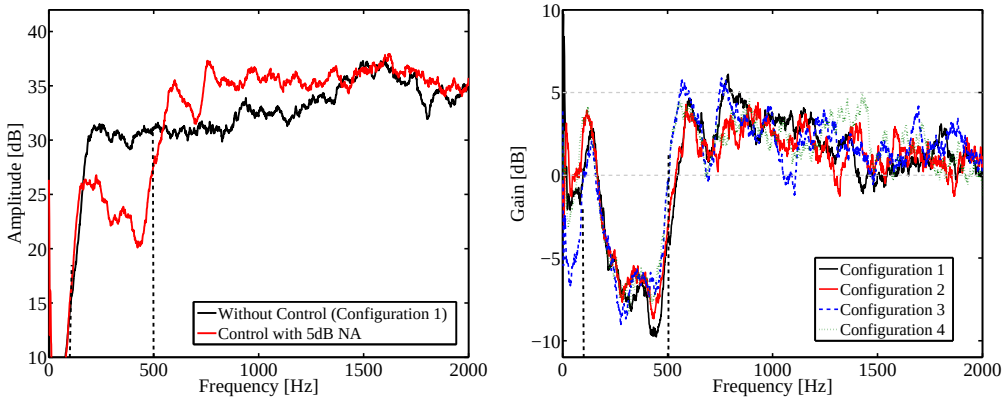

(a) SPL before and after control under configuration 1

(b) Sensitivity $|\boldsymbol{E}(z)|/|\boldsymbol{D}(z)|$ under the four different configurations

Figure 2.19: Performance of the offline-designed controller in the experiment

presents a comparison of sensitivity $|\boldsymbol{E}(z)|/|\boldsymbol{D}(z)|$ obtained in the four experiment configurations. The results indicate that about 8 dB noise attenuation, which is similar to the results obtained in the simulations, can be achieved within the target band of control for all of the four different configurations, and the noise amplification can also be confined effectively within the given 5 dB even if the uncertainties exist in the secondary path model. The experiment results validate the effectiveness of the proposed method for designing a robust fixed controller.

The second experiment is to verify the effectiveness of the proposed method for the online controller design process. This experiment is conducted under configuration 2, where a different error microphone is used because the uncertainties under this configuration are larger than the others. The primary noise is a white noise filtered by a low-pass with a cut-off frequency of 1 kHz. The maximum noise amplification is set as 5 dB, so that the calculated time domain constraint c_{Lim} is 0.12. The control filter coefficients are updated by the FX-LMS algorithm, where the step-size parameter is set as 0.0001.

Figure. 2.20 shows the performance of online updated controller. Within the target band of control, about 3 dB noise attenuation can be obtained even if the secondary path model is not accurate. As indicated in the simulations, it can be confirmed that a wider control bandwidth leads to less noise attenuation by comparing the online control experiment results with the offline control results, where the control bandwidth is narrower. The noise amplification can also be limited to within the given value effectively. These results indicate that the proposed method is also effective for online controller design process.

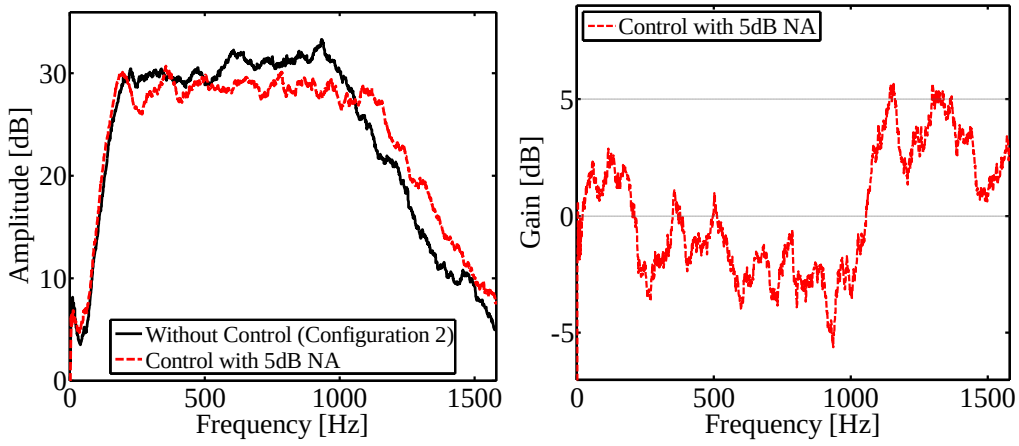

(a) SPL before and after control

(b) Sensitivity $|\boldsymbol{E}(z)|/|\boldsymbol{D}(z)|$

Figure 2.20: Performance of the online-designed controller under the experiment configuration 2

2.5 Summary

This chapter proposed two adaptive methods for designing a robust FB controller. The first method applies an MFDB-LMS algorithm to update the control filter in the FB controller, and the robust stability condition and the noise amplification constraint is verified in the adaptive process. Several simulations were conducted to validate the effectiveness of the method. The results demonstrate that the proposed method can effectively ensure the robust stability of an FB-ANC system, and can limit the noise amplification to within a given value. However, the MFDB-LMS algorithm is of higher computational cost in comparison with the time domain LMS algorithm. Therefore, a time domain method was proposed subsequently. This method determines an equivalent time domain constraint for the robust stability condition and the noise amplification constraint in the frequency domain, which is a maximum value constraint for the FIR filter coefficients. Consequently, a robust IMC controller can be designed by using any time domain adaptive algorithms. Several simulations and experiments were conducted to validate the effectiveness of the method. The simulation and experimental results indicate that the proposed method is effective for designing a robust controller and for limiting the maximum noise amplification for both the online and offline controller design processes.

Chapter 3

Hybrid Active Noise Barrier

3.1 Introduction

This chapter investigates the noise attenuation performance of the proposed ANB system. First, an HB control strategy, which controls the diffracting edge of the ANB and the sound pressure at the head position of the listener simultaneously, is proposed to improve the noise attenuation performance. In the ANB applying the HB control strategy, FB control is used to realize the active control of the diffracting edge, and the sound pressure control part is implemented by FF control. The time domain method proposed in Chapter 2 is exploited to design the FB controllers. Although the noise amplification constraint can be considered in the design process, the noise attenuation provided by the FB controller will become small if the noise amplification is limited to within a small value. Therefore, in order to avoid the trade-off between reducing the primary noise and limiting the noise amplification, a waterbed effect cancellation technique, which reduces the noise amplification propagating into the control area behind the ANB rather than limits it inside the FB controller by exploiting the HB control structure, is proposed. Then, the system implementation of the control strategies is presented. A prototype of the ANB using the HB control strategy is developed, and the noise attenuation performance of the ANB under different sound field conditions is investigated by simulations and experiments. Finally, an experiment in an office room is conducted to verify the effectiveness of the proposed ANB in the practical environment.

3.2 Control strategies

This section introduces the control strategies of the proposed ANB system.

3.2.1 Hybrid control

The schematic diagram of the HB control strategy is shown in Fig. 3.1. In the ANB, the diffracting edge of the partition is controlled by an FB controller, and the sound pressure at the control point, which is supposed to be located at the head position of

the target person behind the partition, is controlled by an FF controller simultaneously to improve the noise attenuation performance of the ANB.

The controlled sound pressure at the FB and FF control points, $\boldsymbol{p}_B(\omega)$ and $\boldsymbol{p}_F(\omega)$, shown in Fig. 3.1 can be expressed as

$$\boldsymbol{p}_B(\omega) = \boldsymbol{p}_N(\omega)\boldsymbol{W}_{ref}(\omega) + \boldsymbol{p}_{BC}(\omega)\boldsymbol{G}_B(\omega), \tag{3.1}$$

$$\boldsymbol{p}_F(\omega) = \boldsymbol{p}_N(\omega)\boldsymbol{W}(\omega) + \boldsymbol{p}_{FC}(\omega)\boldsymbol{G}_F(\omega), \tag{3.2}$$

where $\boldsymbol{p}_N(\omega)$ is the sound pressure of the noise source, $\boldsymbol{p}_{BC}(\omega)$ and $\boldsymbol{p}_{FC}(\omega)$ are the control sound pressure at the surface of the FB and FF control sources, $\boldsymbol{W}_{ref}(\omega)$ and $\boldsymbol{W}(\omega)$ are the transfer functions of the acoustic paths from the noise source to the FB and FF control points, $\boldsymbol{G}_B(\omega)$ and $\boldsymbol{G}_F(\omega)$ are the secondary paths from the FB and FF control sources to the control points. Supposing the control performance of the FB and FF control can be expressed as a ratio $\eta(\omega)$ between the residual noise and the primary noise as

$$\boldsymbol{p}_B(\omega) = \eta_B(\omega)\boldsymbol{p}_N(\omega)\boldsymbol{W}_{ref}(\omega), \tag{3.3}$$

$$\boldsymbol{p}_F(\omega) = \eta_F(\omega)\boldsymbol{p}_N(\omega)\boldsymbol{W}(\omega), \tag{3.4}$$

where $|\eta| < 1$, the control sound pressure can be obtained from Eq. (3.1) – Eq. (3.4) as

$$\boldsymbol{p}_{BC}(\omega) = -(1-\eta_B(\omega))\boldsymbol{p}_N(\omega)\frac{\boldsymbol{W}_{ref}(\omega)}{\boldsymbol{G}_B(\omega)}, \tag{3.5}$$

$$\boldsymbol{p}_{FC}(\omega) = -(1-\eta_F(\omega))\boldsymbol{p}_N(\omega)\frac{\boldsymbol{W}(\omega)}{\boldsymbol{G}_F(\omega)}. \tag{3.6}$$

If FB and FF control are conducted simultaneously, the controlled sound pressure at the FF control point $\boldsymbol{p}_{F(HB)}(\omega)$ can be expressed as

$$\boldsymbol{p}_{F(HB)}(\omega) = \boldsymbol{p}_N(\omega)\boldsymbol{W}(\omega) + \boldsymbol{p}_{FC}(\omega)\boldsymbol{G}_F(\omega) + \boldsymbol{p}_{BC}(\omega)\boldsymbol{G}_{BF}(\omega), \tag{3.7}$$

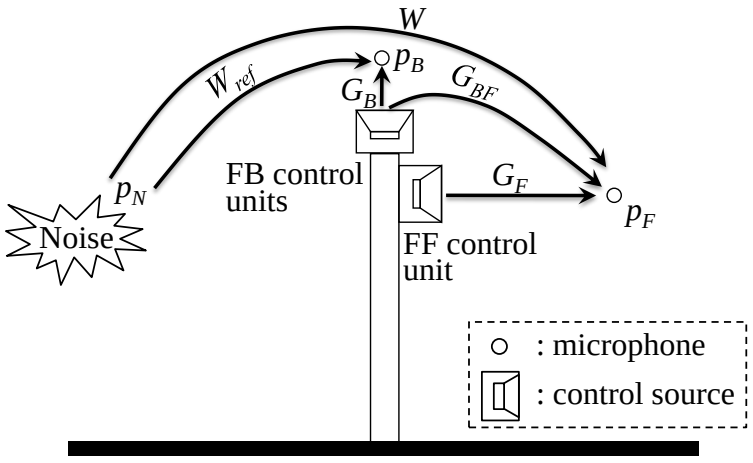

Figure 3.1: Schematic diagram of the hybrid control strategy

where $\boldsymbol{G}_{BF}(\omega)$ is the acoustic path from the FB control source to the FF control point. By substituting $\boldsymbol{p}_{BC}(\omega)$ and $\boldsymbol{p}_{FC}(\omega)$ with Eq. (3.5) and Eq. (3.6), Eq. (3.7) can be rewritten as

$$\boldsymbol{p}_{F(HB)}(\omega) = \eta_F(\omega)\boldsymbol{p}_N(\omega)\boldsymbol{W}(\omega) - (1-\eta_B(\omega))\boldsymbol{p}_N(\omega)\frac{\boldsymbol{W}_{ref}(\omega)\boldsymbol{G}_{BF}(\omega)}{\boldsymbol{G}_B(\omega)}. \tag{3.8}$$

As the distance between the FB control point and the FB control source is very small, it is assumed that the following relations,

$$\boldsymbol{G}_B(\omega) = 1, \tag{3.9}$$

$$\boldsymbol{W}(\omega) = \boldsymbol{W}_{ref}(\omega)\boldsymbol{G}_{BF}(\omega), \tag{3.10}$$

can be established in the free field or in the sound field with low reverberation such as the office room with the sound absorption treatments. Then, Eq. (3.8) can be reduced to

$$\boldsymbol{p}_{F(HB)}(\omega) = (\eta_B(\omega) + \eta_F(\omega) - 1)\boldsymbol{p}_N(\omega)\boldsymbol{W}(\omega). \tag{3.11}$$

Equation (3.11) implies that the performance of the HB control can be expressed as a form of superposition of the FB and FF control results, and higher noise attenuation can be obtained by the HB control strategy if $|\eta_B(\omega)+\eta_F(\omega)-1|$ is smaller than $|\eta_B(\omega)|$ and $|\eta_F(\omega)|$, which means

$$1 - 2\eta_F(\omega) < \eta_B(\omega) < 1. \tag{3.12}$$

This condition also indicates that if the FF control can cancel almost all of the primary noise ($|\eta_F(\omega)| \ll 1$), performing FB control at the same time will increase the noise and reduce the overall control performance. In practice, however, the residual noise must exist and cannot be ignored. Therefore, controlling the diffracting edge and the sound pressure at the control point simultaneously by using the HB control can be an effective strategy to improve the performance of the ANB.

3.2.2 Waterbed effect cancellation

The waterbed effect of the FB controller in the HB-ANC system causes noise amplification. This noise amplification can be seen as a new noise source located at the surface of the FB control source, of which the sound pressure propagates to the control area through the acoustic path $\boldsymbol{G}_{BF}(\omega)$. Actually, a time-advanced reference signal of the noise amplification can be obtained from the signals in the FB controller. Therefore, it is possible to construct an FF controller to cancel the noise amplification in the control area behind the partition even though the noise amplification at the FB control source still exists.

The concept of the noise amplification canceling strategy is shown in Fig. 3.2. By denoting the sound pressure of the noise amplification at the surface of the FB control

source as $\boldsymbol{p}_{WB}(\omega)$ and denoting the control sound pressure as $\boldsymbol{p}_{WBC}(\omega)$, the controlled sound pressure of the noise amplification at the FF control point $\boldsymbol{p}_{F(WB)}(\omega)$ can be expressed as

$$\boldsymbol{p}_{F(WB)}(\omega) = \boldsymbol{p}_{WB}(\omega)\boldsymbol{G}_{BF}(\omega) + \boldsymbol{p}_{WBC}(\omega)\boldsymbol{G}_{F}(\omega). \tag{3.13}$$

Assuming that the ratio of the residual noise is η_{WB}, $\boldsymbol{p}_{WBC}(\omega)$ can be written as

$$\boldsymbol{p}_{WBC}(\omega) = -(1-\eta_{WB})\boldsymbol{p}_{WB}(\omega)\frac{\boldsymbol{G}_{BF}(\omega)}{\boldsymbol{G}_{F}(\omega)}. \tag{3.14}$$

Therefore, if an FF controller to compute and output the control sound pressure in Eq. (3.14) can be built, the noise amplification propagating to the position of the FF control point can be reduced. However, the signal of the pure noise amplification $\boldsymbol{p}_{WB}(\omega)$ cannot be obtained directly. The available signal is the sound pressure of the residual noise at the FB control point $\boldsymbol{p}_{BE}(\omega)$ or the FB control sound pressure $\boldsymbol{p}_{BO}(\omega)$. $\boldsymbol{p}_{BE}(\omega)$ and $\boldsymbol{p}_{BO}(\omega)$ can be expressed as

$$\boldsymbol{p}_{BE}(\omega) = \begin{cases} \boldsymbol{p}_{B}(\omega), & \omega \text{ in the FB control band} \\ \boldsymbol{p}_{WB}(\omega), & \omega \text{ at the other frequencies} \end{cases}, \tag{3.15}$$

$$\boldsymbol{p}_{BO}(\omega) = \begin{cases} \boldsymbol{p}_{BC}(\omega), & \omega \text{ in the FB control band} \\ \boldsymbol{p}_{WB}(\omega), & \omega \text{ at the other frequencies} \end{cases}, \tag{3.16}$$

where $\boldsymbol{p}_{B}(\omega)$ and $\boldsymbol{p}_{BC}(\omega)$ are the components at the frequencies where the waterbed effect does not exist. Both of $\boldsymbol{p}_{BE}(\omega)$ and $\boldsymbol{p}_{BO}(\omega)$ containing the component of $\boldsymbol{p}_{WB}(\omega)$ can be used instead in Eq. (3.14) to calculate the control sound pressure. However, the sound pressure components within the FB control band may reduce the noise attenuation performance. Therefore, in order to decrease the influence of the waterbed effect cancellation part on the FB control performance, the amplitude of the reference signal within the FB control bandwidth should be small. This requirement can be realized by using a band-stop filter. Actually, the residual noise $\boldsymbol{p}_{BE}(\omega)$, which can be expressed as

$$\boldsymbol{p}_{BE}(\omega) = \begin{cases} \eta_{B}(\omega)\boldsymbol{p}_{N}(\omega)\boldsymbol{W}_{ref}(\omega), & \omega \text{ in the FB control band} \\ \boldsymbol{p}_{WB}(\omega), & \omega \text{ at the other frequencies} \end{cases}, \tag{3.17}$$

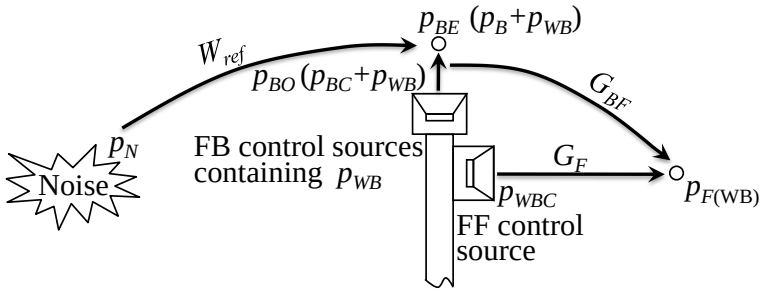

Figure 3.2: Concept of canceling the waterbed effect induced noise amplification

according to Eq. (3.3) and Eq. (3.15), is naturally of small amplitude within the control bandwidth if the FB control is effectively conducted ($|\eta_B(\omega)| \ll 1$). Therefore, using $\boldsymbol{p}_{BE}(\omega)$ as the reference signal can be satisfy the amplitude requirement of the reference signal, which can also save the computation of band-stop filtering. Additionally, as the waterbed effect cancellation is conducted by using FF control, low coherence between the reference signal and the error signal within the control bandwidth can also reduce the performance loss of the FB control. The coherence between $\boldsymbol{p}_{BE}(\omega)$ and the sound pressure signal at the FF control point within the FB control bandwidth will be investigated by simulation in Section 3.4.3.

3.3 System implementation

Figure 3.3 shows the block diagram of the control system to realize the HB control strategy and the waterbed effect cancellation. In the block diagram, $x(n)$ is the noise source signal. $d_B(n)$, $y_B(n)$ and $e_B(n)$ are the noise signal, FB control signal and error signal at the FB control point, respectively. $d_F(n)$, $y_{BF}(n)$, $y_F(n)$ and $e_F(n)$ are the noise signal, FB control signal, FF control signal and error signal at the FF control point, respectively. $\boldsymbol{C}_B(z)$ and $\boldsymbol{C}_F(z)$ are the control filters in the FB and FF controller. $\boldsymbol{C}_W(z)$ is a filter to cancel the noise amplification in the control area caused by the waterbed effect. $\boldsymbol{C}_B(z)$, $\boldsymbol{C}_F(z)$ and $\boldsymbol{C}_W(z)$ are implemented by FIR filters. The superscript $\hat{}$ denotes the estimate of signals and transfer functions of the acoustic paths.

The FB control units are driven by a 5-channel IMC structured FB-ANC system. The five control filters $\boldsymbol{C}_B(z)$s are updated offline respectively by the FX-LMS algorithm, and the filter coefficient constraint determined by the time domain method proposed in Chapter 2 is used in the adaptation process to ensure the robustness of the

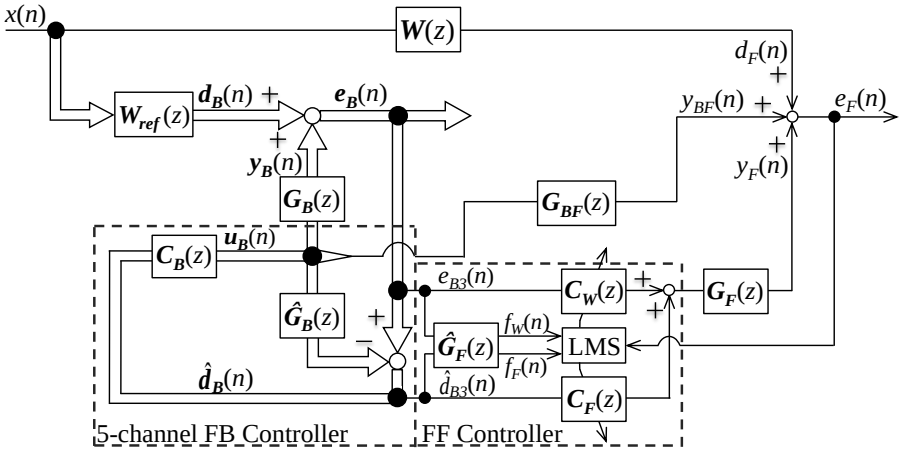

Figure 3.3: Block diagram of the control system

FB control. Only the robust stability condition is considered in the calculation of the filter coefficient constraint because the noise amplification propagating into the control area will be canceled by the filter $\boldsymbol{C}_W(z)$. In the real-time control stage, the FB control filters are applied as fixed filters, and the FB control signal $u_{Bi}(n)$ of the ith channel is calculated as

$$u_{Bi}(n) = \boldsymbol{c}_{Bi}(n)^{\mathrm{T}} \hat{\boldsymbol{d}}_{Bi}(n), \tag{3.18}$$

where

$$\boldsymbol{c}_{Bi}(n) = [c_{Bi1}(n),\ c_{Bi2}(n),\ \ldots,\ c_{BiL}(n)]^{\mathrm{T}}, \tag{3.19}$$

$$\hat{\boldsymbol{d}}_{Bi}(n) = [\hat{d}_{Bi}(n),\ \hat{d}_{Bi}(n-1),\ \ldots,\ \hat{d}_{Bi}(n-L+1)]^{\mathrm{T}}, \tag{3.20}$$

$$\hat{d}_{Bi}(n) = e_{Bi}(n) - \sum_{j=1}^{5} \hat{\boldsymbol{g}}_{Bji}^{\mathrm{T}} \boldsymbol{u}_{Bj}(n), \tag{3.21}$$

$$\hat{\boldsymbol{g}}_{Bi} = [\hat{g}_{Bi1},\ \hat{g}_{Bi2},\ \ldots,\ \hat{g}_{BiL}]^{\mathrm{T}}, \tag{3.22}$$

$$\boldsymbol{u}_{Bi}(n) = [u_{Bi}(n),\ u_{Bi}(n-1),\ \ldots,\ u_{Bi}(n-L+1)]^{\mathrm{T}}, \tag{3.23}$$

$\boldsymbol{c}_{Bi}(n)$ is the FIR filter coefficients of the ith FB control filter, $\hat{\boldsymbol{d}}_{Bi}(n)$ is the time series of the estimated primary noise signal at the ith FB control point, $e_{Bi}(n)$ is the error signal of the ith FB control unit, $\hat{\boldsymbol{g}}_{Bji}$ is a FIR filter expressing the impulse response of the acoustic path from the jth FB control source to the ith control point, $\boldsymbol{u}_{Bi}(n)$ is the time series of the control signal of the ith FB control source, and L denotes the filter length. In Eq. (3.21), the acoustic feedback path from the FF control source to the FB control point is not taken into the calculation of $d_{Bi}(n)$. In comparison with the distance from the FB control source to the FB control point, that from the FF control source to the FB control point is larger so that the distance attenuation effect is also larger. In addition, even though the FF control source is not a directional loudspeaker, the sound power emitted to the back of the loudspeaker is smaller than that to the front. Accordingly, it can be considered that the effect of the acoustic feedback is small to be ignored.

The single channel FF controller is composed of two control filters, $\boldsymbol{C}_F(z)$ to cancel the primary noise and $\boldsymbol{C}_W(z)$ to cancel the noise amplification from the FB control source. $\boldsymbol{C}_F(z)$ applies the estimated primary noise signal at the center FB control point (The configuration of the control devices is shown in Fig. 3.4.) $\hat{d}_{B3}(n)$ as the reference signal, and $\boldsymbol{C}_W(z)$ applies the error signal of the center FB control unit $e_{B3}(n)$ as the reference signal. Both of the signals $\hat{d}_{B3}(n)$ and $e_{B3}(n)$ are obtained from the FB controller so that a reference sensor for the FF controller is not required. In order to obtain a reference signal of high coherence with the sound pressure signal at the FF control point, the estimated primary noise signal at the FB control point that is on the straight line connecting the noise source and the FF control point should be used. As

the position of the FF control point is fixed, it is possible to select an appropriate FB control unit to obtain the reference signal in the real-time control stage by estimating the noise incident angle using a noise source detection algorithm such as the method in Ref. [149]. In the investigations of this thesis, the primary noise source is located on the center line of the ANB so that the signals of the center FB control unit is used. $\boldsymbol{C}_F(z)$ and $\boldsymbol{C}_W(z)$ are updated in sequence by FX-LMS algorithm in the initialization stage of the system, and used as fixed filters during the real-time control. An error sensor located at the control point is necessary for the filter coefficients adaptation, whereas the error sensor can be removed once the adaptation is done. Therefore, in the real-time control stage, it is unnecessary to locate any control devices in the workplace. The FF control filters are updated as

$$\boldsymbol{c}_F(n+1) = \boldsymbol{c}_F(n) - \mu e_F(n)\boldsymbol{f}_F(n), \tag{3.24}$$

$$\boldsymbol{c}_W(n+1) = \boldsymbol{c}_W(n) - \mu e_F(n)\boldsymbol{f}_W(n), \tag{3.25}$$

where

$$\boldsymbol{c}_F(n) = [c_{F1}(n),\ c_{F2}(n),\ \ldots,\ c_{FL}(n)]^{\mathrm{T}}, \tag{3.26}$$

$$\boldsymbol{c}_W(n) = [c_{W1}(n),\ c_{W2}(n),\ \ldots,\ c_{WL}(n)]^{\mathrm{T}}, \tag{3.27}$$

$$\boldsymbol{f}_F(n) = [f_F(n),\ f_F(n-1),\ \ldots,\ f_F(n-L+1)]^{\mathrm{T}}, \tag{3.28}$$

$$\boldsymbol{f}_W(n) = [f_W(n),\ f_W(n-1),\ \ldots,\ f_W(n-L+1)]^{\mathrm{T}}, \tag{3.29}$$

$$f_F(n) = \hat{\boldsymbol{g}}_F^{\mathrm{T}}\hat{\boldsymbol{d}}_{B3}(n), \tag{3.30}$$

$$f_W(n) = \hat{\boldsymbol{g}}_F^{\mathrm{T}}\boldsymbol{e}_{B3}(n), \tag{3.31}$$

$$\hat{\boldsymbol{g}}_F = [\hat{g}_{F1},\ \hat{g}_{F2},\ \ldots,\ \hat{g}_{FL}]^{\mathrm{T}}, \tag{3.32}$$

$$\boldsymbol{e}_{B3}(n) = [e_{B3}(n),\ e_{B3}(n-1),\ \ldots,\ e_{B3}(n-L+1)]^{\mathrm{T}}, \tag{3.33}$$

$\boldsymbol{c}_F(n)$ and $\boldsymbol{c}_W(n)$ are FF control filter coefficients, $\hat{\boldsymbol{g}}_F$ is a FIR filter expressing the impulse response of the secondary path from the FF control source to the control point, $\boldsymbol{f}_F(n)$ and $\boldsymbol{f}_W(n)$ are the time series of the secondary path model filtered reference signals, $\boldsymbol{e}_{B3}(n)$ is the time series of the error signal of the center FB control unit, and μ is the step-size parameter of which the value is determined by trial and error to guarantee the optimal control performance. The FF control signal is calculated by adding the output of $\boldsymbol{C}_F(z)$ and $\boldsymbol{C}_W(z)$ as

$$u_F(n) = \boldsymbol{c}_F(n)^{\mathrm{T}}\hat{\boldsymbol{d}}_{B3}(n) + \boldsymbol{c}_W(n)^{\mathrm{T}}\boldsymbol{e}_{B3}(n). \tag{3.34}$$

3.4 Simulation investigations of the system performance in different sound field configurations

In this section, a prototype ANB using the proposed HB-ANC system is developed, and several computer simulations are conducted to investigate the noise attenuation

performance of the ANB.

3.4.1 Simulation conditions

Figure 3.4 shows the simulation configuration. The prototype ANB consists of an office partition (1280×1024 mm), five sets of loudspeakers and microphones as the FB control units placed on the top of the partition, and a loudspeaker as the FF control source placed on the back of the partition. The distance between the FB control points is 200 mm. In order to investigate the influence of the diffraction from side of the ANB and the sound reflection on the ANB performance, four sound field configurations are set up by placing partition 1 (900×1500 mm), partition 2 (2400×1800 mm), and partition 3 (1200×1200 mm) at position 1 , position 2, and position 3. The ANB is located next to the wall of the anechoic chamber, and the sound diffraction from the acoustic material side is much smaller than the other side. The arrangement of the partitions, existence of the side diffraction, and existence of the sound reflection in these configurations are concluded in Table 3.1. Configuration 1 is for investigating the noise attenuation performance of the ANB in the sound field where neither the diffraction from side nor the reflection exists. In configuration 2, the reflection exists on one side in the control area. Configuration 3 is for investigating the noise attenuation performance in the sound field where the diffraction from side exists, but there is no sound reflection. Configuration 4 is for investigating the noise attenuation performance where both the side diffraction and the reflection exist.

The noise attenuation provided by the ANB for each configuration is calculated in the 600×600 mm measurement area behind the ANB where the measurement points are set at intervals of 100 mm. The noise attenuation at the six points around the control point depicted as black dots (•) in Fig. 3.4 will be especially concerned as this area is supposed to be the head position of the listener.

The simulations are performed according to the block diagram shown in Fig. 3.3. The acoustic paths used in the simulations are expressed as 2048-tap FIR filters, which are identified in the anechoic chamber for each configuration in advance. The FB and FF control filters are 128-tap FIR filters for configuration 1 and 3, and 256-tap FIR filters for configuration 2 and 4 where the reverberation time is longer because of the existence of the sound reflection. The primary noise is white noise. The sampling frequency of the control system is set as 20 kHz. The FB control filters designed for configuration 3 are applied to all of the four configurations by assuming that the setup of partition 1, 2, and 3 hardly influences the secondary path of the FB controller because the distance between the error microphone and the FB control source is very small. The control filters in the FF controller are identified respectively for each configuration. The crosstalk paths among the FB controllers and the FF controller are not considered in the simulations.

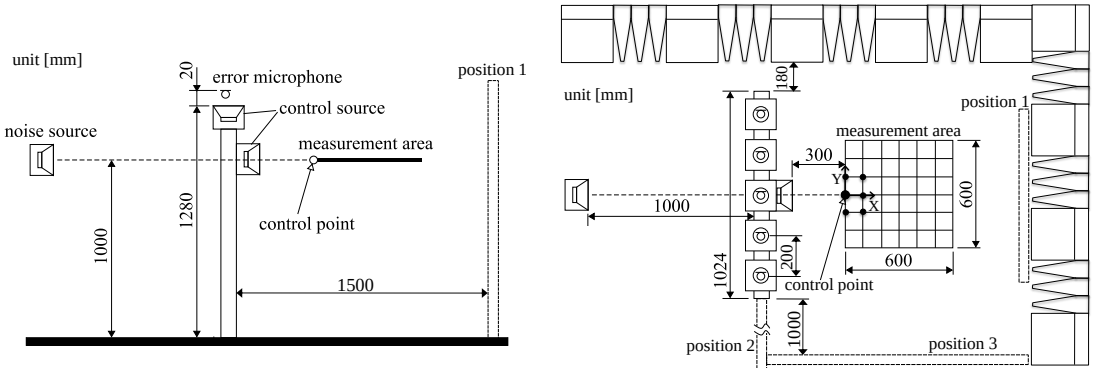

(a) Side view

(b) Top view

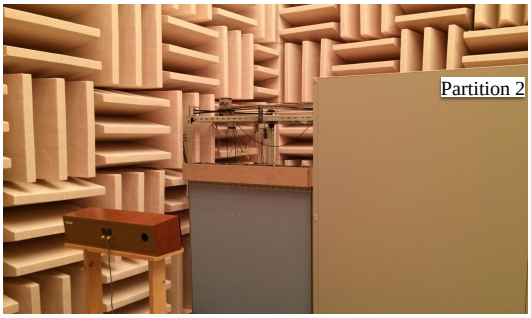

(c) Configuration 1

(d) Configuration 2

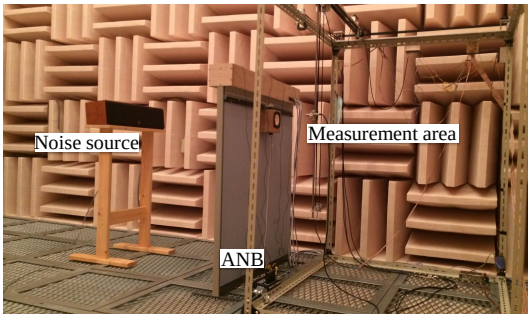

(e) Configuration 3

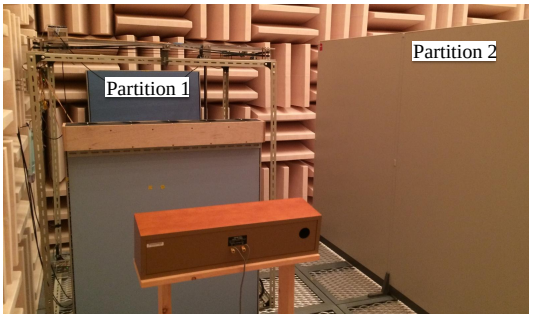

(f) Configuration 4

Figure 3.4: Sound field configurations

Table 3.1: Sound field configurations

	Arrangement of the partitions			Side diffraction	Reflection
	Position 1	Position 2	Position 3		
Configuration 1	–	Partition 2	–	No	No
Configuration 2	–	Partition 2	Partition 3	No	Yes
Configuration 3	–	–	–	Yes	No
Configuration 4	Partition 1	–	Partition 2	Yes	Yes

3.4.2 Feedback controller design

In the offline design process of the FB control filters, the target band of control should be decided firstly. The lower bound of the target band is set as 200 Hz 1/3 octave band due to the frequency response limitation of the loudspeakers used as the control sources. The upper bound is set as 630 Hz 1/3 octave band according to the results of the preceding study [98], in which it has been confirmed that the FB controllers set on the top of the ANB provide active noise attenuation more effectively at lower frequencies. In addition, the upper bound is also determined by considering that the distance between the control points (200 mm) should be shorter than the half-wavelength at the highest frequency of interest (about 240 mm at 708 Hz) to avoid the spatial aliasing [73]. In the design process of the time domain method described in Chapter 2, the primary noise signal for the filter coefficient calculation applies the FB control bandwidth limited white noise ([178, 708] Hz), and the secondary path model applies the one of configuration 3. The calculated FB control filter is shown in Fig. 3.5. In the real-time control stage, this filter is used as the fixed filter so that the designed noise attenuation performance can be realized regardless of the properties of the primary noise.

3.4.3 Validation of the reference signals for the feedforward controller

The appropriateness of using the FB output and error signal as the reference signal of the noise amplification canceling filter $\boldsymbol{C}_W(z)$ is investigated according to the discussion in Section 3.2.2. Figure 3.6(a) compares the amplitude of the FB control output and error signal. Figure 3.6(b) compares the coherence between the HB control error signal and the FB control output and error signal, respectively. Within the target band of FB control, the amplitude of the FB error signal is smaller, and the FB error signal is also less coherent with the HB error signal in comparison with the FB control output signal. Therefore, using the error signal of the FB control as the reference signal of

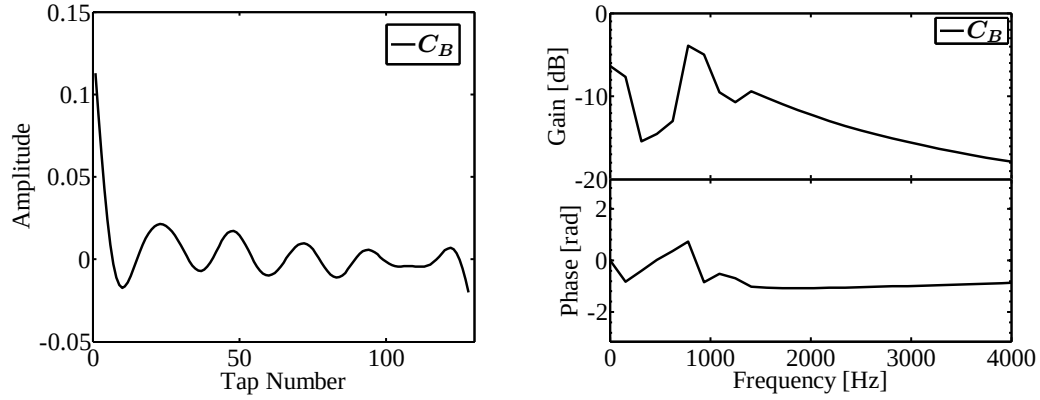

(a) Filter coefficients

(b) Frequency properties

Figure 3.5: FB control filter $\boldsymbol{C}_B$

the filter $\boldsymbol{C}_W(z)$ has less influence on the noise attenuation performance within the FB control bandwidth. At the frequencies where the waterbed effect exists, the FB error and output signal has the similar amplitude and coherence with the HB control error signal. Therefore, both of two signals contains the waterbed effect components and can be an effective reference signal to cancel the waterbed effect induced noise amplification. By considering the above two aspects, the FB error signal is more appropriate to be applied as the reference signal of the noise amplification canceling filter $\boldsymbol{C}_W(z)$.

3.4.4 Noise attenuation at the control points

The noise attenuation at the FB and FF control points for the representative configuration 3 is calculated to confirm the performance of the designed FB control filters and the effectiveness of the proposed HB-ANC system with waterbed effect cancellation.

Figure 3.7 shows the 1/3 octave band SPL before and after control at the center FB control point and the FF control point. At the FB control point, the noise is reduced within the target band of control, whereas the waterbed effect causes noise amplification at other frequencies. Especially, at the 800 Hz and 1 kHz 1/3 octave band, the noise

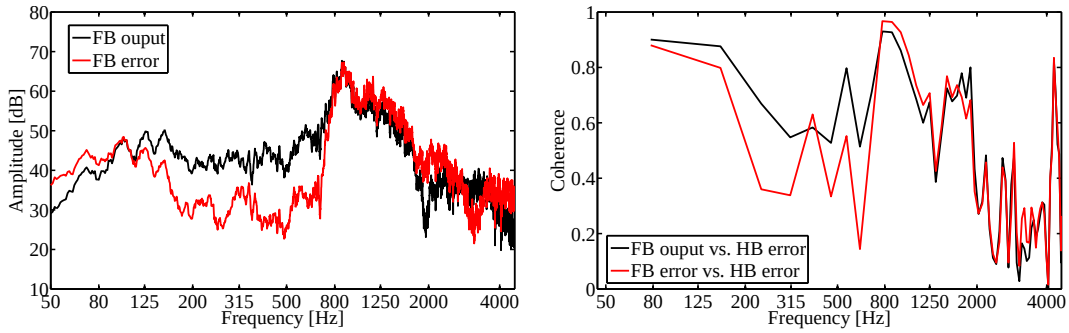

(a) Amplitude (b) Coherence

Figure 3.6: A comparison of using the FB error and output signal as the reference signal of the filter to cancel the waterbed effect induced noise amplification

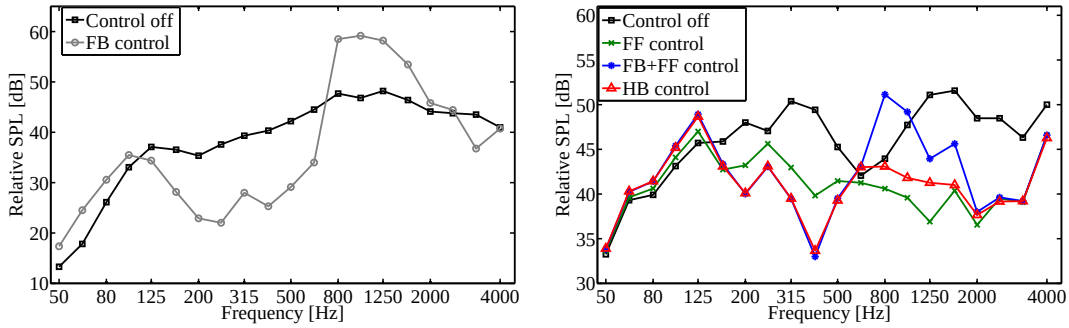

(a) At the center FB control point (b) At the FF control point

Figure 3.7: 1/3 octave band SPL at control points for configuration 3

amplification is more obvious and will propagate to the control area behind the ANB. In the FF control point result shown in Fig. 3.7(b), the performance of the FF control, the simple combination of FF and FB control without waterbed effect cancellation, and the proposed HB control are compared. The FF control applies the microphone of the center FB control unit as the reference sensor. Within the target band of the FB control from 200 Hz to 630 Hz 1/3 octave band, the noise attenuation provided by the FB and FF control superpose so the combination of FF and FB control and the HB control can obtain higher noise attenuation than the FF control. At the frequencies where the waterbed effect of the FB control exists, the HB control with waterbed effect cancellation can reduce it and achieve better noise attenuation performance than the simple combination of FF and FB control. These results validate the effectiveness of the proposed control strategies.

However, at the frequencies where the waterbed effect exists, the noise attenuation provided by the HB control is about 3 dB less than that of the FF control. This is because only the signal of the center FB control unit is used to cancel the noise amplification caused by the waterbed effect so that the noise amplification from the other four FB control units cannot be reduced sufficiently. Figure 3.8 shows the control results of the HB-ANC system using five $\boldsymbol{C}_W(z)$s to cancel the noise amplification from all of the five FB control units. From the results, it can be confirmed that using five $\boldsymbol{C}_W(z)$s can improve the noise amplification cancellation performance. Nevertheless, adding extra filters will increase the computational complexity of the control algorithm so that the real-time implementation of the control system may become difficult. Therefore, in this thesis, only one $\boldsymbol{C}_W(z)$ is used in the HB-ANC system.

3.4.5 Noise attenuation in the control area

The noise attenuation in the measurement area for each sound field configuration is calculated to verify the effectiveness of the ANB. The noise attenuation is defined as

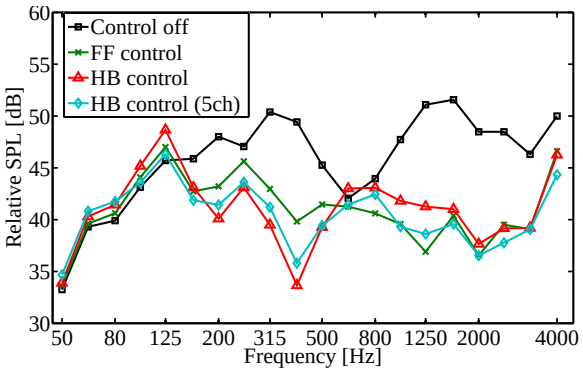

Figure 3.8: A comparison of the performance of FF control, HB control with one $\boldsymbol{C}_W(z)$ and HB control with five $\boldsymbol{C}_W(z)$s

the difference between the SPL before and after control.

First, the performance of the proposed HB control and the conventional control systems is compared to verify the effectiveness of the HB control. Figure 3.9 – Figure 3.12 compares the noise attenuation contours resulted by the FB control, FF control, simple combination of the FB and FF control, and HB control under configuration 3. The results of four 1/3 octave bands, 250 Hz and 500 Hz 1/3 octave band within the FB control bandwidth, 1 kHz 1/3 octave band where the waterbed effect is obvious, and 2 kHz 1/3 octave band apart from the FB control bandwidth, are shown in Fig. 3.9 – Fig. 3.12. Within the FB control bandwidth, the combination of the FB and FF control and the HB control achieves larger noise attenuation in the measurement area behind the ANB than the FB or FF control. Within the 1 kHz 1/3 octave band where the waterbed effect exists, even though the noise attenuation provided by the HB control is smaller than the FF control, the HB control can reduce the noise amplification effectively so that better performance is achieved comparing with the simple combination of the FF and FB control. Especially, the HB control obtains about 5 dB noise attenuation around the control point that is supposed to be the head position of the listener. Within the 2 kHz 1/3 octave band, the HB control performs similarly with the FF control because the FB control has little influence on the control effect. The above results demonstrate that the proposed HB control can improve the noise attenuation performance of the ANB within the FB control bandwidth at low frequencies not only at the control point but in the overall 600mm×600mm measurement area.

The next simulation investigates the influence of the different sound configurations on the ANB performance. Figure 3.13 – Figure 3.16 depict the noise attenuation contours in the measurement area of the representative 250 Hz, 500 Hz, 1 kHz, 2 kHz 1/3 octave band for the four sound field configurations. The effectiveness of the HB control has been confirmed previously, and therefore, only the HB control is investigated in this simulation. Figure 3.13 indicates that high noise attenuation can be achieved in a wide area if there is little diffraction from side and little reflection. Figure 3.14 shows the results for configuration 2. In comparison with configuration 1, a reflector is located on one side of the control area in configuration 2. It is noteworthy that the low frequency noise attenuation deteriorates on the side where the reflector exists, but less influence of the side reflector is found at high frequencies, of which the acoustic wavelength is shorter and the sound wave propagation is more directional. Figure 3.15 shows the results for configuration 3 where only the side diffraction exists. It can be found that the diffraction from side has more negative influence at the low frequencies, of which the wavelength is long enough in comparison with the size of the ANB to diffract from it. The results for configuration 4, in which the side diffraction, and the reflection from the side reflector and from the reflector placed at the propagation direction of the primary noise and the control sound exist, are shown in Fig. 3.16.

The results indicate that the noise attenuation deteriorates due to the side diffraction and the side reflector at low frequencies, and at high frequencies, the reflector located at the propagation direction of the primary noise and the control sound causes the performance deterioration at the positions away from the control point.

Additionally, even in configuration 1 where there is little side diffraction and little sound reflection, the noise attenuation distribution at low frequencies is not symmetric. This is because the sound field condition is also asymmetric in configuration 1 as shown in Fig. 3.4. Although the ANB is located next to the wall of the anechoic chamber, the acoustic material cannot absorb all of the low frequency noise so that the diffraction from this side also exists. However, the diffraction from the acoustic material side is much smaller than the diffraction from the other side that is objective to be investigated in the simulations, and therefore, it does not affect the correctness of the discussion based on the above simulation results.

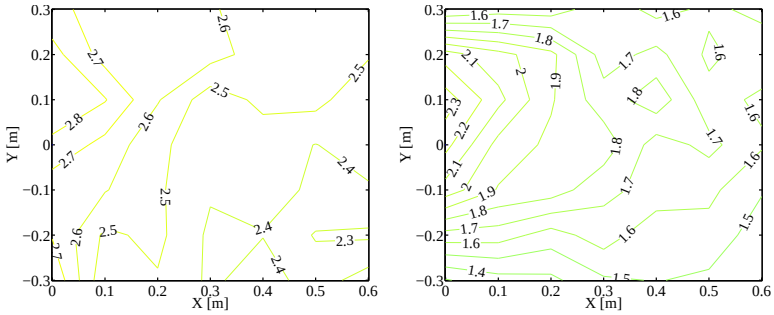

(a) FB control (b) FF control

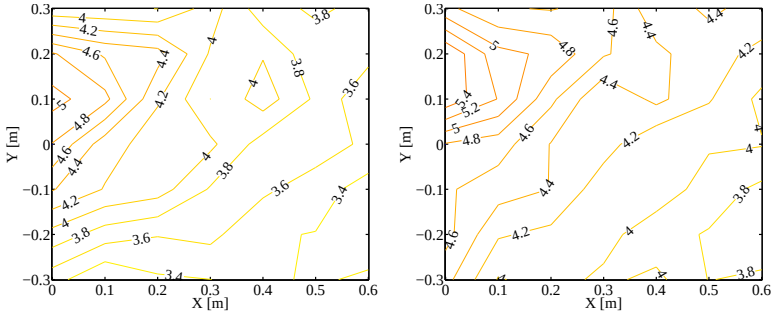

(c) FB+FF control (d) HB control

Figure 3.9: Noise attenuation [dB] at the 250 Hz 1/3 octave band

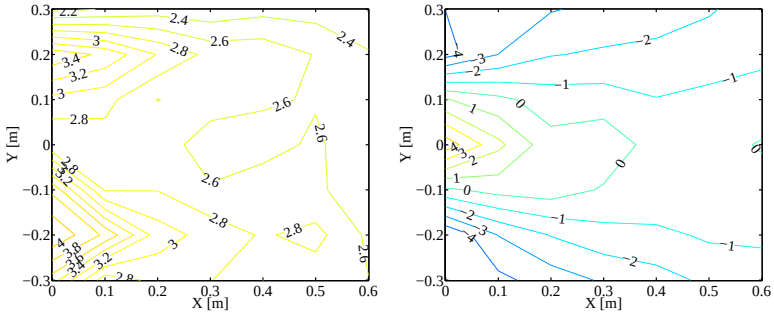

(a) FB control (b) FF control

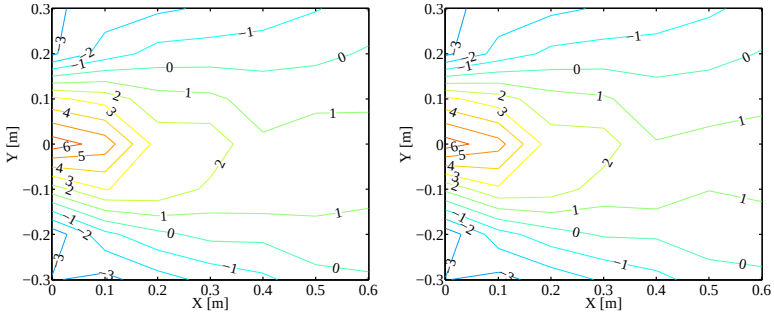

(c) FB+FF control (d) HB control

Figure 3.10: Noise attenuation [dB] at the 500 Hz 1/3 octave band

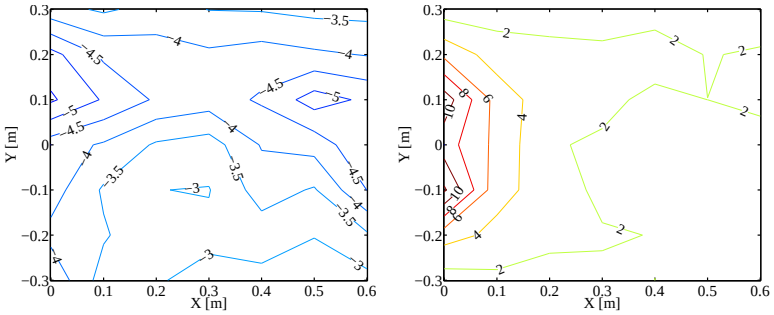

(a) FB control (b) FF control

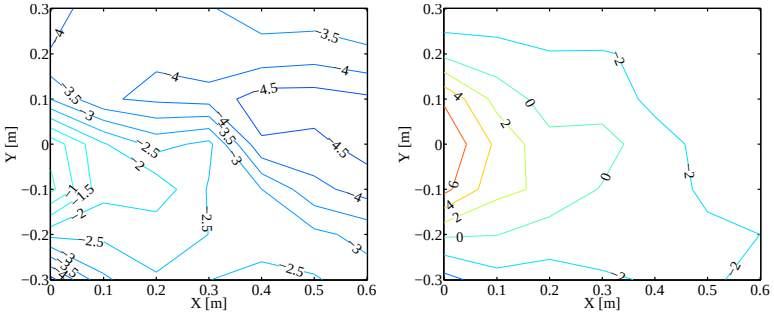

(c) FB+FF control (d) HB control

Figure 3.11: Noise attenuation [dB] at the 1 kHz 1/3 octave band

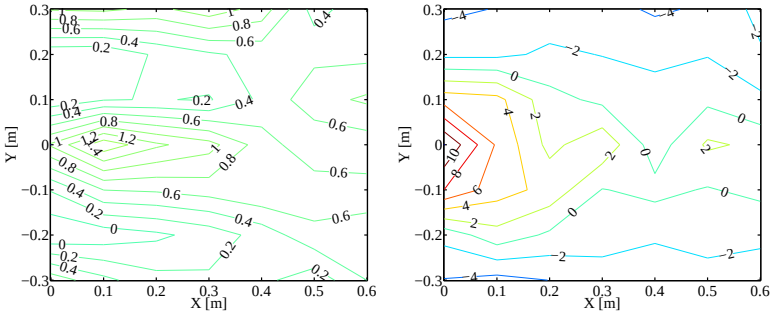

(a) FB control (b) FF control

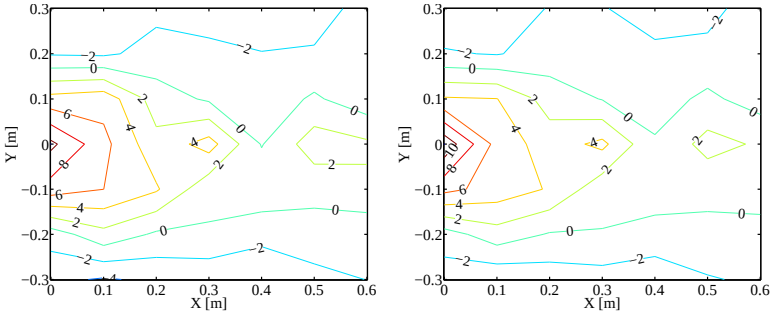

(c) FB+FF control (d) HB control

Figure 3.12: Noise attenuation [dB] at the 2 kHz 1/3 octave band

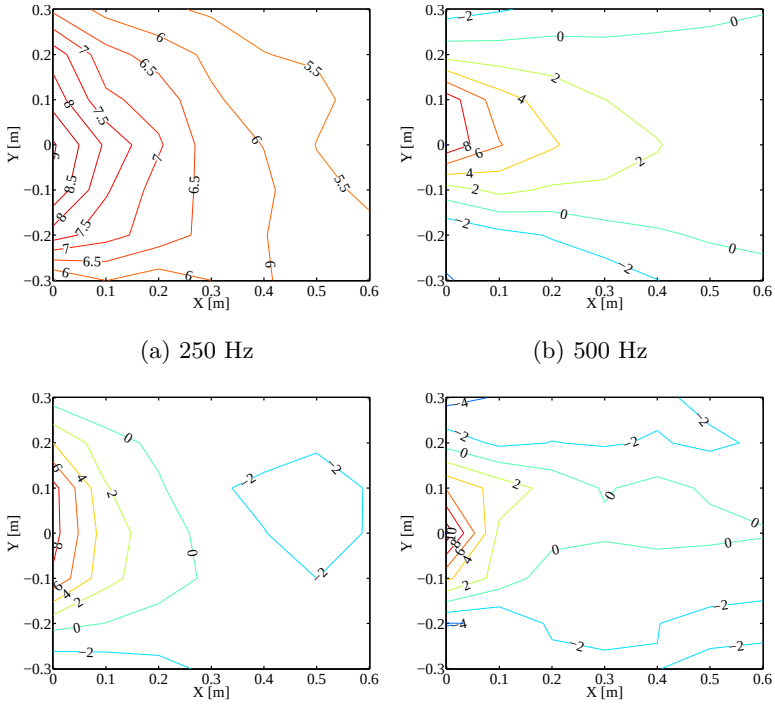

(a) 250 Hz (b) 500 Hz

(c) 1 kHz (d) 2 kHz

Figure 3.13: Noise attenuation [dB] provided by the HB control for configuration 1

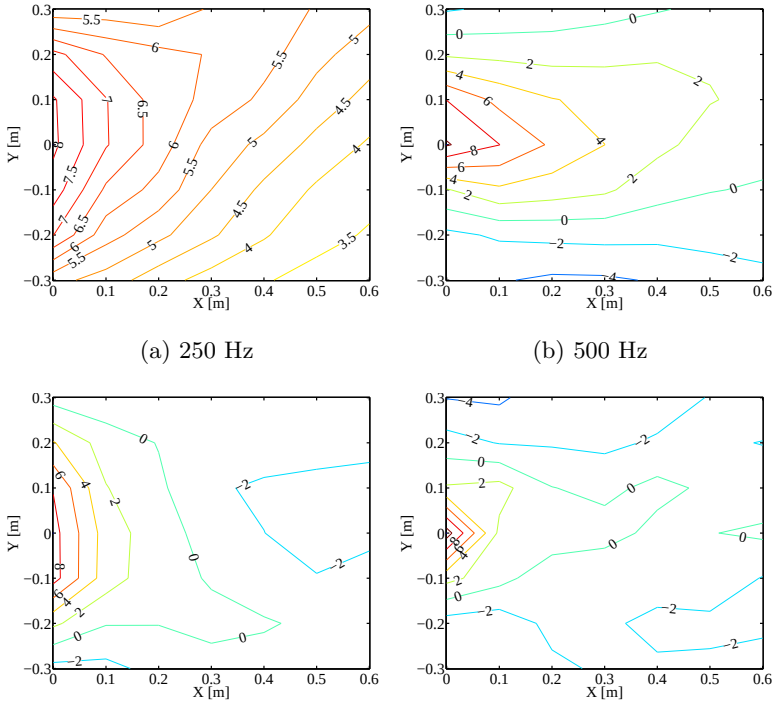

(a) 250 Hz (b) 500 Hz

(c) 1 kHz (d) 2 kHz

Figure 3.14: Noise attenuation [dB] provided by the HB control for configuration 2

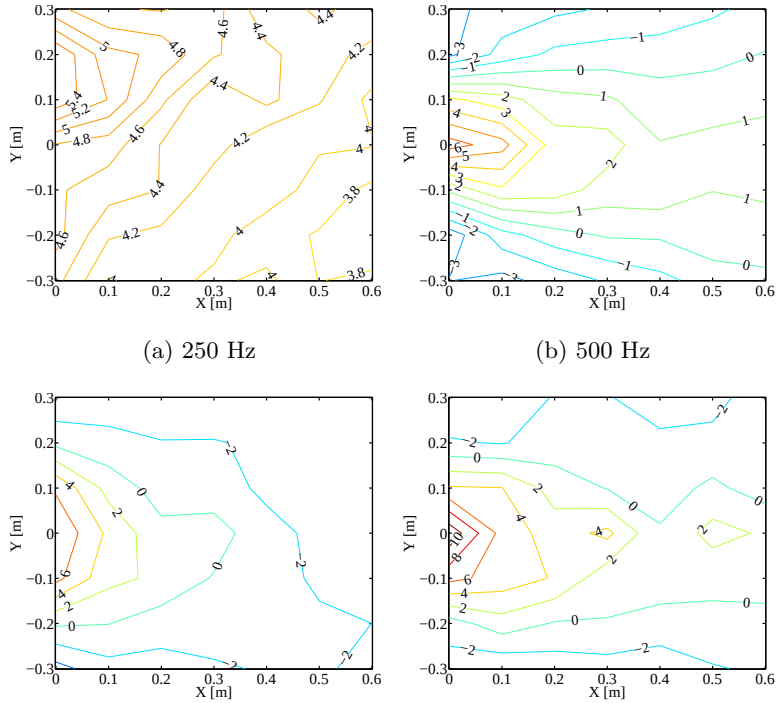

(a) 250 Hz (b) 500 Hz

(c) 1 kHz (d) 2 kHz

Figure 3.15: Noise attenuation [dB] provided by the HB control for configuration 3

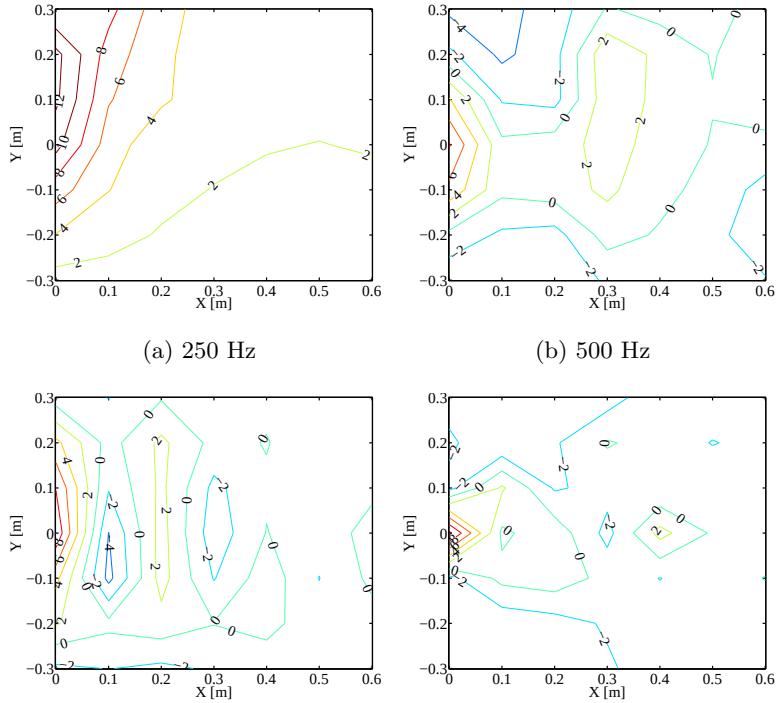

(a) 250 Hz (b) 500 Hz

(c) 1 kHz (d) 2 kHz

Figure 3.16: Noise attenuation [dB] provided by the HB control for configuration 4

As for the head position of the listener, the average noise attenuation of the six points around the control point is calculated and shown in Fig. 3.17. The result indicates the ANB performs better under configuration 1, in which there are little side diffraction and little sound reflection, generally. At low frequencies, the noise attenuation around the control point reduces under configuration 3 where the largest diffraction from side exists. This is also because the side diffraction abates the coherence between the reference signal of the FF control, which is the signal of the noise diffracted from the top of the ANB, and the noise signal at the control point. This will deteriorate the noise attenuation performance of the FF control part itself. At high frequencies, the ANB performs worse under configuration 4 where both of the side diffraction and the sound reflection exist. However, about 2 dB noise attenuation can be still obtained within the 1 kHz and 2 kHz 1/3 octave band.

The above simulation results reveal that the ANB is most effective for the sound field where there is little diffraction from side and little reflection. For other three sound fields, even though the diffraction from side and the reflection lead to the spatial non-uniformity and deterioration of the noise attenuation, the low frequency noise attenuation can be achieved in a wide area behind the ANB, and noise attenuation for a wide frequency range can be ensured around the control point.

3.4.6 Experimental verification of the reliability of the simulations

A real-time experiment in the anechoic chamber is conducted under the representative configuration 3 in order to verify the correctness of the simulation results. Configuration 3 is adopted because of its simplicity.

The HB-ANC system is implemented on a DSP with a TMS 320C6713 DSK chip. The control filters are 128-tap FIR filters, and the secondary path models apply 512-tap FIR filters. The primary noise is white noise. The sampling frequency is set as 20 kHz for the FB controllers and 10 kHz for the FF controller. The FF controller applies the estimated the primary noise signal and the error signal at the center FB

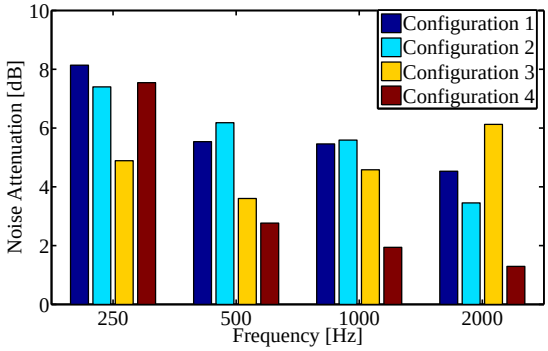

Figure 3.17: Average noise attenuation of the six measurement points around the control point

control point as the reference signals of the primary noise control filter $\boldsymbol{C}_F(z)$ and the waterbed effect cancellation filter $\boldsymbol{C}_W(z)$, respectively. The crosstalk among the FB controllers is canceled internal the system.

Figure 3.18 depicts the experiment results of the 1/3 octave band SPL before and after control at the center FB control point and the FF control point. The results indicate that the HB control can provide higher noise attenuation at low frequencies, and cancel the noise amplification effectively at the frequencies where the waterbed

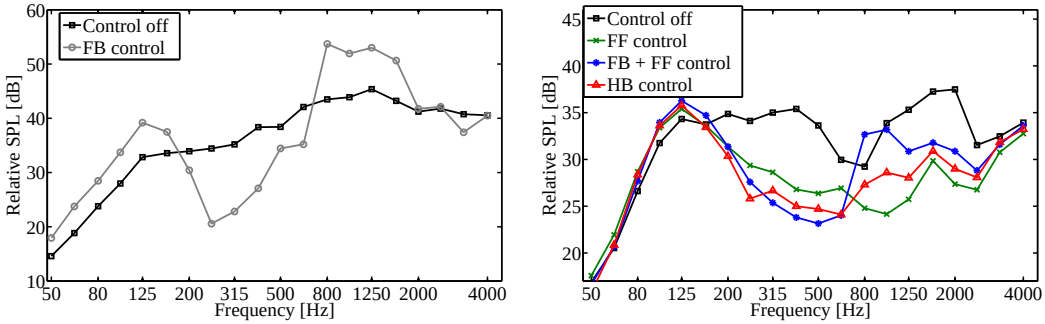

(a) at the center FB control point (b) at the FF control point

Figure 3.18: 1/3 octave band SPL at control points for configuration 3 (Experiment result)

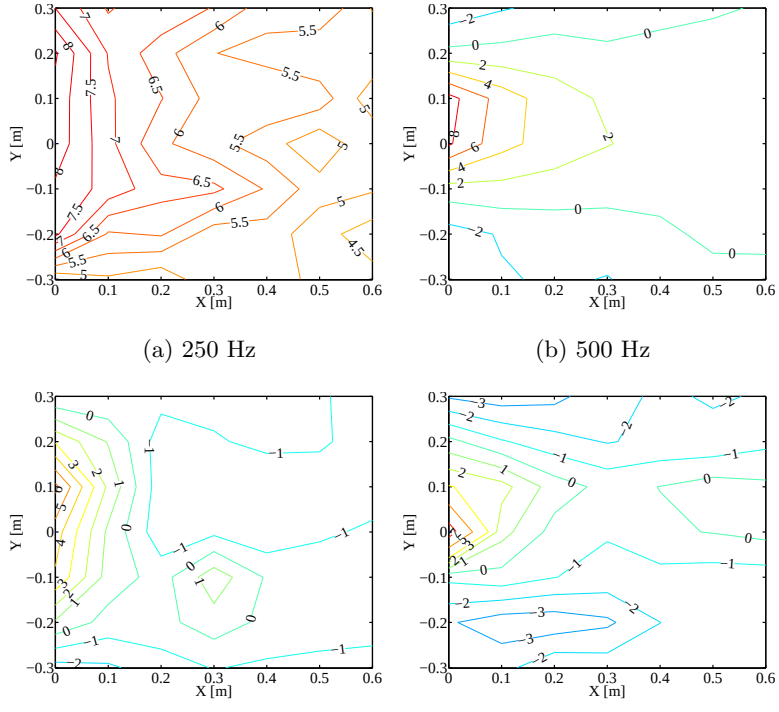

(a) 250 Hz (b) 500 Hz

(c) 1 kHz (d) 2 kHz

Figure 3.19: Noise attenuation [dB] provided by the HB control for configuration 3 (Experiment result)

effect exists. Figure 3.19 shows the noise attenuation in the measurement area. The experiment results accord with the simulation results well that validates the simulation investigations.

3.5 Experiment in an office room

This section presents a real-time experiment in an office room to verify the noise attenuation performance of the ANB for practical application.

3.5.1 Experimental conditions

The experiment is conducted in an L9000 × W5500 × H2600 mm office room with the reverberation time T60 of 0.42 that is measured according to JIS A 1417 : 2000 [150]. The experimental configuration is shown in Fig. 3.20. In order to investigate the influence of the background noise on the noise attenuation performance of the ANB, a loudspeaker located on the control area side outputs pink noise, which is used to simulate the environment noise, to adjust the background noise level. The noise

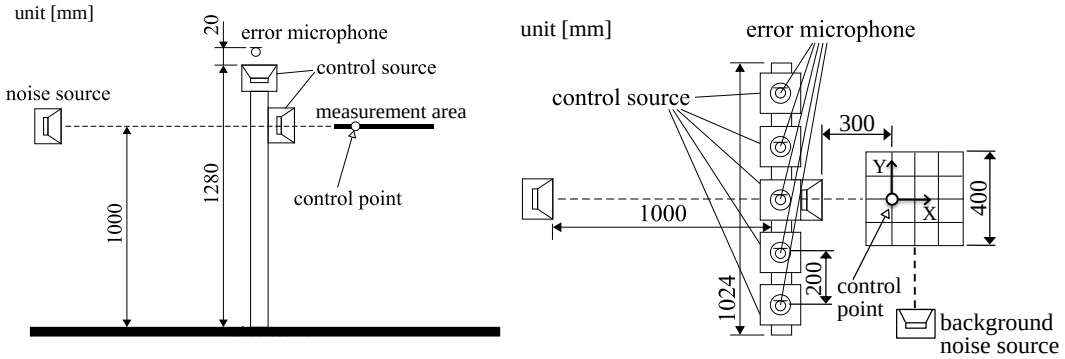

(a) Side view

(b) Top view

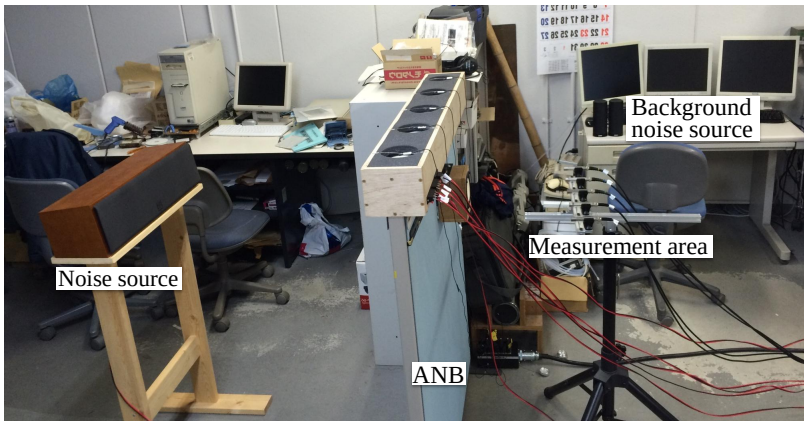

(c) A picture of the experiment configuration in an office room

Figure 3.20: Experiment configuration

attenuation in the measurement area provided by the ANB is calculated based on the measured sound pressure before and after control at the measurement points.

The HB-ANC system is implemented on a DSP with a TMS 320C6713 DSK chip. The FB control filters are 128-tap FIR filters. The target band of the FB control is set as from 200 Hz to 630 Hz 1/3 octave band that is same with the bandwidth in the simulations.The time domain method in Chapter 2 is used to design the FB control filters, and only the robust stability condition is considered in the design process. The FF control filters apply 512-tap FIR filters. The sampling frequency is set as 20 kHz for the FB controller and 10 kHz for the FF controller. The primary noise applies white noise.

3.5.2 Noise attenuation at the control points

The SPL at the FB and FF control points before and after control are calculated to confirm the performance of the offline designed FB control filters and the effectiveness of the HB-ANC system to cancel the primary noise and the noise amplification caused by the FB control at the FF control point.

Figure 3.21 depicts the 1/3 octave band SPL before and after control at the center FB control point and the FF control point. At the FB control point, about 10 dB noise attenuation is achieved by the offline designed FB control filters within the control band. However, the waterbed effect induces noise amplification at other frequencies, which will also propagate to the control area behind the partition. In the result at the FF control point, the performance of the FF control, the simple combination of FF and FB control without noise amplification cancellation, and the HB control are compared. Within the FB control band, both of the simple combination of FF and FB control and the HB control can obtain higher noise attenuation than the FF control due to the superposition of the two noise attenuations provided by the FB and FF control. At the frequencies where the waterbed effect exists, the HB control can cancel the

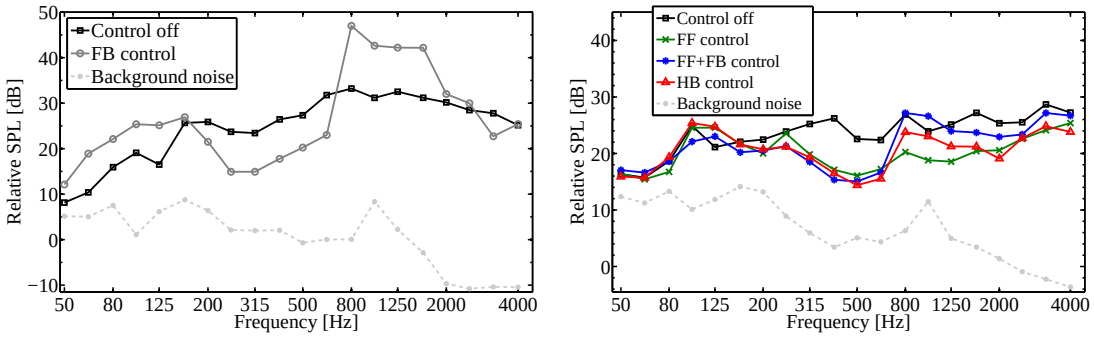

(a) At the center FB control point

(b) At the FF control point

Figure 3.21: 1/3 octave band SPL at the control points

noise amplification and achieve about 4 dB higher noise attenuation than the simple combination of FF and FB control. The above results indicate that the proposed HB control can achieve higher noise attenuation within the target band of the FB control, and can effectively reduce the noise amplification propagating to the control area.

3.5.3 Noise attenuation in the control area

The noise attenuation, which is the difference of the SPL before and after control, in the measurement area provided by the FF control, the FB control, the simple combination of FF and FB control, and the HB control are calculated and compared.

The noise attenuation contours for 250 Hz and 500 Hz 1/3 octave bands within the FB control band, 800 Hz 1/3 octave band where the waterbed effect exists, and 4 kHz 1/3 octave band apart from the FB control band are depicted in Fig. 3.22 – Fig. 3.25. Within the FB control band, the superposition of the noise attenuations provided by the FB and FF control can be obtained not only at the FF control point but also the other points in the control area, and therefore, the HB control obtains larger noise attenuation than the FB or FF control in a wide area behind the partition. Within the 800 Hz 1/3 octave band, in comparison with the FB control and the simple combination of FB and FF control, which lead to the amplification of the primary noise in the control area due to the waterbed effect, the HB control can cancel the noise amplification in the control area and achieve about 3 dB noise attenuation around the control point. At higher frequencies, such as the 4 kHz 1/3 octave band, the FB control has little influence so that the HB control performs similarly with the FF control. The above results validate the effectiveness of the HB control and show that the proposed ANB system can obtain 3 – 8 dB noise attenuation in the sound field of a real office room.

3.5.4 Influence of the background noise on the system performance

In order to investigate the influence of the background noise on the noise attenuation performance of the ANB, in addition to the original background noise (BGN 0), other two background noises numbered 1 and 2 (BGN 1 and 2) are considered in the experiment. BGN 1 and BGN 2 are composed of the original background noise and the pink noise of different power output from the background noise source shown in Fig. 3.20. The noise attenuation performance at the center FB control point and the FF control point in the control area behind the ANB are investigated.

The 1/3 octave band SPL of the primary noise and the background noises are shown in Fig. 3.26. At the center FB control point, the primary noise signal to background noise ratio (SNR) is 22 dB, 20 dB and 19 dB for BGN 0, BGN 1 and BGN 2, respectively. At the FF control point, the SNR is 11 dB, 9 dB and 8 dB for BGN 0, BGN 1 and BGN 2, respectively.

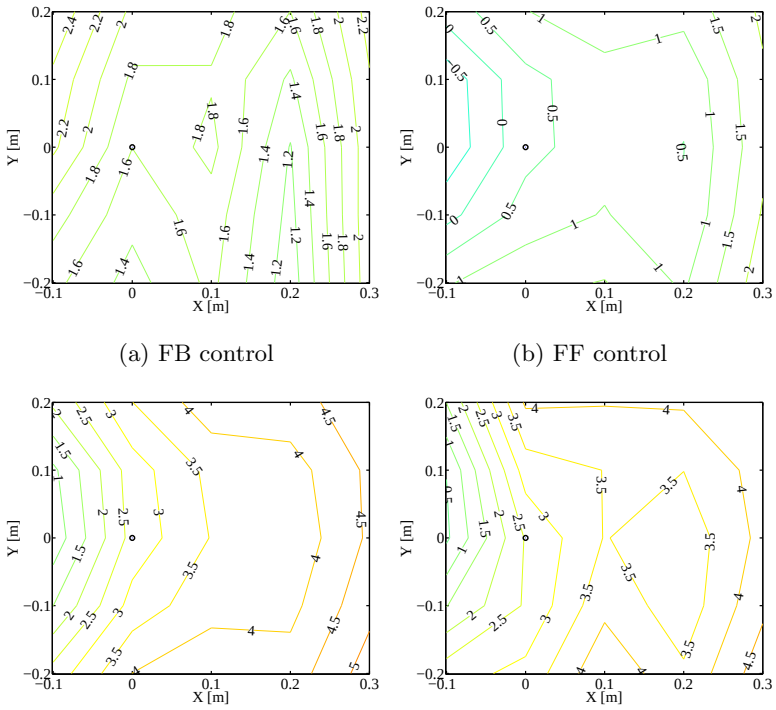

(a) FB control (b) FF control

(c) FF+FB control (d) HB control

Figure 3.22: Noise attenuation [dB] in the measurement area for 250 Hz 1/3 octave band

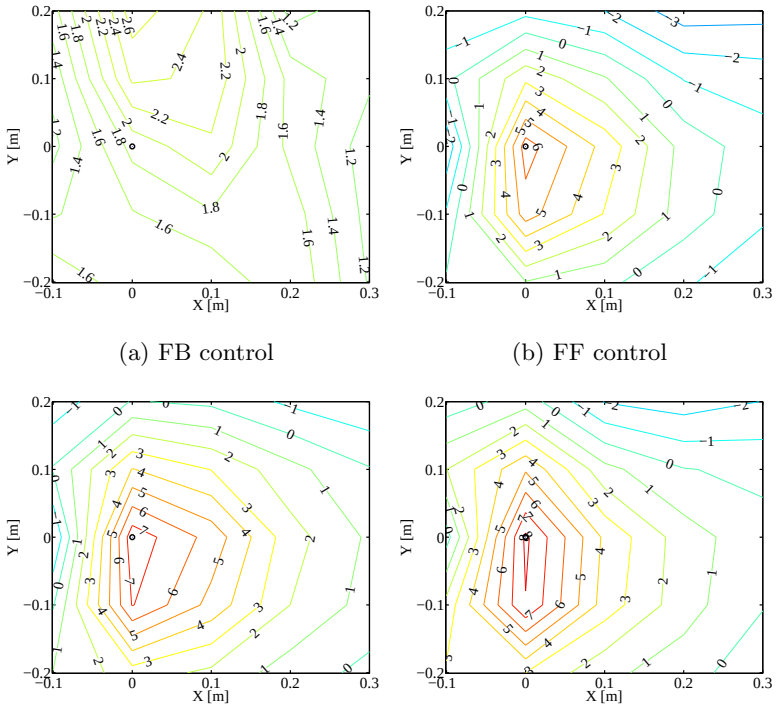

(a) FB control (b) FF control

(c) FF+FB control (d) HB control

Figure 3.23: Noise attenuation [dB] in the measurement area for 500 Hz 1/3 octave band

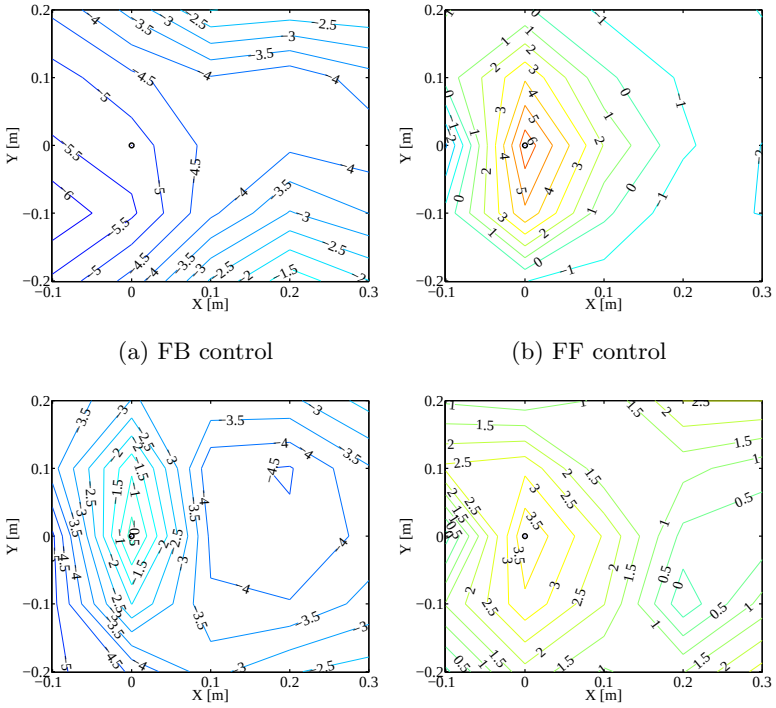

(a) FB control (b) FF control

(c) FF+FB control (d) HB control

Figure 3.24: Noise attenuation [dB] in the measurement area for 800 Hz 1/3 octave band

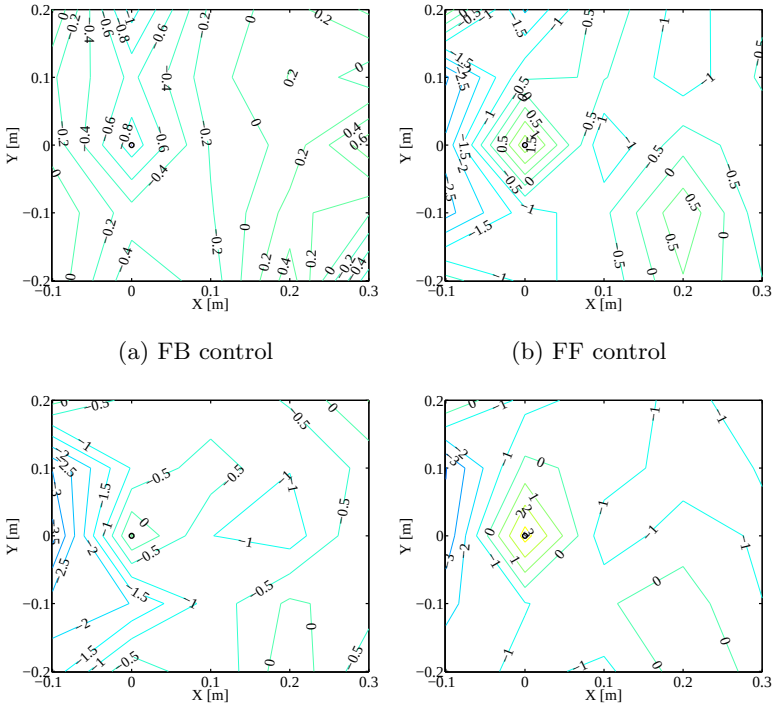

(a) FB control (b) FF control

(c) FF+FB control (d) HB control

Figure 3.25: Noise attenuation [dB] in the measurement area for 4 kHz 1/3 octave band

Figure 3.27 shows the results of the noise attenuation at the center FB control point and the FF control point under different background noises. In Fig. 3.27(b), it can be found that the noise attenuation performance deteriorates more obviously within the 315 Hz – 500 Hz 1/3 octave bands at the FF control point. The reason for the performance deterioration at the FF control point and other points in the control area is that the background noise, which is incoherent with the primary noise, cannot be canceled by the FF control. However, it can be seen from Fig. 3.28 that the extent

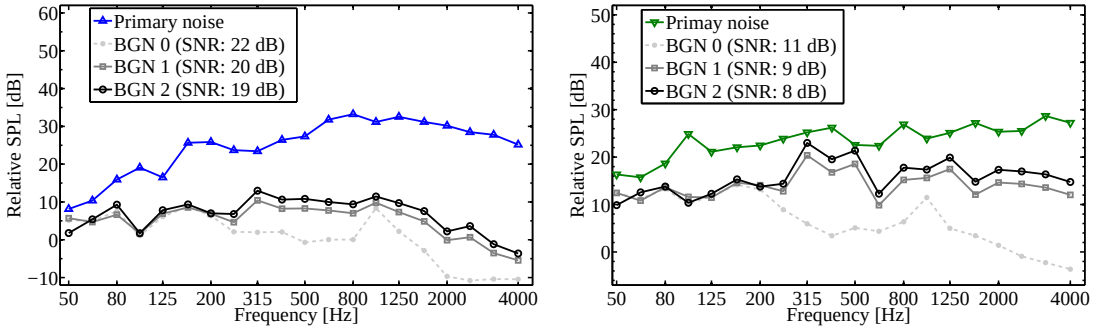

(a) At the center FB control point

(b) At the FF control point

Figure 3.26: 1/3 octave band SPL of the primary noise and the three background noises

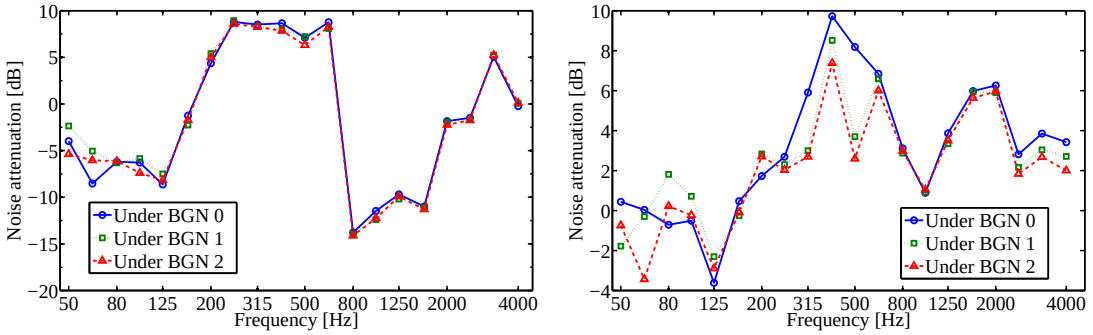

(a) At the center FB control point

(b) At the FF control point

Figure 3.27: Noise attenuation at the control points under different background noises

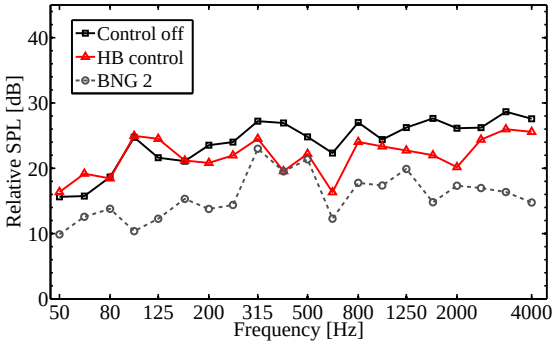

Figure 3.28: 1/3 octave band SPL at the FF control point under BGN 2.

of the deterioration depends on the ratio between the amplitude of the residue noise and the background noise. Figure 3.28 depicts the SPL at the FF control point before and after HB control under BGN 2. Within the 315 Hz – 500 Hz 1/3 octave bands, the background noise having a similar level of the residual noise causes more obvious deterioration of the noise attenuation. On the other hand, at the frequencies where the sound pressure is dominated by the residual noise, the performance deterioration is relatively small. For the results at the center FB control point shown in Fig. 3.27(a), almost the same noise attenuation results are obtained under three background noises because the FB control is able to cancel the incoherent noise. However, the noise attenuation in the control area provided by the FB control may reduce for the same reason with the FF control. The above results indicate that the background noise has little negative influence on the noise attenuation at the FB control points. However, the noise attenuation in the control area may be deteriorated according to the ratio between the amplitude of the residue noise and the background noise.

3.6 Summary

This chapter investigated the noise attenuation performance of the proposed ANB system. First, the control strategies used in the ANB system and the system implementation of them were presented. Then, a prototype ANB was developed, and the noise attenuation performance of the ANB under different sound field conditions was investigated by simulations and experiments. It was confirmed that the proposed HB control can improve the ANB performance at low frequencies, and the waterbed effect cancellation technique can reduce the noise amplification propagating into the control area effectively. The simulation results also indicate that the ANB is more effective for the sound field where there are little side diffraction and little reflection. For other sound fields, even though the side diffraction and the reflection lead to the spatial non-uniformity and deterioration of the noise attenuation, the low frequency noise attenuation can be achieved in a wide area behind the ANB, and noise attenuation for a wide frequency range can be ensured around the control point. Finally, an experiment was conducted to verify the effectiveness of the proposed ANB in a real office room. In this practical application, the ANB achieved about 3 – 8 dB noise attenuation in the control area when the background noise is relatively small. The experiment results also validate that the proposed HB control system can achieve larger noise attenuation than the FB or FF control, and can effectively suppress the waterbed effect induced noise amplification in the control area.

Chapter 4

Evaluation of Maskers

4.1 Introduction

This chapter focuses on the selection of the maskers used in the sound masking part of the proposed sound proof system. Sound masking in the workspace has two aims. One of those is to protect the speech privacy, and another is to help the employees concentrate. These mean that a masker with high masking efficiency for the aim of making speech incomprehensible and low annoyance for the aim of relieving the acoustic distraction is desired for the sound masking systems used in offices. In this chapter, therefore, two listening experiments are conducted to evaluate the masking efficiency and the annoyance of several representative maskers, respectively. Then, a selection criterion for the maskers is considered according to the experimental results.

4.2 Generation of the maskers

This section introduces the generation methods and the features of the maskers which will be investigated in the listening experiments. There are two kinds of sound masking: energetic masking and informational masking. Therefore, five representatives of the energetic and informational maskers including band-limited pink noise, target spectrum based random noise, frequency-reversed masker, time-reversed masker, and a synthesized environment noise are selected and investigated in this chapter. Several sound masking simulations are conducted, and the results are used to present the generation process and the features of these maskers. In the simulations, the target speech sound is a Japanese news audio.

4.2.1 Band-limited pink noise

Pink noise is a steady random noise of which the amount of the noise power is equal in each octave band, and it is an often-used masker because of the easiness to generate it. This pink noise masker primarily leads to energetic masking. It has been confirmed that the band-limited ([177, 5656] Hz) pink noise has higher masking efficiency than a

broadband pink noise [110]. Therefore, the band-limited pink noise will be investigated in the experiments.

Figure 4.1 shows the 1/3 octave band amplitude of the band-limited pink noise, the target speech signal, and the masking result. The target speech has low power spectral density above 2 kHz, whereas the pink noise masker has an equal power spectrum in all 1/3 octave bands. Therefore, the noise power in the high frequency domain can be decreased in order to cover the target sound more efficiently.

4.2.2 Target spectrum based random noise

Target spectrum based masker is a steady random noise which is generated according to the power spectrum of the target speech in order to cover it more efficiently. The generation method of the target spectrum based masker is as follows.

Step 1: Obtain the target speech signal.

Step 2: Extract the spectral shape curve of the target speech signal by performing moving average to the amplitude. However, the amplitude of the target speech signal should be smoothed sufficiently by the moving average because if the component at formant frequencies [151, 152], which is a feature value for human speech, remains in the spectral shape curve, the generated sound could be still intelligible so that it cannot be an effective masker. The degree of smoothness of the shape curve is determined by error and trial. Figure 4.2 shows the amplitude and extracted shape curve of the target speech signal.

Step 3: Perform exponential average to the spectral shape curves obtained at each discrete time to avoid the sudden and large change in the masker property. In this thesis, the forgetting factor of the exponential average is set as 0.985. Then, by using the shape curve result of the exponential average as the amplitude, an FIR filter can be calculated by IFFT. Figure 4.3 depicts the filter coefficients and the frequency properties of the obtained FIR filter.

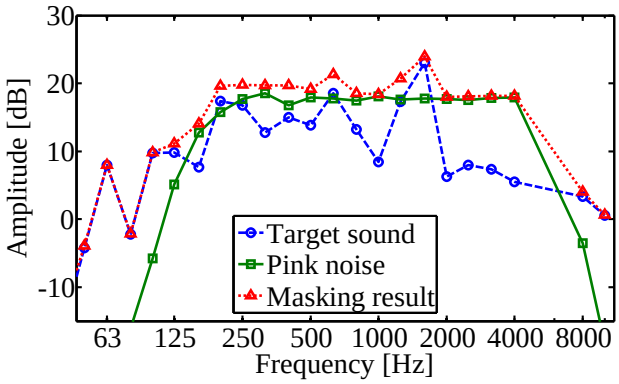

Figure 4.1: Masking result by pink noise

Step 4: Filter the band-limited ([177, 5656] Hz) white noise by the FIR filter obtained in Step 3, and use the result as the target spectrum based masker.

Figure 4.4 shows the 1/3 octave band amplitude of the target spectrum based masker, the target speech signal, and the masking result. In comparison with the band-limited pink noise, the target spectrum based masker has a similar shape of the

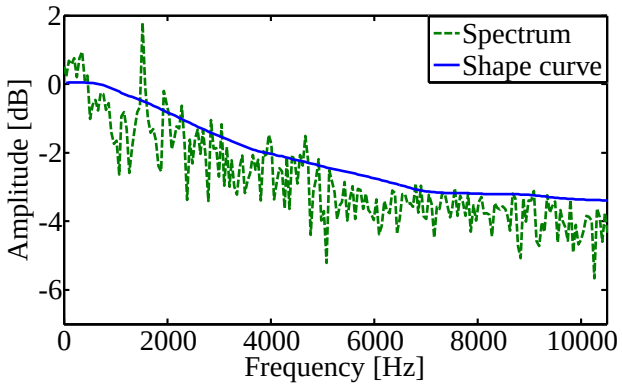

Figure 4.2: Spectrum and shape curve of the target sound

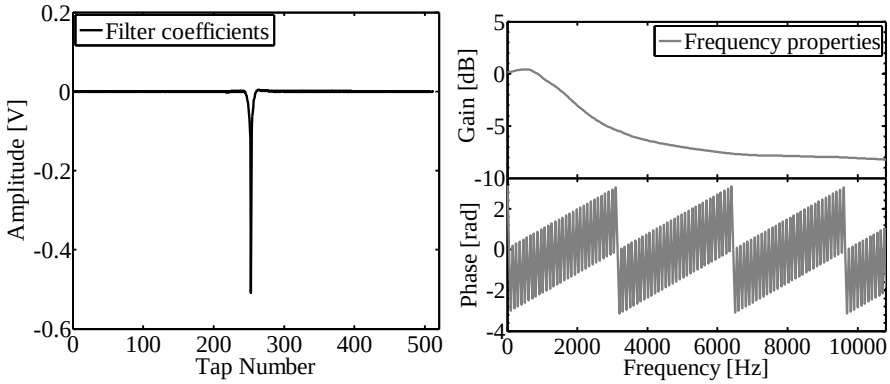

(a) Filter coefficients (b) Frequency properties

Figure 4.3: FIR filter generated from the target shape curve

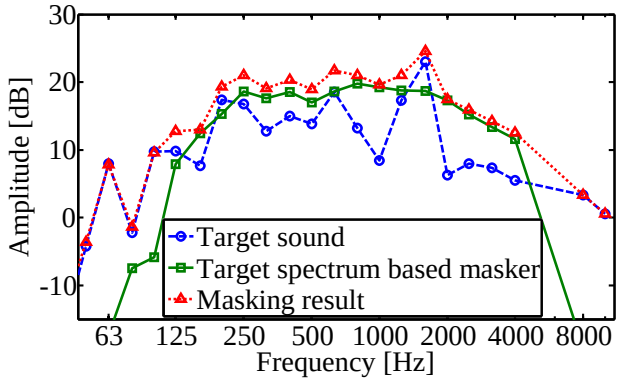

Figure 4.4: Masking result by target spectrum based masker

spectrum with the target speech signal. This masker can be generated in real-time if the target speech signal can be detected online so that the masker can track the changes in the target sound spectrum. In this case, a higher masking effectiveness can be expected. However, as multiple FFT and IFFT computations are required in the generation process and a high sampling frequency must be used according to the audible range ([20, 20000] Hz) of human, a DSP with high computational capability is necessary. Moreover, as the time-variant sound is often more annoying for people. The online generated target spectrum based masker may be of high annoyance even higher masking efficiency and effectiveness is expectable. To solve this problem, one can perform Step 1 – 3 to calculate the FIR filter in real-time for a certain time, and then use this FIR filter as a fixed filter to generate masker sound. In this case, the target spectrum based masker becomes a steady random noise with the time-averaged spectrum of the target sound. Therefore, it could be an energetic masker which covers the target speech more efficiently. This thesis investigates the steady target spectrum based masker.

4.2.3 Frequency-reversed masker

The concept of the frequency-reversed masker is to equalize the power spectral density after masking in order to change the relation between the formant frequencies [114]. The generation process can be described as follows.

Step 1: Obtain the target speech signal.

Step 2: Extract the spectral shape curve of the target speech signal by performing moving average to the amplitude. Figure 4.5 shows the amplitude and extracted shape curve of the target speech signal. It has not to smooth the shape curve much as the target spectrum based random noise because the following reversing process makes the masker sound meaningless.

Step 3: Reverse the spectral shape curve. The frequency band to be reversed is set

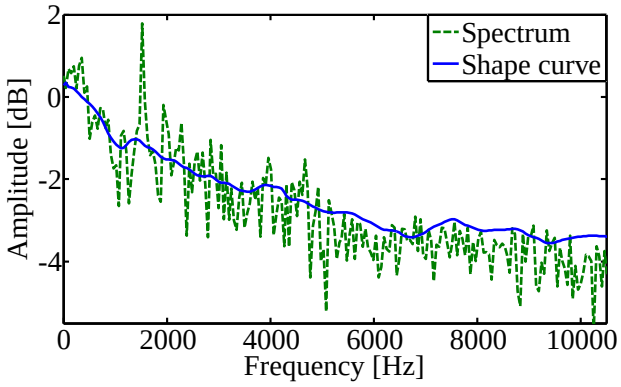

Figure 4.5: Spectrum and shape curve of the target sound

as [1, 4000] Hz. The reversing axis applies the straight line connecting the two ends of the shape curve within the reversing frequency band. Figure 4.6 shows the target shape curve and the reversed one.

Step 4: Perform exponential average to the spectral shape curves obtained at each discrete time to avoid the sudden and large change in the masker property. The forgetting factor of the exponential average is set as 0.985. Then, by using the shape curve result of the exponential average as the amplitude, an FIR filter can be calculated by IFFT. Figure 4.7 depicts the filter coefficients and the frequency properties of the obtained FIR filter.

Step 5: Filter the band-limited ([177, 5656] Hz) white noise by the FIR filter obtained in Step 4 and use the result as the frequency-reversed masker.

Figure 4.8 shows the 1/3 octave band amplitude of the frequency-reversed masker, the target speech signal, and the masking result. The frequency-reversed masker has larger power in the 1 kHz and 2 kHz 1/3 octave band in which the power of the target sound is low. Therefore, the masking result has a flatter power spectral density. The frequency-reversed masker can also be generated in real-time if the target speech

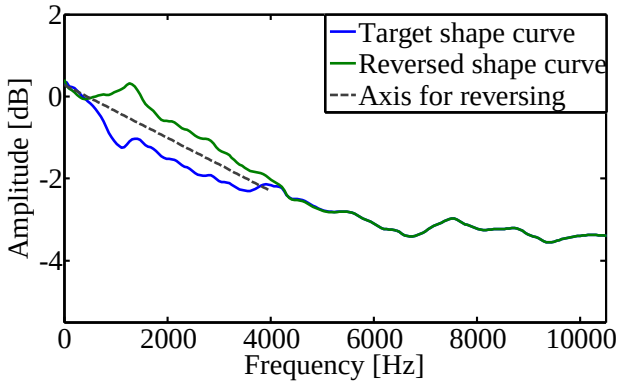

Figure 4.6: Shape curves of the target sound and the masker

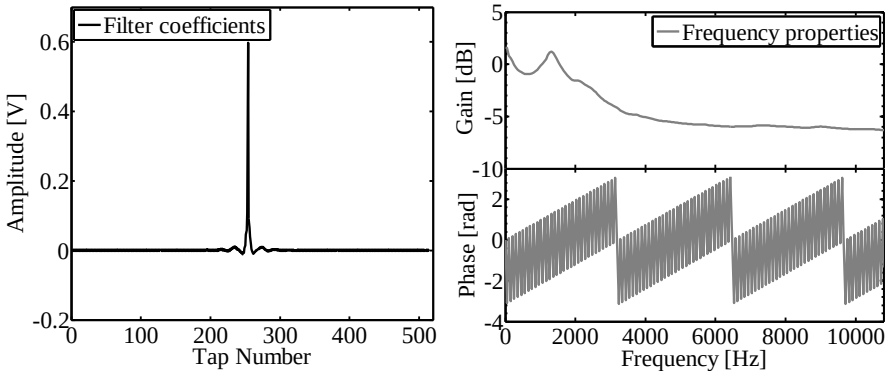

(a) Filter coefficients (b) Frequency properties

Figure 4.7: FIR filter generated from the reversed shape curve

signal can be detected online, and as the target spectrum based random noise, the high computational load and the time-variant property may be the problems. A steady frequency-reversed masker can be generated if the FIR filter generated in Step 4 is used as a fixed filter. In this case, the frequency-reversed masker becomes a special energetic masker of which the spectrum covers that of the target sound partially. In this thesis, the steady frequency-reversed masker will be investigated.

4.2.4 Time-reversed masker

The time-reversed masker [112, 113] is a meaningless sound created by reversing the time frames of the recorded target sound signal. The specific generation procedures of the masker is as follows.

Step 1: Obtain the target speech signal.

Step 2: Split the target speech signal into time frames with a certain length, and reverse the signals in each time frame. If the length of the time frame is shorter than the length of a syllable, the meaning of the reversed time frame is still meaningful so that it cannot be an effective masker [113]. In this thesis, the length of the time frame

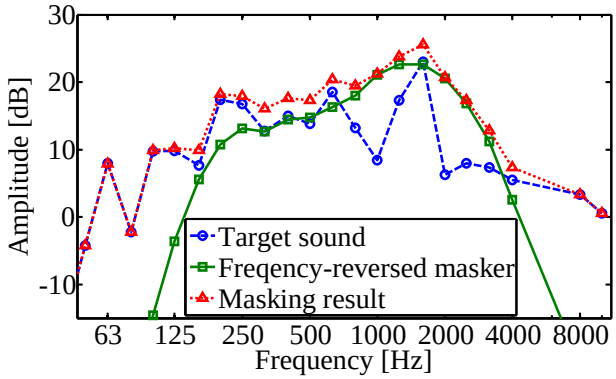

Figure 4.8: Masking result by frequency-reversed masker

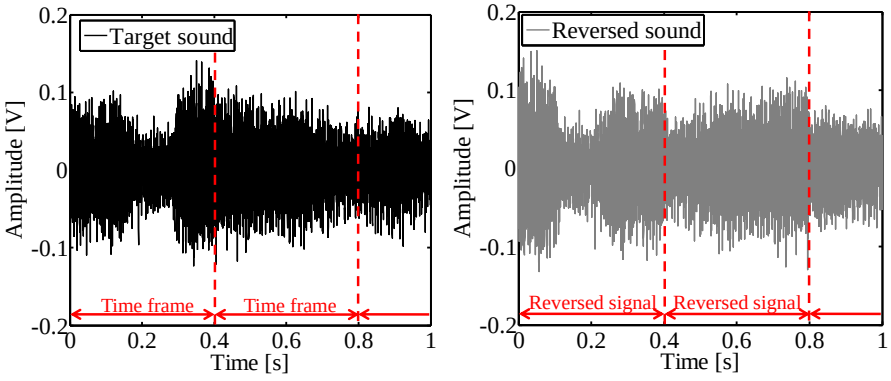

(a) Target sound signal (b) Reversed sound signal

Figure 4.9: Target sound and reversed sound signal

to be reversed is set as 400 ms. Figure 4.9 shows an example of the target and the reversed speech signals.

Step 3: Connect the reversed time frames and use it as the time-reversed masker.

Figure 4.10 shows the 1/3 octave band amplitude of the time-reversed masker, the target speech signal, and the masking result. The time-reversed masker is one of the informational maskers. The amount of the informational masking depends on the similarity between the masker and the target sound and the uncertainty of the masker [106, 153]. The similarity means the masker has a similar spectrum with the target sound, and the uncertainty refers to that the masker sound is meaningless, unpredictable, and unfamiliar for people. The time-reversed masker is a meaningless sound having the same time-averaged spectrum with the target sound, which is of high similarity and uncertainty so that it can be expected to have high masking efficiency. Nevertheless, the time-reversed masker is a time-variant sound so the annoyance of the masker may be a problem, which will be investigated in the listening experiments. In addition, if the time-reversed masker is generated in real-time, a time delay that is equal to the length of the time frame exists between the target sound and the masker, which will reduce the sound masking performance [113]. However, if the target sound signal can be obtained in advance such as the occasion of playing a secret video or audio, the time-reversed masker can be generated offline with the compensation of the time delay. In this case, the time-reversed masker will be more effective.

4.2.5 Environmental noise

The environment noise masker is a mixture of several everyday sounds [107] and noises including news audio sounds, the sound of sea waves, background noises in a railway station and in a cafe, and fan noise. This masker contains steady meaningless noises and unsteady sounds so that it can be seen as a combination of the informational maskers and the energetic maskers.

Figure 4.11 shows the 1/3 octave band amplitude of the environment noise masker,

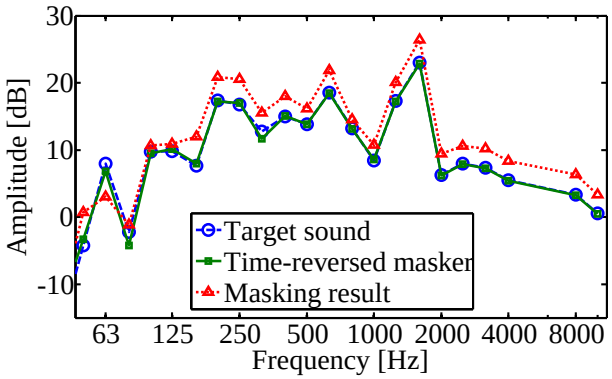

Figure 4.10: Masking result by time-reversed masker

the target speech signal, and the masking result. The environment noise has a similar spectrum with the target sound so that it can be expected to have high masking efficiency. Additionally, it is easy to generate the environment noise masker and play it as a masker. However, there are various environment noises so a different mixture of the noises may lead to different masking efficiency and annoyance.

In the following two sections, two listening experiments are performed to investigate the masking efficiency and the annoyance of the above five maskers.

4.3 Listening experiment I to evaluate sound masking performance

Experiment I is to compare the masking efficiency of the maskers. A list of Japanese words with sound masking are presented to the subjects, then the subjects are required to write down the words they heard. The speech intelligibility, which is the percentage of the correctly answered words, is used to evaluate the performance of the maskers.

4.3.1 Experimental conditions

The subject group consists of eight male college students aged between 20 – 25 with normal hearing. The target word lists are chosen from the familiarity-controlled Japanese word lists 2003 [154] (FW03). There are 50 words in each list. The five maskers are combined into the target sounds with different SNR ranged from -15 dB to 0 dB incremented in 5 dB steps. SNR is defined as

$$\mathrm{SNR} = 10\log_{10}\frac{\sum_{n=1}^{N}\boldsymbol{t}(n)^2}{\sum_{n=1}^{N}\boldsymbol{m}(n)^2}, \tag{4.1}$$

where $\boldsymbol{t}(n)$ is the target sound signal, $\boldsymbol{m}(n)$ is the masker signal, N is the length of the signals. Therefore, there are 16 experimental cases (4 maskers $\times$ 4 SNRs). Eight word lists pronounced by male Japanese and another eight pronounced by female Japanese

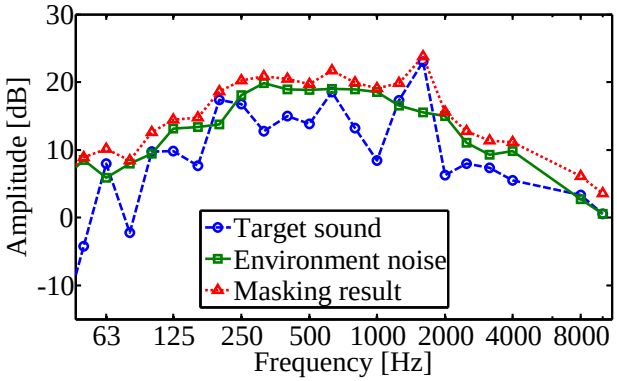

Figure 4.11: Masking result by environmental noise

are selected from the word lists of familiarity rank 2 and 4, and one word list is used for one experimental case. The experiment is conducted in an anechoic chamber, where the background noise is small enough to be ignored in the listening experiments. A laptop computer is used to produce the words and collect the answers. The stimuli are presented to the subjects via a headphone. The SPL of the target sound without masking is adjusted to the same 60 dB for each experimental case.

4.3.2 Results and discussion

Figure 4.12 depicts the mean speech intelligibility and the standard deviation for each experimental case. At the SNRs below -10 dB, the speech intelligibility scores for all of the five maskers are less than 10%, which means high speech privacy can be achieved. The environment noise has the highest masking performance, and the frequency-reversed masker has the lowest masking performance in general. The pink noise and the target spectrum based masker, which are energetic maskers, performs better than the informational time-reversed masker at the low SNRs, especially at -15 dB. On the other hand, at the larger SNRs such as -5 and 0 dB, the informational time-reversed masker has better masking performance than the energetic random noise maskers. At the SNR of -5 dB, the environment noise achieves similar masking performance with the time-reversed masker. These results imply that increasing the power of the maskers is a more effective method to improve the masking performance of the energetic maskers than the informational maskers. However, the informational maskers perform better if the power of the maskers is relatively small. The environment noise masker contains both of the energetic and informational masking can provide higher masking performance, and a masker which only covers the target spectrum partially such as the frequency-reversed masker perform worse in general.

The standard deviation of the speech intelligibility scores, which is caused by the individual difference of the subjects and the different properties of the target sounds,

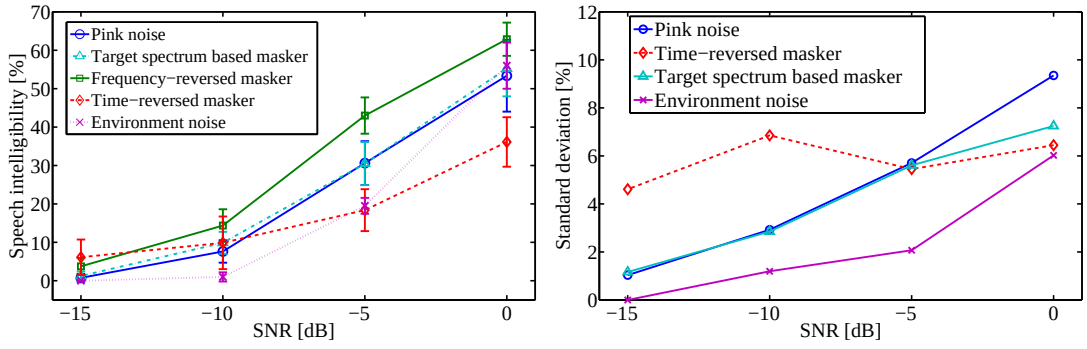

(a) Error bar of the speech intelligibility score

(b) Standard deviation

Figure 4.12: Speech intelligibility scores for the five maskers

can be used to evaluate the robustness of the maskers. In Fig. 4.12(b), it can be seen that the standard deviations of the energetic random noise maskers decrease with the increment of the masker power. However, the time-reversed masker has large standard deviations even at the SNRs of -10 dB and -15 dB. The result of the environment noise has the smallest standard deviation at all of the four SNRs. This implies that the mixed-type environment noise masker has high robustness to the individual difference of the listeners and to the different target sounds, and the energetic maskers can achieve high robustness if the power of the maskers is large; however, the performance of the informational time-reversed masker varies more obviously than the other two types of maskers under different listening conditions.

The above results suggest that if high speech privacy is required, the energetic maskers or the mixed-type maskers of large power are more effective. For the situation that large background noise is not allowed and speech privacy is not required so strictly, the informational maskers, which can achieve higher speech privacy at lower SNRs, may be preferred.

4.4 Listening experiment II to evaluate annoyance

Experiment II is to investigate the annoyance of the maskers, and the masking performance to conversations. The target conversation sounds with masking are presented to the subjects, then the subjects are required to grade the annoyance of the sounds based on a 5-point scale rating method recommended in Ref. [155] with the score between 1

Table 4.1: Meaning of the scores to evaluate the annoyance

Scores	Meaning
1	Extremely annoying
2	Very annoying
3	Annoying
4	Slightly annoying
5	Not annoying at all

Table 4.2: Meaning of the scores to evaluate the speech intelligibility

Scores	Meaning
1	Unintelligible and the speech is not aware
2	Unintelligible but it is aware that the sound is speech
3	Details are unintelligible but the general meaning can be understood
4	Sometimes unintelligible but the details in conversation can still be understood
5	Clearly intelligible

and 5, and also to grade the speech intelligibility with the score between 1 and 5. The meanings of the scores are concluded in Table 4.1 and Table 4.2.

4.4.1 Experimental conditions

The subject group consists of ten male college students aged between 20 – 25 with normal hearing. The target sounds apply several Japanese news audios with a length of about 30 sec. The five maskers are combined into the target sounds with different SNR ranged from -15 dB to 0 dB incremented in 5 dB steps. Therefore, there are 16 experimental cases. Each case uses the different stimulus. The experiment is conducted in an anechoic chamber. The stimuli are presented to the subjects via a loudspeaker. The SPL of the target sound without masking is adjusted to 55 dB.

4.4.2 Results and discussion

The experiment results are shown in Fig. 4.13. In the annoyance result, the random noise maskers and the environment noise masker show that the annoyance of them increases with the increase of masker power (or with the decrease of SNR). On the other hand, the subjects feel annoyed even if the power of the time-reversed masker is small. In general, the stationary energetic random noises are relatively acceptable for the subjects. Especially, the frequency-reversed masker, of which the concept is to flatten the spectrum of the sound after masking, is of the smallest annoyance. The time-reversed masker, which is an artificially synthesized non-stationary masker, is the most annoying one. The environment noise has a score between the stationary random noises and the non-stationary time-reversed masker.

The intelligibility scores in Experiment II confirms the speech intelligibility results of Experiment I, in which Japanese words are used as the target sounds. This result also demonstrates that the quantitative evaluation of the maskers by using word lists is a reliable reference for selecting a masker for practical application where the target

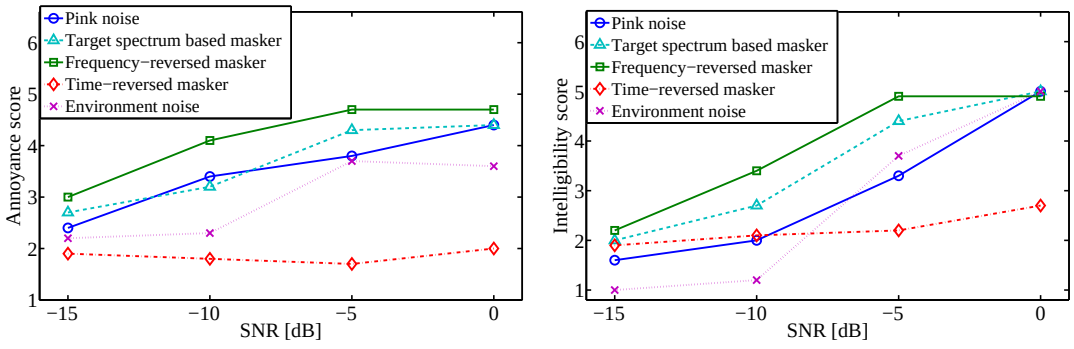

(a) Annoyance scores

(b) Intelligibility scores

Figure 4.13: Annoyance and masking performance for conversations

sounds are conversations.

The two results of Experiment II imply that the stationary energetic maskers are preferred if the main purpose of the sound masking is to improve the concentration of the employees in the workplace.

4.5 Comprehensive evaluation of the maskers

This section evaluate the five maskers by considering the masking efficiency and the annoyance comprehensively according to the previous experimental results.

Figure 4.14 shows the speech intelligibility of the five maskers with respect to the annoyance. The horizontal axis depicts the annoyance results of Experiment II, and the vertical axis depicts the speech intelligibility scores obtained in Experiment I. The curves in the graph represent the masking results of each masker at the different SNRs. Figure 4.14 can be divided into 4 domains. Domain 1 means the sound masking can neither protect the speech privacy nor relieve the acoustic distractions. On the other hand, the masking results in the domain 4, where the sound masking can protect speech privacy well, and meanwhile does not increase the annoyance much, are the most desired results. From Fig. 4.14, one can identify a masker that can achieve the objective speech privacy with the lowest annoyance. The results demonstrate that the informational time reversed masker can achieve better sound masking performance with lower masker power, whereas it may not the preferred selection for the sound masking in offices if the annoyance is taken into the consideration. However, even if the frequency-reversed masker is not an efficient masker, which can be confirmed from Fig. 4.12, it has the lowest annoyance at a certain speech intelligibility score in comparison with other maskers. Therefore, by considering the masking performance and the annoyance comprehensively, the frequency-reversed masker can be a good choice for the sound masking systems used in the workspace.

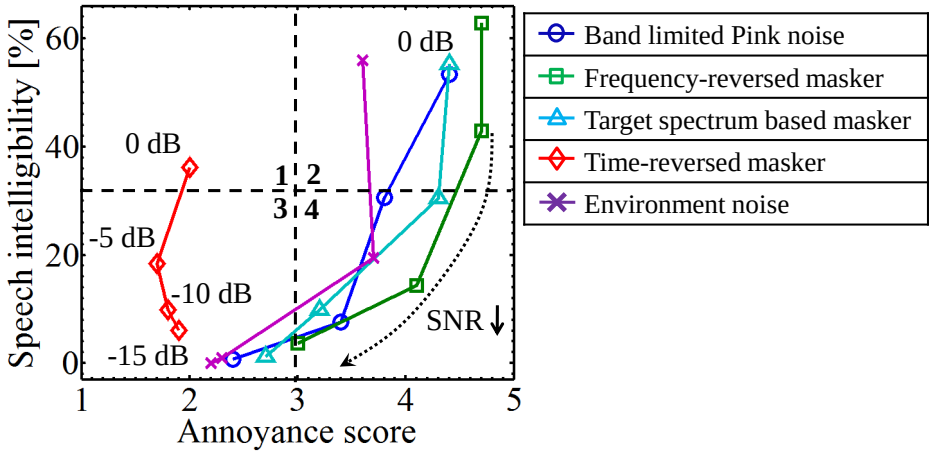

Figure 4.14: Speech intelligibility with respect to the annoyance scores

4.6 Summary

This chapter investigated several typical energetic and informational maskers including band-limited pink noise, target spectrum based random noise, frequency-reversed masker, time-reversed masker, and a synthesized environment noise in order to select an appropriate masker for the sound masking systems used in the workspace. First, the principles and the generation methods of the maskers were introduced. Then, the masking efficiency and the annoyance of the maskers were evaluated by two listening experiments. The results of Experiment I suggest that if the requirement of speech privacy is strict, the energetic maskers or the mixed-type maskers of large power are more effective than the informational maskers. The results of Experiment II imply that the stationary maskers are preferred if the main purpose of the sound masking is to improve the concentration of the employees in the workplace rather than to protect the speech privacy. Finally, according to the experimental results, a comprehensive evaluation criterion that identifies the masker achieving a certain speech intelligibility with the lowest annoyance was presented.

Chapter 5

Hybrid Active Noise Barrier with Sound Masking

5.1 Introduction

This chapter presents a sound proof system which combines the sound masking with the ANB investigated in Chapter 3. In practice, the ANB cannot cancel the undesired sound completely. Therefore, the sound masking technique is integrated into the ANB in order to cover the residue undesired sound. As the target sound level has been reduced by the ANC part of the ANB, less masker power is required to achieve the same sound masking effect in comparison with the conventional sound masking systems. Consequently, it is expected that the proposed sound proof system can achieve the quietness and the speech privacy simultaneously in the private workspace behind the ANB. In this chapter, the control system combining the HB-ANC and the sound masking techniques is presented, first. The performance of the ANB using the control system is investigated by simulations.

5.2 Hybrid active noise control system combining sound masking

Figure 5.1 shows the block diagram of the control system that integrates sound masking into the HB-ANC system. The masker signal $m(n)$ is output via the loudspeaker used as the FF control source. For the sound masking part, in comparison with the simple signal processing, selecting an appropriate masker for the sound masking in offices is more important, which has been discussed in Chapter 4. The results of Fig. 4.14 has confirmed that the time-invariant frequency-reversed masker is preferred for the sound masking in offices by considering the masking performance and the annoyance simultaneously. Therefore, the masker generator in the control system applies the time-invariant frequency-reversed masker generation method described in Section 4.2.3 to synthesize the masker signal $m(n)$.

By adding the sound masking part into the HB-ANC system, the system operation process becomes three steps.

Step 1: ANC part initialization. Control filters $\boldsymbol{C}_F(z)$ and $\boldsymbol{C}_W(z)$ are updated in this stage.

Step 2: Sound masking part initialization. The FIR filter to generate the frequency-reverse masker is calculated in this stage. The target speech signal applies the reference signal of the FF control filter $\boldsymbol{C}_F(z)$, which is obtained from the center FB control unit.

Step 3: Real-time control stage. The offline-designed FB control filters $\boldsymbol{C}_B(z)$, and the control filters $\boldsymbol{C}_F(z)$ and $\boldsymbol{C}_W(z)$ are used as fixed filters to calculated the control signal to cancel the target sound. The masker generator synthesizes the masker sound by filtering the band-limited white noise by the FIR filter obtained in Step 2 to cover the residual sound. In this stage, the output signal of the FF control source $u_{FO}(n)$ is calculated as

$$u_{FO}(n) = u_F(n) + m(n). \tag{5.1}$$

5.3 Simulation investigations

In this section, the performance of the proposed sound proof system is investigated by simulations.

5.3.1 Simulation conditions

Figure 5.2 shows the sound field configuration considered in the simulations. One side of the ANB is located next to the wall of the anechoic chamber, and a large partition is placed on the other side of the ANB to block the side diffraction. Therefore, there is little sound diffraction from the side of the ANB in this configuration. The sound pressures in the measurement area behind the ANB are calculated to evaluate the system performance.

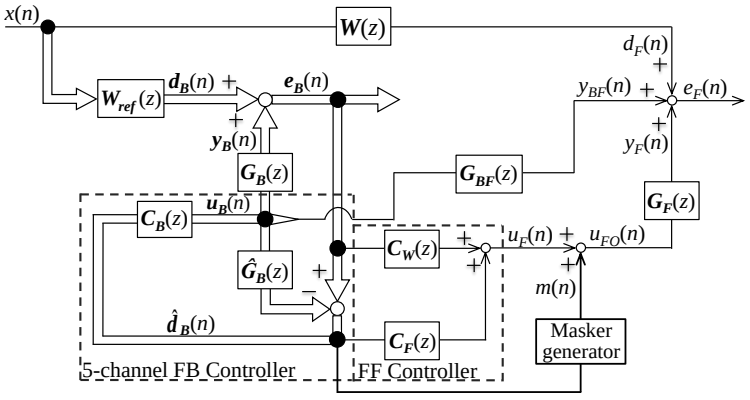

Figure 5.1: Acoustic control system combining HB-ANC with sound masking

The simulations are performed according to the block diagram in Fig. 5.1. The acoustic paths used in the simulations are expressed as 2048-tap FIR filters, which are identified in the anechoic chamber. The FB and FF control filters apply 128-tap FIR filters. The target band of the FB control is set as from 200 Hz to 630 Hz 1/3 octave band, and the FB and FF control filters are obtained by the same procedures in Chapter 3. A Japanese news audio is used as the primary noise source. The FIR filter in the masker generator for synthesizing the time-invariant frequency-reversed masker signal applies a 512-tap FIR filter. The sampling frequency of the control system is set as 20 kHz. The crosstalk paths among the FB controllers and the FF controller are not considered in the simulations. The reliability of this simulation method has been verified in Section 3.4.6.

5.3.2 Sound attenuation at the control points

In this simulation, the attenuation of the target speech at the control points is calculated to verify the effectiveness of the ANC part for the case in which the primary noise is the time-variant speech signal.

Figure 5.3 shows the time-averaged 1/3 octave band SPL before and after control at the center FB control point and the FF control point. At the FB control point, the noise is reduced within the target band of control, and the control result at the

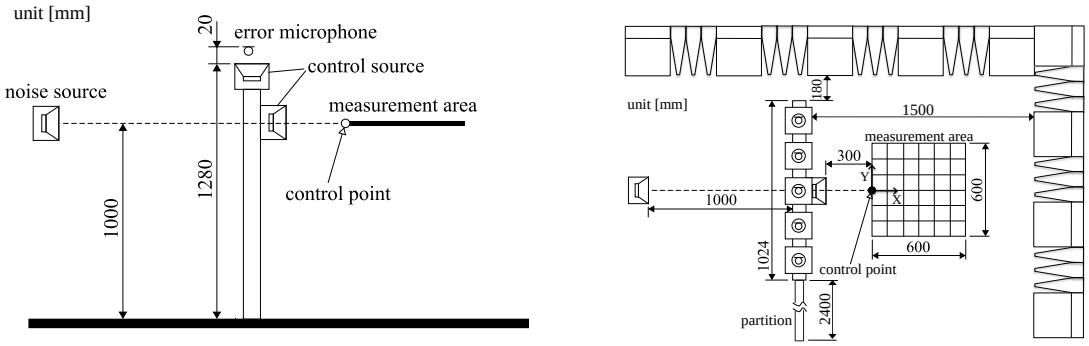

(a) Side view

(b) Top view

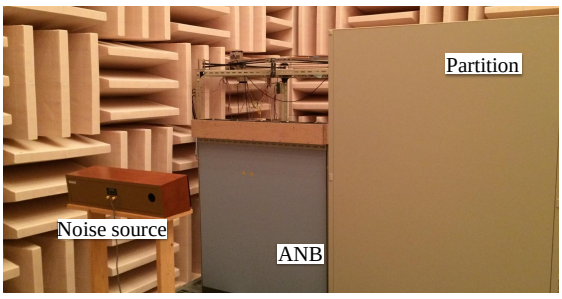

(c) Configuration in the anechoic chamber

Figure 5.2: Sound field configuration

FF control point demonstrates the HB control can reduce the target speech in a wide frequency band. Figure 5.4 shows the speech signal at the FF control point before and after HB control. The result indicates that the ANC part of the proposed sound proof system can effectively reduce the time-variant target speech.

5.3.3 Sound masking performance in the control area

The simulations in this section investigate the sound masking performance of the proposed sound proof system.

Figure 5.5 shows the 1/3 octave band amplitude of the original speech signal and the masker to confirm if the masker sound is generated successfully. The amplitude of the masker is lower at low frequencies and higher within the bandwidth from 1 kHz to 4 kHz where the power of the target speech is smaller. Therefore, the sound masking result can be expected to have a flat spectrum, which is the desired result.

Then, the sound masking effect at the FF control point is confirmed by observing the spectral shape of the target speech before and after control. Figure 5.6 shows the spectrogram of the target speech at the FF control point before control. The power of the target speech is high at low frequencies because of the passive noise attenuation

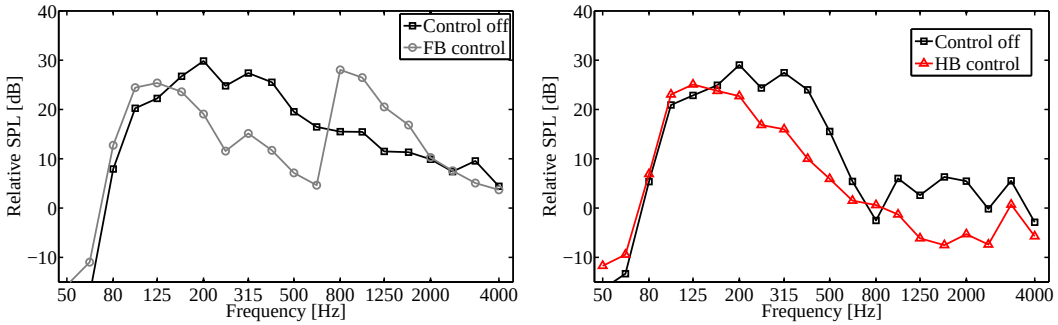

(a) at the center FB control point (b) at the FF control point

Figure 5.3: 1/3 octave band SPL at control points

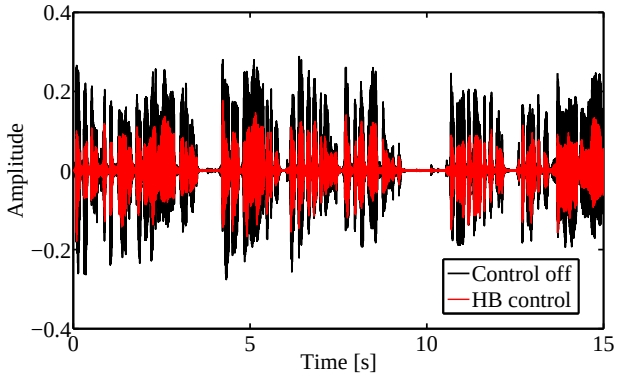

Figure 5.4: Speech signal at the FF control point before and after control

effect of the partition. However, the passive noise attenuation is insufficient so that the speech can still be recognized. Figure 5.7 shows the result of the HB control. After control, the target speech is further reduced. However, the spectral shape is not changed sufficiently, and the formant components at the frequencies 500 Hz – 1.5 kHz and 2.5 kHz – 3.5 kHz can still be found, which means the residual speech may be still intelligible.

In order to improve the speech privacy, the masker shown in Fig. 5.8 is output via the

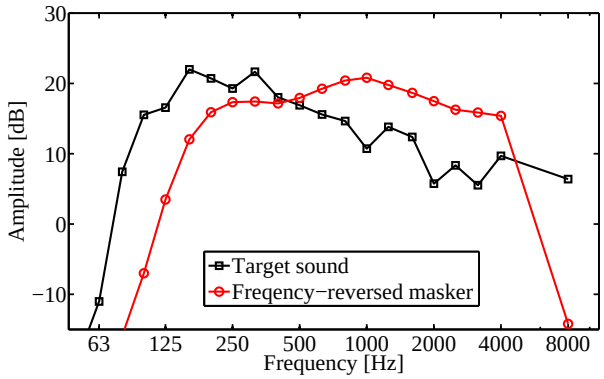

Figure 5.5: Amplitudes of the target speech and the masker

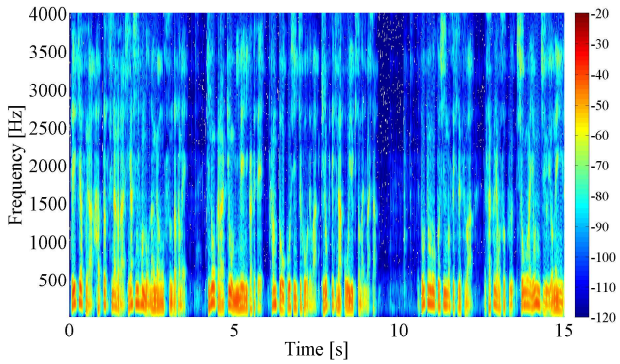

Figure 5.6: Spectrogram of the target speech before control

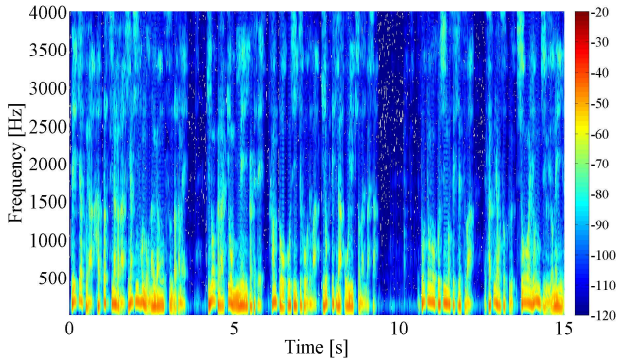

Figure 5.7: Spectrogram of the target speech after HB control

FF control source. In order to realize the "Normal Privacy" level in offices, the speech intelligibility should be below 50% [26]. According to Fig. 4.12, the frequency-reversed masker with the SNR of -5 dB can achieve this. Therefore, the SNR, which is defined by Eq. (4.1), is set as -5 dB in the following sound masking simulations. Figure 5.9 shows the spectrogram of the target speech after the HB control and the sound masking. The result indicates that the spectrum of the target speech becomes time-invariant and the flat, in which the formant components cannot be found. Therefore, it is expected that the speech privacy can be protected well.

In the next simulation, the SNR distribution in the measurement area is calculated to confirm the sound masking performance behind the ANB. The SNR is associated with the speech intelligibility [31–33], and for one certain masker, the same SNR can be considered as the same speech privacy level. Figure 5.10 shows the SNR distribution with and without HB control. When the HB control is not performed, the SNR is -5 dB at the FF control point, whereas the SNR increases at other positions. If the SNR increases to 0 dB, the speech intelligibility becomes about 60% according to Fig. 4.12, and the privacy level degraded to "Transitional Privacy". On the other hand, by HB control, the target speech is reduced so that the SNR decreases, and therefore, the

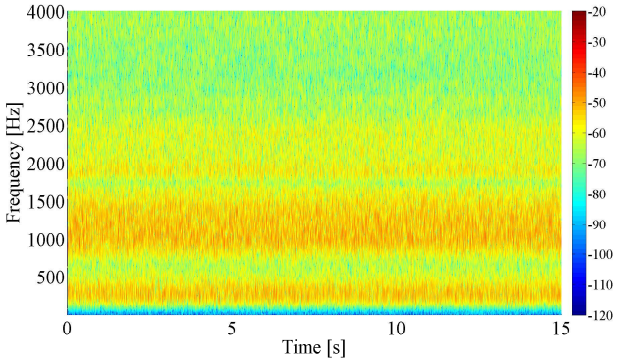

Figure 5.8: Spectrogram of the masker

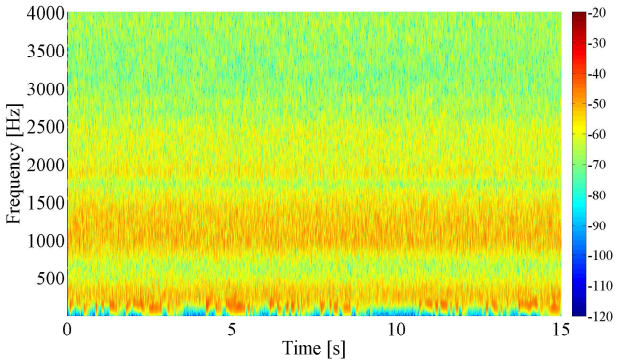

Figure 5.9: Spectrogram of the target speech after HB control and sound masking where the SNR is set as -5 dB

"Normal Privacy" can be guaranteed in the whole measurement area. In other words, one can achieve the same SNR (or same privacy level) by smaller masker sound if the proposed sound proof system, which actively reduces and covers the target speech simultaneously, is used.

5.4 Summary

In this chapter, a sound proof system which combines the sound masking with the ANB was presented. The ANB applies the HB-ANC system to cancel the target speech, and the frequency-reversed masker is output via the loudspeaker used as the FF control source to cover the residual speech. The control system combining the HB-ANC and the sound masking techniques was presented, firstly. Then, the performance of the proposed system was validated by simulations. The results demonstrate that the proposed system can achieve the same privacy level by using smaller masker sound, which means the simultaneous realization of the quietness and the speech privacy in the workspace can be expected.

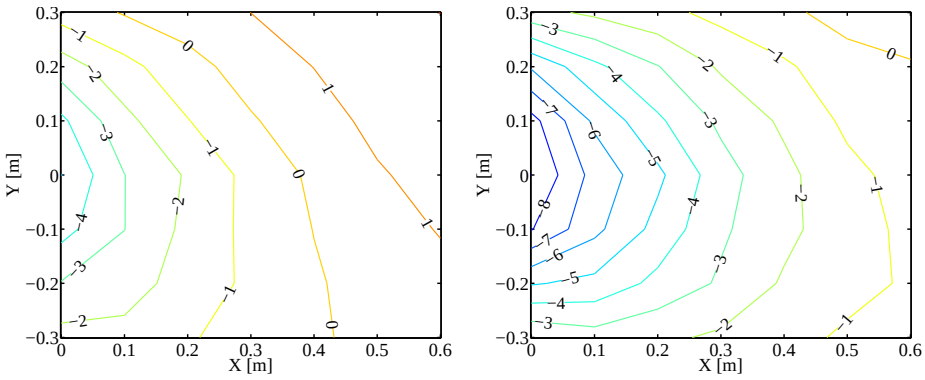

(a) SNR without HB control

(b) SNR with HB control

Figure 5.10: SNR [dB] in the control area with and without HB control

Chapter 6

Global Active Noise Control Based on Wavefront Synthesis

6.1 Introduction

This chapter presents a global ANC approach which is supposed to be used in the FF control part of the proposed sound proof system to enlarge the quiet zone behind the ANB. The extent of the quiet zone created by the ANC technique depends on the wavelength at the frequency of interest, and the spatial distribution of the primary noise and the control sound [37]. As the frequency increases, the quiet zone becomes small. This can also be confirmed from the noise attenuation distribution results in Chapter 3. A multi-input and multi-output (MIMO) ANC system with optimized arrangement of the control sources and control points [56] can be used to enlarge the quiet zone. However, as the target area becomes wide, more control channels have to be used, which will increase the computational burden of the control algorithm and the complexity of the hardware configuration. These two disadvantages limit the use of MIMO ANC systems.

To overcome these problems, an approach to global noise reduction in a certain area based on the concept of wavefront synthesis is proposed in this chapter. The basic idea is to divide a global ANC system into two sub-systems according to the different control objectives. One sub-system is to reproduce the shape of the wavefront of the incident noise into the target area, and the other is to adjust the amplitude and phase of the reproduced wavefront to be the anti-noise. The first one can be realized by any sound field reproduction methods such as the wave field synthesis method [156], the spectral division method [157], and the least squares (LS) method [158]. In this thesis, the LS method, which minimizes the errors between the reproduced sound field and the desired sound field, is used because it only requires the sound pressure information in the target area. The second objective can be realized by using an adaptive single-input and single-output (SISO) ANC system to control one point in the target area. Therefore, by using the proposed approach, the global noise control can be achieved

by minimizing the sound pressure at a local point, in which the control algorithm and the hardware configuration are simpler than those of the MIMO global ANC systems. Additionally, the modularization of a global ANC system can also simplify system design process in comparison with the MIMO ANC system. The effectiveness of the proposed approach is verified by numerical simulations.

6.2 Description of the method

Figure 6.1 illustrates a diagrammatic sketch of the proposed approach. The design process of a global ANC system according to the proposed approach can be divided into two stages: the design of an input filter for the loudspeaker array to reproduce the wavefront of the incident noise into the target area and the computation of the control source strength for canceling the noise at a local point in the target area. These procedures are realized as follows.

6.2.1 Reproduction of the noise field

The LS method has been widely used in the ANC applications [35], and it can also be applied to the sound field reproduction problem [158]. By denoting the matrix of the transfer functions from each unit of the loudspeaker array to the points in the target area as $\boldsymbol{G}$, the input filter of the loudspeaker array as $\boldsymbol{h}$, the sound pressure distribution $\boldsymbol{p}_R$ generated by the loudspeaker array with a set of unit input signals can be expressed as

$$\boldsymbol{p}_R = \boldsymbol{G}\boldsymbol{h}, \tag{6.1}$$

in which

$$\boldsymbol{G} = \begin{bmatrix} G(\boldsymbol{r}_{T,1}|\boldsymbol{r}_{C,1}) & G(\boldsymbol{r}_{T,1}|\boldsymbol{r}_{C,2}) & \dots & G(\boldsymbol{r}_{T,1}|\boldsymbol{r}_{C,m}) \\ G(\boldsymbol{r}_{T,2}|\boldsymbol{r}_{C,1}) & G(\boldsymbol{r}_{T,2}|\boldsymbol{r}_{C,2}) & \dots & G(\boldsymbol{r}_{T,2}|\boldsymbol{r}_{C,m}) \\ \vdots & \vdots & \ddots & \vdots \\ G(\boldsymbol{r}_{T,n}|\boldsymbol{r}_{C,1}) & G(\boldsymbol{r}_{T,n}|\boldsymbol{r}_{C,2}) & \dots & G(\boldsymbol{r}_{T,n}|\boldsymbol{r}_{C,m}) \end{bmatrix}, \tag{6.2}$$

$$\boldsymbol{h} = [h_1, \quad h_2, \quad \dots, \quad h_m]^{\mathrm{T}}, \tag{6.3}$$

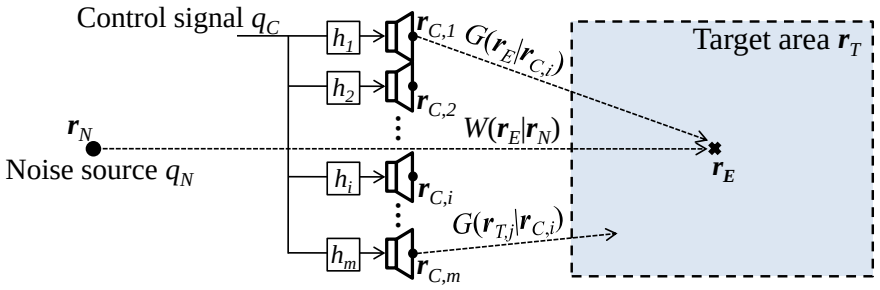

Figure 6.1: Diagrammatic sketch of the proposed global ANC approach

the superscript $^{\mathrm{T}}$ denotes the transpose, $\boldsymbol{r}_{T,j}$ ($\boldsymbol{r} = [x, y]$) is the position of a measurement point in the target area, $\boldsymbol{r}_{C,i}$ is the location of a unit in the loudspeaker array, n is the number of the measurement points in the target area, m is the number of the loudspeaker units, $G(\boldsymbol{r}_{T,j}|\boldsymbol{r}_{C,i})$ represents the transfer function of the acoustic path from the loudspeaker unit located in $\boldsymbol{r}_{C,i}$ to the point $\boldsymbol{r}_{T,j}$ in the target area.

The LS method minimizes the error $\boldsymbol{e}_R$ between the reproduced sound field $\boldsymbol{p}_R$ and the target sound field $\boldsymbol{p}_T$ to obtain the optimal input filter of the loudspeaker array. This is realized by minimizing the following cost function [158],

$$J_R = \boldsymbol{e}_R^{\mathrm{H}}\boldsymbol{e}_R + \lambda_R(\boldsymbol{h}^{\mathrm{H}}\boldsymbol{h} - h_0) = (\boldsymbol{G}\boldsymbol{h} - \boldsymbol{p}_T)^{\mathrm{H}}(\boldsymbol{G}\boldsymbol{h} - \boldsymbol{p}_T) + \lambda_R(\boldsymbol{h}^{\mathrm{H}}\boldsymbol{h} - h_0), \tag{6.4}$$

where the superscript $^{\mathrm{H}}$ denotes the Hermitian transpose. The second term of Eq. (6.4) is for limiting the input power $\boldsymbol{h}^{\mathrm{H}}\boldsymbol{h}$ to within a given value h_0, and λ_R is the Lagrange multiplier that is a real and positive number. The optimal input filter $\boldsymbol{h}$ of the loudspeaker array given by the LS method is

$$\boldsymbol{h} = (\boldsymbol{G}^{\mathrm{H}}\boldsymbol{G} + \lambda_R\boldsymbol{I})^{-1}\boldsymbol{G}^{\mathrm{H}}\boldsymbol{p}_T, \quad \boldsymbol{h}^{\mathrm{H}}\boldsymbol{h} = h_0. \tag{6.5}$$

The value of Lagrange multiplier λ_R is determined by satisfying the input power constraint $\boldsymbol{h}^{\mathrm{H}}\boldsymbol{h} = h_0$.

The target sound field $\boldsymbol{p}_T$ is determined according to the properties of the primary noise. If the locations of the primary noise sources and the transfer functions from the noise sources to the target area can be predicted, $\boldsymbol{p}_T$ can be easily given. When the information of the noise sources is unknown, $\boldsymbol{p}_T$ can be estimated according to the specific occasions where the system is used. For example, if the noise sources are far from the target area of control, such as the occasion in the application of an active window [75] reducing the incident traffic noise into a room where the noise sources are the vehicles on the road, the primary noise waves in the target area can be approximated by a series of planar waves, and therefore, $\boldsymbol{p}_T$ can be set as the sound pressure distribution of planar waves.

6.2.2 Calculation of the source strength for active noise control

The global ANC system using the proposed approach minimizes the sound pressure at the position of the control point $\boldsymbol{r}_E$ by using the loudspeaker array as the control source, of which the input signal is filtered by the filter $\boldsymbol{h}$ obtained above. Therefore, the cost function of the system to be minimized can be defined as

$$J_C = e_C^* e_C = (q_N W + q_C \boldsymbol{G}_E \boldsymbol{h})^*(q_N W + q_C \boldsymbol{G}_E \boldsymbol{h}), \tag{6.6}$$

where the superscript * denotes the complex conjugate, q_N is the strength of the noise source, q_C is the control source strength. $W(\boldsymbol{r}_E|\boldsymbol{r}_N)$ is the transfer function of the

primary path from the location of the noise source $\boldsymbol{r}_N$ to the control point $\boldsymbol{r}_E$, and $(\boldsymbol{r}_E|\boldsymbol{r}_N)$ is omitted in Eq. (6.6) for convenience. $\boldsymbol{G}_E$ is a row of the matrix $\boldsymbol{G}$ denoting the transfer functions from the loudspeaker units to the control point $\boldsymbol{r}_E$, which is defined as

$$\boldsymbol{G}_E = [G(\boldsymbol{r}_E|\boldsymbol{r}_{C,1}), \quad G(\boldsymbol{r}_E|\boldsymbol{r}_{C,2}), \quad \ldots, \quad G(\boldsymbol{r}_E|\boldsymbol{r}_{C,m})]\,. \tag{6.7}$$

Accordingly, the control source strength q_C to minimize the cost function based on the FF control strategy can be given by

$$q_C = -(\boldsymbol{G}_E\boldsymbol{h})^{-1}Wq_N. \tag{6.8}$$

In Eq. (6.8), the noise source strength q_N is applied as the reference signal of the FF control by assuming the signal of the primary noise can be obtained by a microphone ideally.

In order to compare the ANC system using the proposed approach with the conventional SISO and MIMO ANC systems, the calculation of the control strengths for the SISO and MIMO ANC system are also given here. The SISO ANC system uses one loudspeaker to control the noise sound pressure at the control point $\boldsymbol{r}_E$ so that the cost function of the system is

$$J_S = e_S^* e_S = (q_N W + q_S G_S)^*(q_N W + q_S G_S), \tag{6.9}$$

where q_S is the control strength for the SISO ANC system, G_S is the transfer function from the control source $\boldsymbol{r}_{C,i}$ to the control point $\boldsymbol{r}_{C,i}$, and $(\boldsymbol{r}_E|\boldsymbol{r}_{C,i})$ is omitted for convenience. Therefore, q_S to minimize the cost function can be written as [36]

$$q_S = -G_S^{-1}Wq_N, \tag{6.10}$$

The MIMO ANC system minimizes the sound pressures at a number of control points. Therefore, the cost function can be defined as

$$J_M = \boldsymbol{e}_M^{\mathrm{H}}\boldsymbol{e}_M = (\boldsymbol{W}_M q_N + \boldsymbol{G}_M\boldsymbol{q}_M)^{\mathrm{H}}(\boldsymbol{W}_M q_N + \boldsymbol{G}_M\boldsymbol{q}_M), \tag{6.11}$$

where $\boldsymbol{W}_M$ is a vector of the transfer functions from the noise source $\boldsymbol{r}_N$ to the control points $\boldsymbol{r}_E$, and $\boldsymbol{G}_M$ is a matrix of the transfer functions from the control sources $\boldsymbol{r}_{C,i}$ to the control points $\boldsymbol{r}_E$, which are respectively defined as

$$\boldsymbol{W}_M = [W(\boldsymbol{r}_{E,1}|\boldsymbol{r}_N), \quad W(\boldsymbol{r}_{E,2}|\boldsymbol{r}_N), \quad \ldots, \quad W(\boldsymbol{r}_{E,l}|\boldsymbol{r}_N)]^{\mathrm{T}}\,, \tag{6.12}$$

$$\boldsymbol{G}_M = \begin{bmatrix} G(\boldsymbol{r}_{E,1}|\boldsymbol{r}_{C,1}) & G(\boldsymbol{r}_{E,1}|\boldsymbol{r}_{C,2}) & \ldots & G(\boldsymbol{r}_{E,1}|\boldsymbol{r}_{C,m}) \\ G(\boldsymbol{r}_{E,2}|\boldsymbol{r}_{C,1}) & G(\boldsymbol{r}_{E,2}|\boldsymbol{r}_{C,2}) & \ldots & G(\boldsymbol{r}_{E,2}|\boldsymbol{r}_{C,m}) \\ \vdots & \vdots & \ddots & \vdots \\ G(\boldsymbol{r}_{E,l}|\boldsymbol{r}_{C,1}) & G(\boldsymbol{r}_{E,l}|\boldsymbol{r}_{C,2}) & \ldots & G(\boldsymbol{r}_{E,l}|\boldsymbol{r}_{C,m}) \end{bmatrix}, \tag{6.13}$$

and l is the number of the control points. Accordingly, the control source strength vector $\boldsymbol{q}_M$ can be given by [36]

$$\boldsymbol{q}_M = -(\boldsymbol{G}_M^{\mathrm{H}}\boldsymbol{G}_M)^{-1}(\boldsymbol{G}_M^{\mathrm{H}}\boldsymbol{W}_M)q_N, \tag{6.14}$$

Comparing with Eq. (6.8), the inverse problem of $(\boldsymbol{G}_M^{\mathrm{H}}\boldsymbol{G}_M)^{-1}$ to calculate the control strength $\boldsymbol{q}_M$ in Eq. (6.14) means more complex control algorithm. A comparison of the performance of the proposed system and the SISO, MIMO ANC systems will be conducted in Section 6.3.2.

6.3 A global active noise control system using planar wave synthesis

This section presents a system realization of the proposed approach to global ANC using wavefront synthesis, and the performance of this system is investigated by numerical simulations to demonstrate the effectiveness of the approach.

6.3.1 System description

The scenario considered here is shown in Fig. 6.2(a), where the control objective is to achieve the overall noise reduction in an area around the listener. A linear loudspeaker array is used as the control source to cancel the noise at the control point $\boldsymbol{r}_E$ that is supposed to be located at the head position of the listener. If the noise source is far from the listener, the incident noise propagates in the target area as planar waves. Therefore, the target field $\boldsymbol{p}_T$ can be set as a series of the sound pressures associated with the planar wave as

$$\boldsymbol{p}_T(\boldsymbol{r}) = A\mathrm{e}^{jk\boldsymbol{n}_p\boldsymbol{r}^{\mathrm{T}}}, \tag{6.15}$$

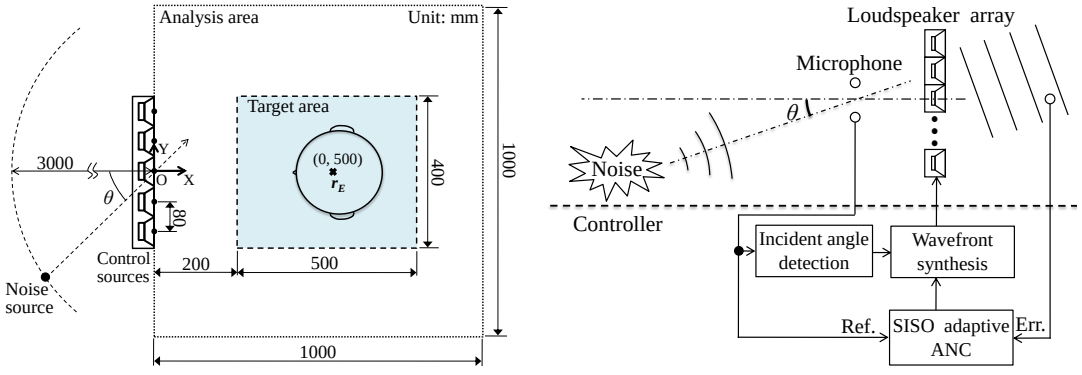

(a) An illustration to show the control objective and the analysis geometry

(b) Block diagram of the assumed system structure

Figure 6.2: ANC system based on planar wave synthesis

to obtain the loudspeaker array input filter $\boldsymbol{h}$ according to Eq. (6.5), where A is the complex amplitude of the planar wave, j is the imaginary unit, k is the wave number, $\boldsymbol{n}_p = [\cos\theta, \sin\theta]$ is the normal vector of the planar wavefront, and θ is the incident angle of the primary noise.

Figure 6.2(b) shows the assumed system structure that consists of three parts. The first part is to detect the incident angle θ, which can be realized by any sound source localization techniques such as the method using two microphones proposed in Ref. [159]. The second part is a loudspeaker array system to synthesize planar waves according to the incident angle θ. The high computational complexity of solving the inverse problem in Eq. (6.5) makes the calculation of the input filter $\boldsymbol{h}$ of the loudspeaker array difficult to be implemented in the real-time control system. Therefore, an approach that prepares a set of input filters for different incident angles in advance, and switches the input filter during the control process could be more practical. The third part is a SISO ANC system to reduce the sound pressure at the control point where an error microphone is located. The reference signal of the ANC system can be obtained from the microphones used to detect the incident angle.

6.3.2 Numerical simulations

The simulations are conducted according to the analysis geometry in Fig. 6.2(a). The primary noise source and the loudspeaker units are considered as point sources, and the transfer functions of the acoustic paths use the free field Green's function which is defined as

$$G_{mn} = -j\omega\rho_0 \frac{\mathrm{e}^{jk\|\boldsymbol{r}_m - \boldsymbol{r}_n\|}}{4\pi\|\boldsymbol{r}_m - \boldsymbol{r}_n\|}, \tag{6.16}$$

where $\|\ \|$ denotes the norm of a vector. Five loudspeaker units are used in the simulations. The frequencies of interest are up to 2 kHz, and therefore, the distance between the loudspeaker units is set to be shorter than the half-wavelength at 2 kHz as 80 mm to avoid the spatial aliasing. The incident angle θ is assumed to be detected at the origin of the coordinate r_O. Because the distance between the noise source and the target area is much longer than the distance between r_O and the target area, θ is approximately equal to the real incident angle into the target area. A specified input power constraint is not considered in the simulations so that the Lagrange multiplier λ_R in Eq. (6.5) is set to be a very small number as 10^{-10}. The target area is discretized by 25×20 points at intervals of 2 cm, and the transfer functions from the loudspeakers to these discrete points are assumed to be known to calculate the input filter $\boldsymbol{h}$ of the loudspeaker array. The distance of 2 cm is small enough in comparison with the half-wavelength of the frequency of interest to ensure the reproduction performance. In addition, as the design process of $\boldsymbol{h}$ is supposed to be performed offline, a relatively large number of the discrete points in the target area will not increase the computational burden of the

real-time control system.

The first simulation investigates the quality of the reproduced planar waves in the target area. Figure 6.3 depicts the normalized reproduction error e_{RN}, which is defined

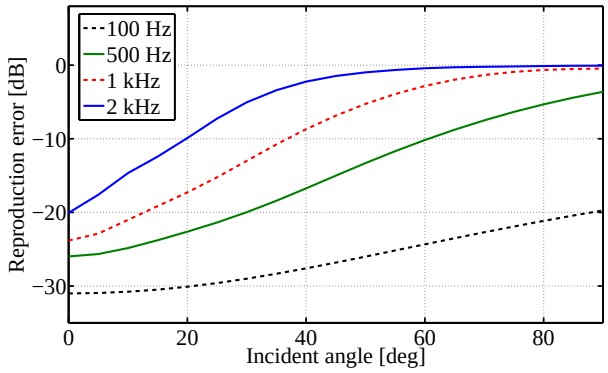

Figure 6.3: Normalized reproduction error with respect to the incident angles and the frequencies

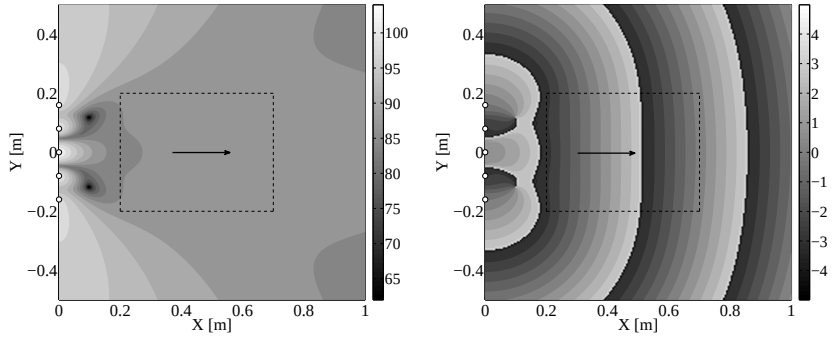

(a) Sound pressure level [dB] (b) Phase [rad]

Figure 6.4: The reproduced 1 kHz planar waves for $\theta = 0°$. "○" represents the point control source, and "→" represents the desired direction of the planar wave.

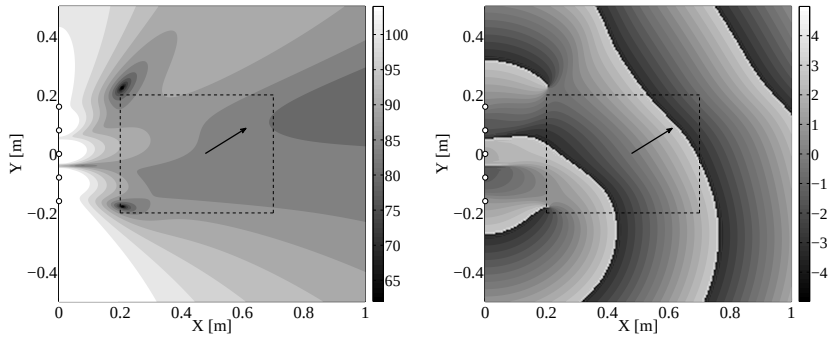

(a) Sound pressure level [dB] (b) Phase [rad]

Figure 6.5: The reproduced 1 kHz planar waves for $\theta = 45°$. "○" represents the point control source, and "→" represents the desired direction of the planar wave.

as

$$e_{RN} = 10 \log_{10} \frac{\boldsymbol{e}_R^{\mathrm{H}} \boldsymbol{e}_R}{\boldsymbol{p}_T^{\mathrm{H}} \boldsymbol{p}_T}, \tag{6.17}$$

with respect to the frequencies of interest and the incident angles. The result shows that planar waves can be reproduced more accurately at the low frequencies where the size of the target area is relatively small comparing with the wavelengths. When the incident angle is smaller than 20°, a reproduction of the planar waves with the errors smaller than -10 dB can be achieved for all of the frequencies below 2 kHz. However, as the incident angle increases, the high-quality reproduction can only be realized at low frequencies such as 100 Hz and 500 Hz. The reproduced 1 kHz tonal sound field with the incident angle of 0°, of which the normalized reproduction error is -24 dB, is shown in Fig. 6.4, and the reproduced sound field with the incident angle of 45°, of which the normalized reproduction error is -7 dB, is shown in Fig. 6.5 as examples. A uniform distribution of the sound pressure level (SPL), which is the desired field, is realized in the target area, and the phase distribution shows that the planar wavefronts propagate according to the incident angles in the target area.

Then, the effectiveness of the proposed system is validated by comparing it with the SISO and MIMO ANC systems. The SISO ANC system applies the center unit of the loudspeaker array as the control source to reduce the noise at the control point $\boldsymbol{r}_E$. The MIMO ANC system reduces the sound pressures at 5 × 5 control points, which are distributed equally in the control area. To evaluate the system performance, the reduction of the acoustic potential energy (APE) ER in the target area is used. ER is defined as

$$ER = 10 \log_{10} \frac{\boldsymbol{p}_E^{\mathrm{H}} \boldsymbol{p}_E}{\boldsymbol{p}_N^{\mathrm{H}} \boldsymbol{p}_N}, \tag{6.18}$$

where $\boldsymbol{p}_N$ is the sound pressures of the primary noise in the target area, and $\boldsymbol{p}_E$ is the sound pressures in the target area after control.

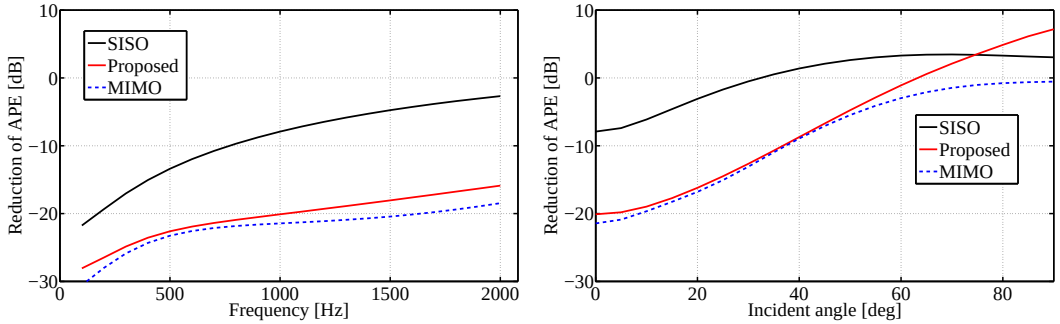

(a) Reduction of the APE with respect to the frequencies for $\theta = 0°$

(b) Reduction of the APE with respect to the incident angles for the 1 kHz tonal sound

Figure 6.6: A comparison of the performance of the SISO, MIMO and proposed ANC system

Figure 6.6(a) shows the reduction of the APE with respect to the frequencies of interest where the incident angle θ is 0°. In this case, all of the three ANC systems can reduce the APE in the target area over the frequency band of interest. However, the reduction of the APE decreases at higher frequencies due to the smaller quiet zone in the target area according to the wavelength. The proposed and MIMO system provide much larger noise reduction than the SISO system. The result reveals that the proposed system, which controls the sound pressure at one control point, can achieve a similar level of noise reduction with the MIMO system for the case $\theta = 0°$. Even though the noise reduction performance difference between the proposed and MIMO system becomes larger as the frequency increases, it is still less than 3 dB at 2 kHz. To demonstrate the noise reduction result in detail, Fig. 6.7 shows the noise reduction contour for the 1 kHz tonal sound in the analysis area. The SISO system can guarantee the noise reduction around the control point. However, the noise reduction at the positions close to the control source decreases because of the different propagation property of the primary noise and the control sound in the near field of the control

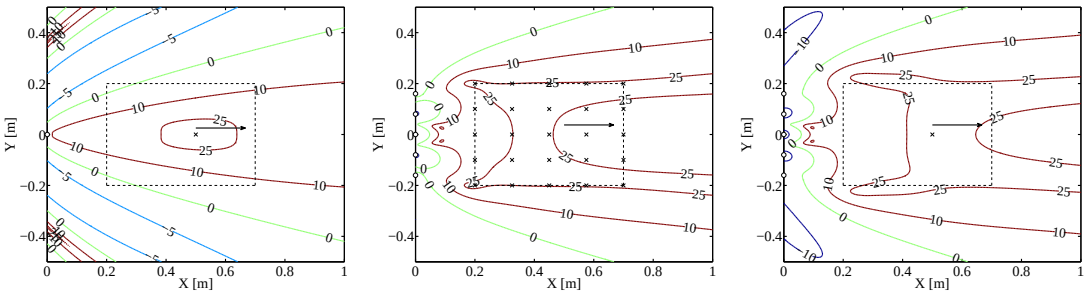

(a) SISO (b) MIMO (c) Proposed

Figure 6.7: Reduction of the SPL [dB] for the 1 kHz tonal sound where $\theta = 0°$. "○" represents the point control source, "→" represents the propagation direction of the primary noise wave, and "×" represents the control point.

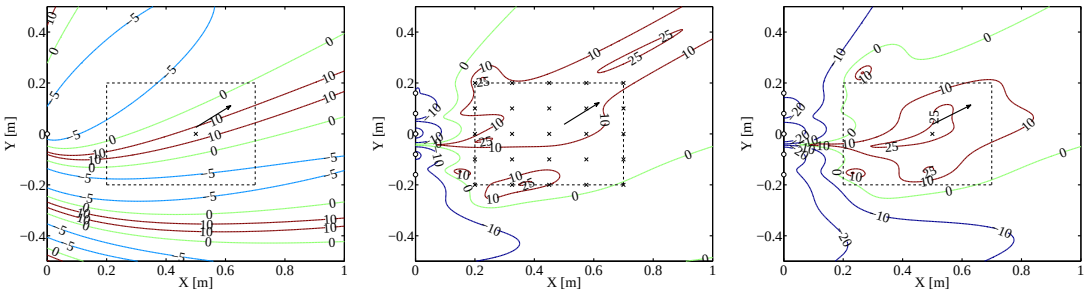

(a) SISO (b) MIMO (c) Proposed

Figure 6.8: Reduction of the SPL [dB] for the 1 kHz tonal sound where $\theta = 45°$. "○" represents the point control source, "→" represents the propagation direction of the primary noise wave, and "×" represents the control point.

source [48]. The proposed and MIMO system can create a larger quiet zone, and the result also indicates that the proposed system can create a similar noise reduction distribution with the MIMO system.

Figure 6.6(b) shows the reduction of the APE with respect to the incident angles for the 1 kHz tonal sound. The performance of the three systems reduces as the incident angle increases. When the incident angle is small, all of the three systems can effectively reduce the APE in the target area. For the incident angles larger than about 35°, however, the SISO system increase the APE in the target area. The proposed system can reduce the APE for a larger incident angle up to about 65°, and the MIMO system has the best noise reduction performance that will not increase the APE regardless of the incident angles. The proposed and MIMO system has the similar noise reduction performance if the incident angle of the noise is smaller than about 45° because the planar wave reproduction accuracy is relatively high for the small the incident angles. Figure 6.8 depicts the noise reduction contour for the 1 kHz tonal sound where the incident angle is 45°. Although the MIMO system can reduce the APE better than the proposed system, the resulted noise reduction is distributed unequally in the target area, and the largest noise reduction is obtained outside the target area. The proposed system creates a large enough quiet zone with at least 10 dB noise reduction around the control point in the target area.

In the above simulations, the distance between the noise source and the control source is set as 3 m. This distance relates to the distribution of the primary noise in the target area that influences the noise reduction performance. Therefore, the last simulation investigates the relation between the reduction of the APE in the target area and the noise source distance that is normalized by the wavelength λ. Figure 6.9 shows the result for the 1 kHz tonal sound. The performance of the SISO and MIMO system reduces as the distance becomes large, whereas the proposed system shows a different trend. When the distance is small, the reduction of the APE provided by the proposed

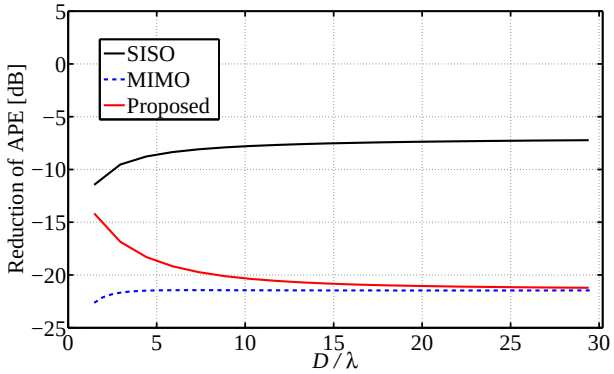

Figure 6.9: Reduction of the APE with respect to the normalized distance of the noise source

system is smaller than that of the MIMO system. However, as the noise source distance increases, the primary noise field can be approximated by a planar wave field so that the performance difference between the proposed and MIMO system becomes small. When the normalized distance is larger than about 10λ, the proposed system can achieve a good noise reduction performance steadily. Figure 6.10 shows the change in the SPL for the different normalized distance D/λ. When $D = 1\lambda$, the primary noise wavefronts which are still spherical mismatch with the planar wavefronts of the control sound so that quiet zone is small. When $D = 3\lambda$, the area with at least 10 dB noise reduction becomes large, whereas the area with higher noise reduction in the target area does not enlarged in comparison with the $D = 1\lambda$ case. When $D = 10\lambda$, the primary noise wavefronts becomes planar, and therefore, in the target area, the extent of quiet zone with high noise reduction is the largest among these three normalized distance cases, which is the most desired control result.

6.4 Summary

This chapter proposed an approach to global noise reduction in the target area by controlling the sound pressure at a local point. The basic concept is to divide a global ANC system into two sub-systems according to the different control objectives. One is a loudspeaker array system to reproduce the shape of the incident noise wavefront into the target area, and the other is a SISO ANC system to adjust the amplitude and phase of the reproduced wavefront. A realization of the proposed global control approach, which is supposed to be used in the occasion where the noise source is far from the target area and the incident noise wave can be seen as a series of planar waves, was presented. This system applies a linear loudspeaker array to reproduce a planar control sound field with different incident angles and applies a SISO ANC system to compute the control sound signal. The effectiveness of this system was verified by

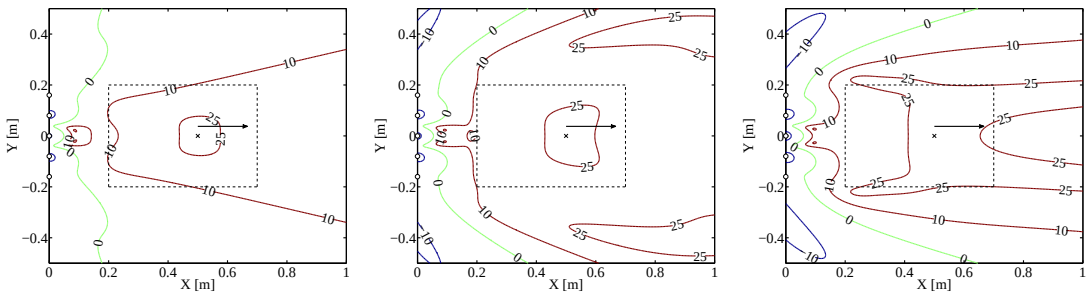

(a) $D = 1\lambda$ (b) $D = 3\lambda$ (c) $D = 10\lambda$

Figure 6.10: Reduction of the SPL [dB] for the different normalized distance where $\theta = 0°$. "$\circ$" represents the point control source, "$\rightarrow$" represents the propagation direction of the primary noise wave, and "$\times$" represents the control point.

several numerical simulations. The results show that the proposed system can achieve an overall noise reduction in the target area regardless of the incident angles of the noise by controlling the sound pressure at a local point. When the noise source locates from the target area by a distance larger than about ten times of the wavelength of interest, the ANC system based on the planar wave synthesis can achieve a similar noise reduction performance with a MIMO global ANC system. It is noteworthy that the control sound waves have not to be planar. In the case when the property of the noise source is predictable, the input filter of the loudspeaker array can be designed to the reproduce the primary noise wavefronts, and the proposed approach will also be effective in achieving the global noise reduction. In Appendix D, the concept of performing ANC by using a wavefront controlled loudspeaker array in this chapter is expanded, and an approach to creating a quiet zone of arbitrary shape is presented and investigated.

Chapter 7

Conclusions

Two primary problems of the acoustic environment in open-plan offices are the unacceptable background noise level and the insufficient speech privacy. This thesis focuses on the development of a small-typed ANB system in order to improve the acoustic quality in open-plan offices. This ANB system is composed of an office partition and an active sound control system integrated into the partition, which exploits the ANC and the sound masking techniques simultaneously to relieve the acoustic problems in the workspace related to the background noise and the speech privacy. The ANC part in the proposed ANB system aims to create a quiet zone around the listener behind the partition, and the sound masking part covers the residual sound to improve the speech privacy and to reduce the acoustic distractions. The ANC and the sound masking parts were investigated respectively, and then, the sound proof system combining these two active control techniques was constructed and investigated in the thesis.

In the context of ANC, in order to improve the noise attenuation performance of the ANB, a novel HB control strategy, which controls the diffracting edge of the noise barrier using FB control and reduces the noise at the head position of the listener behind the partition using FF control simultaneously, was proposed.

First, the robustness and waterbed effect induced noise amplification problem of the FB control, which is important for a practical controller, was investigated. Two adaptive methods for designing a robust FB controller was proposed. The first method applies the proposed MFDB-LMS algorithm to update the FB control filter, and the robust stability condition and the noise amplification constraint is verified in the frequency domain adaptation. Several simulations were conducted to validate the effectiveness of the method. The results demonstrate that the proposed frequency domain method can effectively guarantee the robust stability of an FB-ANC system, and can limit the noise amplification to within a given value. However, the MFDB-LMS algorithm is of higher computational cost in comparison with the time domain LMS algorithm. Therefore, a time domain method was also proposed. This method determines an equivalent time domain constraint for the robust stability condition and maximum noise amplification

constraint in the frequency domain, which is a maximum value constraint for the FIR filter coefficients. Consequently, a robust IMC controller can be designed by using any time domain adaptive algorithms. Several simulations and experiments were conducted to validate the effectiveness of the method. The simulation and experimental results indicate that the proposed method is effective for designing a robust controller and for limiting the maximum noise amplification for both the online and offline controller design processes. In comparison with the conventional design methods of the robust FB controllers, both of the proposed design methods can keep the FB controller adaptive so that it can be more effective in the practical applications where the primary noise is time-variant.

Then, the ANB using the HB control strategy was investigated. In order to suppress the waterbed effect induced noise amplification propagating into the control area, a technique that exploits the HB control structure to cancel the noise amplification was proposed. The system implementation of these control strategies was presented, and a prototype ANB was implemented. The noise attenuation performance of the ANB system under different sound field configurations was investigated by simulations and experiments. It was confirmed from the results that the HB control can improve the ANB performance at low frequencies, and the waterbed effect cancellation technique can reduce the noise amplification propagating into the control area effectively. The simulation results also indicate that the ANB is most effective for the sound field where there is little side diffraction and little reflection. For other sound fields, even though the side diffraction and the reflection lead to the spatial non-uniformity and deterioration of the noise attenuation, the low frequency noise attenuation can be achieved in a wide area behind the ANB, and noise attenuation for a wide frequency range can be ensured around the control point. Eventually, an experiment was conducted to verify the performance of the proposed ANB in a real office room. In this practical application, the ANB achieved about 3 – 8 dB noise attenuation in the control area when the background noise is relatively small, which confirms the effectiveness of using this ANB system to reduce undesired sounds in offices.

The aim of the sound masking part in this thesis is to select an appropriate masker for the sound masking systems used in offices. Using sound masking systems in the workspace has two objectives. One is to prevent the information leakage, and the other is to help the employees concentrate. The first objective requires high masking efficiency and effectiveness, and the latter one requires low annoyance of the maskers. Accordingly, five representative energetic and informational maskers including band-limited pink noise, target spectrum based random noise, frequency-reversed masker, time-reversed masker, and a synthesized environment noise were investigated from the viewpoints of sound masking efficiency and annoyance by two listening experiments. The results of Experiment I suggest that if the requirement of speech privacy is strict,

the energetic maskers or the mixed-type maskers of large power are more effective than the informational maskers. Experiment II implies that the stationary maskers are preferred if the main purpose of the sound masking is to improve the concentration of the employees in the workplace rather than to protect the speech privacy. According to the experimental results, a comprehensive evaluation criterion that identifies the masker achieving a certain speech intelligibility with the lowest annoyance was presented.

Based on the above investigations, a sound proof system that integrates the sound masking techniques into the ANB system was proposed and implemented. The ANB applies the HB-ANC system to cancel the target speech, and the frequency-reversed masker is output via the loudspeaker used as the FF control source to cover the residual sound. The performance of the proposed system was validated by simulations. The results demonstrate that the proposed system can achieve the same privacy level by using smaller masker sound, which implies the simultaneous realization of the quietness and the speech privacy in the workspace can be expected.

Additionally, an approach to achieving overall noise attenuation in a certain area by using simple system configuration was proposed with the aim of improving the performance of the FF control part of the HB control strategy. The basic idea of this approach is to divide a global ANC system into two sub-systems according to the different control objectives. One is a loudspeaker array system to reproduce the incident noise wavefront into the target area, and the other is a SISO ANC system to synthesize the control sound. A system realization using the proposed approach, which is supposed to be used in the case where the noise source is far from the target area and the incident noise wave can be seen as a series of planar waves, was presented. The effectiveness of this system was verified by numerical simulations. The results show that the proposed system can achieve an overall noise reduction in the target area by controlling the sound pressure at a local point. It is noteworthy that the control sound waves have not to be planar. In the case when the property of the noise source is predictable, the input filter of the loudspeaker array can be designed to the reproduce the primary noise wavefronts, and the proposed approach will also be effective in achieving the global noise reduction. By introducing this approach into the ANB system, the actively created quiet zone can be enlarged without increasing the complexity of the control algorithm and the hardware configuration of the system much.

Appendix A

Definitions of the Causality Operators

This appendix presents the definitions and properties of the causality operator $\{\ \}_+$ [142]. By expressing the frequency domain signal of a time series $x(n)$ as

$$\boldsymbol{X}(n) = \boldsymbol{F}[x(n-2L+1),\ x(n-2L+2),\ \ldots,\ x(n)], \tag{A.1}$$

where $\boldsymbol{F}$ denotes the DFT and L is the length of the vector, the causal part $\{\boldsymbol{X}(n)\}_+$ and the non-causal part $\{\boldsymbol{X}(n)\}_-$ are respectively defined as

$$\{\boldsymbol{X}(n)\}_+ = \boldsymbol{F}[x(n-2L+1),\ \ldots,\ x(n-L), \boldsymbol{0}_{1\times L}], \tag{A.2}$$

$$\{\boldsymbol{X}(n)\}_- = \boldsymbol{F}[\boldsymbol{0}_{1\times L},\ x(n-L+1),\ \ldots,\ x(n)]. \tag{A.3}$$

To obtain the causal part of frequency domain signals by the calculation of matrices and vectors, a partial zero matrix $\boldsymbol{Z}_{L,0}$,

$$\boldsymbol{Z}_{L,0} = \begin{bmatrix} \boldsymbol{I}_{L\times L} & \boldsymbol{0}_{L\times L} \\ \boldsymbol{0}_{L\times L} & \boldsymbol{0}_{L\times L} \end{bmatrix}, \tag{A.4}$$

is defined [140] so that the causal part $\{\boldsymbol{X}(n)\}_+$ can be calculated by

$$\{\boldsymbol{X}(n)\}_+ = \boldsymbol{F}\boldsymbol{Z}_{L,0}\boldsymbol{F}^{-1}\boldsymbol{X}(n), \tag{A.5}$$

as the usage in Section 2.3.1.

The following properties of the causality operators can be easily obtained from the definitions in Eq. (A.2) and Eq. (A.3).

$$\boldsymbol{X}(n) = \{\boldsymbol{X}(n)\}_+ + \{\boldsymbol{X}(n)\}_-, \tag{A.6}$$

$$\{\boldsymbol{X}(n) + \boldsymbol{Y}(n)\}_+ = \{\boldsymbol{X}(n)\}_+ + \{\boldsymbol{Y}(n)\}_+, \tag{A.7}$$

$$\{\boldsymbol{X}(n) + \boldsymbol{Y}(n)\}_- = \{\boldsymbol{X}(n)\}_- + \{\boldsymbol{Y}(n)\}_-. \tag{A.8}$$

There are also several additional properties which can only be approximately true in practice, whereas the errors are small when the length of the signal buffer is long

enough [142].

$$\{\{\boldsymbol{X}(n)\}_+\{\boldsymbol{Y}(n)\}_+\}_+ = \{\boldsymbol{X}(n)\}_+\{\boldsymbol{Y}(n)\}_+, \tag{A.9}$$

$$\{\{\boldsymbol{X}(n)\}_-\{\boldsymbol{Y}(n)\}_-\}_- = \{\boldsymbol{X}(n)\}_-\{\boldsymbol{Y}(n)\}_-, \tag{A.10}$$

$$\{\{\boldsymbol{X}(n)\}_+\{\boldsymbol{Y}(n)\}_+\}_- = 0, \tag{A.11}$$

$$\{\{\boldsymbol{X}(n)\}_-\{\boldsymbol{Y}(n)\}_-\}_+ = 0. \tag{A.12}$$

Appendix B

A Reference to Determine the Feedback Control Bandwidth

This appendix presents a steady-state performance analysis of the IMC structured FB-ANC system shown in Fig. 2.3(a) and a numerical method to calculated the potential noise attenuation (PNA) of it.

B.1 Performance analysis based on the ideal secondary model

Equation (2.3) indicates that if the control filter is the negative inverse property of the secondary path, the IMC structured FB-ANC system can cancel the primary noise entirely. However, as the secondary path of an ANC system inevitably contains time delay that is composed of the propagation time of the control sound and the processing time of the electronic devices, the inverse property of such a non-minimum phase system, which is the desired controller property, is unstable. If an inherently stable FIR filter is used to approximate the inverse secondary path, the stability of the FB-ANC system can be easily ensured. Therefore, the optimal property of such an FIR filter is derived firstly in order to investigate the steady-state performance of the IMC structured FB-ANC system.

The optimal Wiener FIR filter can be written as follows [145] :

$$\boldsymbol{C}_{wopt}(z) = -\left\{\frac{\boldsymbol{P}_{xd}(z)}{\boldsymbol{P}_{xx}(z)}\right\}_{+} = -\frac{1}{\boldsymbol{S}(z)}\left\{\frac{\boldsymbol{P}_{xd}(z)}{\boldsymbol{S}(z^{-1})}\right\}_{+}, \tag{B.1}$$

where

$$\boldsymbol{P}_{xx}(z) = \boldsymbol{S}(z^{-1})\boldsymbol{S}(z). \tag{B.2}$$

$\boldsymbol{P}_{xd}(z)$ is the cross spectral density of the reference signal and the desired signal, $\boldsymbol{P}_{xx}(z)$ is the power spectral density of the reference signal, $\boldsymbol{S}(z)$ and $\boldsymbol{S}(z^{-1})$ are the spectral factors of $\boldsymbol{P}_{xx}(z)$. For the IMC structured FB-ANC system shown in Fig. 2.3(a), $\hat{d}_f(n)$ and $d(n)$ are the reference signal and the desired signal, respectively. By considering

$z = e^{j\omega}$,

$$\boldsymbol{S}(z^{-1}) = \boldsymbol{S}^*(z). \tag{B.3}$$

The non-minimum phase secondary path containing t-sample time delay can be expressed as

$$\boldsymbol{G}(z) = z^{-t}\boldsymbol{G}_{min}(z), \tag{B.4}$$

where $\boldsymbol{G}_{min}(z)$ is the minimum phase part of the secondary path $\boldsymbol{G}(z)$. The power spectral density $\boldsymbol{P}_{xx}(z)$ can be written as

$$\boldsymbol{P}_{xx}(z) = |\hat{\boldsymbol{G}}(z)|^2 \boldsymbol{P}_{\hat{d}\hat{d}}(z), \tag{B.5}$$

in which,

$$|\hat{\boldsymbol{G}}(z)|^2 = \hat{\boldsymbol{G}}^*_{min}(z)\hat{\boldsymbol{G}}_{min}(z), \tag{B.6}$$

$$\boldsymbol{P}_{\hat{d}\hat{d}}(z) = \boldsymbol{S}^*_{\hat{d}}(z)\boldsymbol{S}_{\hat{d}}(z), \tag{B.7}$$

$\boldsymbol{P}_{\hat{d}\hat{d}}(z)$ is the power spectral density of $\hat{d}(n)$, and $\boldsymbol{S}_{\hat{d}}(z)$ is its spectral factor. From the above equations,

$$\boldsymbol{S}(z) = \hat{\boldsymbol{G}}_{min}(z)\boldsymbol{S}_{\hat{d}}(z), \tag{B.8}$$

$$\boldsymbol{P}_{xx}(z) = [\hat{\boldsymbol{G}}^*_{min}(z)\boldsymbol{S}^*_{\hat{d}}(z)][\hat{\boldsymbol{G}}_{min}(z)\boldsymbol{S}_{\hat{d}}(z)], \tag{B.9}$$

can be established. The cross spectral density $\boldsymbol{P}_{xd}(z)$ can be written as

$$\boldsymbol{P}_{xd}(z) = \hat{\boldsymbol{G}}^*(z)\boldsymbol{S}^*_{\hat{d}}(z)\boldsymbol{S}_d(z), \tag{B.10}$$

where $\boldsymbol{S}_d(z)$ is the spectral factor of the desired signal $d(n)$. Substitute Eq. (B.9) and Eq. (B.10) to Eq. (B.1),

$$\boldsymbol{C}_{wopt}(z) = -\frac{1}{\hat{\boldsymbol{G}}_{min}(z)} \frac{\{z^t \boldsymbol{S}_d(z)\}_+}{\boldsymbol{S}_{\hat{d}}(z)}, \tag{B.11}$$

can be obtained. The relation between $d(n)$ and $\hat{d}(n)$ can be derived from the block diagram shown in Fig. 2.3(a) as

$$\boldsymbol{D}(z) = [1 - \boldsymbol{C}(z)(\boldsymbol{G}(z) - \hat{\boldsymbol{G}}(z))]\hat{\boldsymbol{D}}(z). \tag{B.12}$$

In the ideal secondary path model case, $\boldsymbol{D}(z) \approx \hat{\boldsymbol{D}}(z)$, so that

$$\boldsymbol{S}_d(z) \approx \boldsymbol{S}_{\hat{d}}(z). \tag{B.13}$$

Therefore, Eq. (B.11) can be rewritten as

$$\boldsymbol{C}_{wopt}(z) = -\frac{1}{\boldsymbol{G}_{min}(z)} \frac{\{z^t \boldsymbol{S}_d(z)\}_+}{\boldsymbol{S}_d(z)}. \tag{B.14}$$

where $\left\{z^t \boldsymbol{S}_d(z)\right\}_+ / \boldsymbol{S}_d(z)$ is the optimal property of a linear predictor to estimate the primary noise signal in t-sample advance. Therefore, in the ideal case where the inverse property of the minimum phase system $\boldsymbol{G}_{min}(z)$ can be calculated precisely, the IMC structured FB-ANC system is equivalent to a linear prediction system shown in Fig. B.1, and its noise attenuation performance depends on the time delay t and the predictability of the primary noise. This result derived from the optimal frequency response of the casual FIR filter is same with that obtained in Ref. [127] by directly solving the Wiener-Hopf equation of the IMC structured FB-ANC system.

B.2 Potential noise attenuation

The PNA of the IMC structured FB-ANC system can be predicted according to the optimal Wiener filter theory in order to determine the system parameters such as the target bandwidth of control. The power of the error signal $e^2_{min}(n)$ in a system using the optimal Wiener filter can be expressed as follows [35] :

$$E[e^2_{min}(n)] = E[d^2(n)] + \boldsymbol{c}^{\mathrm{T}}_{opt}\boldsymbol{R}\boldsymbol{c}_{opt} - 2\boldsymbol{c}^{\mathrm{T}}_{opt}\boldsymbol{p} = E[d^2(n)] - \boldsymbol{p}^{\mathrm{T}}\boldsymbol{R}^{-1}\boldsymbol{p}. \tag{B.15}$$

where $E[\ ]$ is the expectation operator, $\boldsymbol{c}_{opt}$ is the optimal filter coefficient vector, $\boldsymbol{R}$ is the auto-correlation matrix of the reference signal $\hat{d}_f(n)$, and $\boldsymbol{p}$ is the cross-correlation vector between the reference signal $\hat{d}_f(n)$ and the desired signal $d(n)$. In the ideal case, $\hat{d}_f(n)$ is a t-sample delayed signal of $d(n)$.

By reforming Eq. (B.15), PNA can be written as

$$PNA = 10\log_{10}\left(\frac{E[e^2_{min}(n)]}{E[d^2(n)]}\right) = 10\log_{10}\left(1 - \frac{\boldsymbol{p}^{\mathrm{T}}\boldsymbol{R}^{-1}\boldsymbol{p}}{E[d^2(n)]}\right). \tag{B.16}$$

Therefore, if the time delay t and the statistic properties of the primary noise can be predicted in advance, the PNA of the FB-ANC system can be calculated by using Eq. (B.16).

For an example, the PNA for the band-limited white noise is calculated. Figure B.2(a) depicts the PNA for the white noise with the normalized bandwidth (NB) of 0.1 with respect to the time delay t. The NB is defined as the ration between the

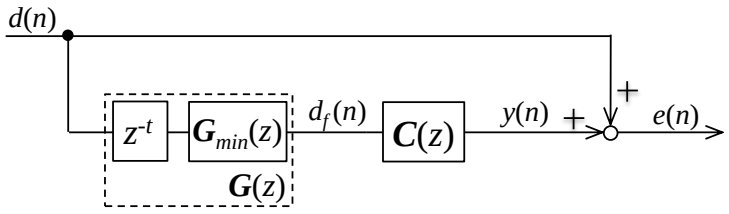

Figure B.1: Block diagram of the equivalent IMC structured FB-ANC system based on the ideal secondary path model

noise bandwidth b_w and the Nyquist frequency f_{Ny} that is the one-half of the sampling frequency,

$$NB = \frac{b_w}{f_{Ny}}. \tag{B.17}$$

Figure B.2(b) shows the PNA result with respect to the NB in the case where the time delay is 0.25 ms. The results suggest that in order to obtain sufficient noise attenuation, it is necessary to shorten the time delay in the FB-ANC system and to use a large enough sampling frequency comparing with the bandwidth of the primary noise. In addition, for the case in which the FB-ANC system is used to reduce the broadband noise within a certain frequency bandwidth, the PNA can be seen as the achievable noise attenuation within the target bandwidth.

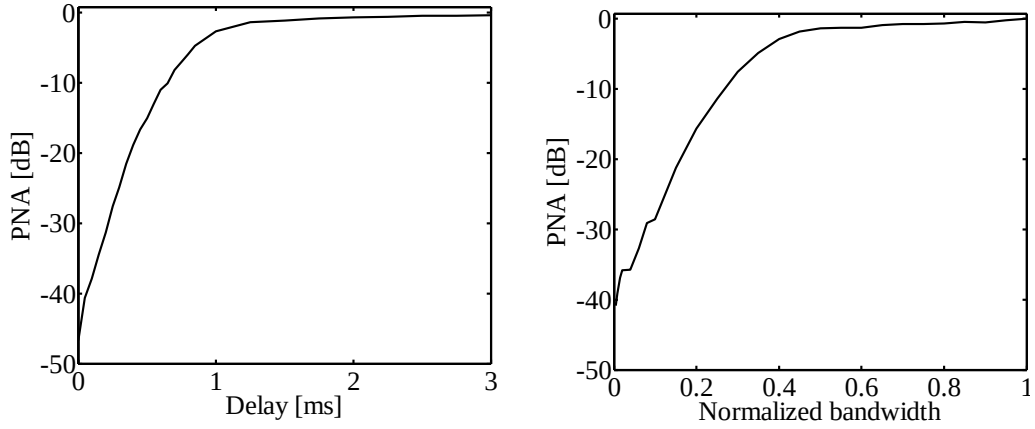

(a) PNA against delay ($NB = 0.1$) (b) PNA against NB ($t = 0.25$ ms)

Figure B.2: PNA of the IMC feedback ANC system for the band-limited white noise

Appendix C

Influence of Feedback Controller Performance on the Active Noise Barrier Performance

This appendix investigates the trade-off between the noise amplification constraint of the FB controller and the noise attenuation performance of the ANB using FB control by simulations.

The simulations are performed under the sound field configuration 1 shown in Fig. 3.4 where the sound reflection and the side diffraction from one side of the ANB do not exist. The FB controller is designed by the frequency domain method proposed in Chapter 2, and it is assumed that the model uncertainties are 5% at 1 Hz and 25% at 4 kHz. Two noise amplification constraints, 5 dB maximum noise amplification and only robust stability without noise amplification constraint, are considered in the simulations.

Figure C.1 shows the noise attenuation at the center FB control point. When the noise amplification is limited to within 5 dB, the noise attenuation at the control point becomes small due to the classic trade-off of the FB control.

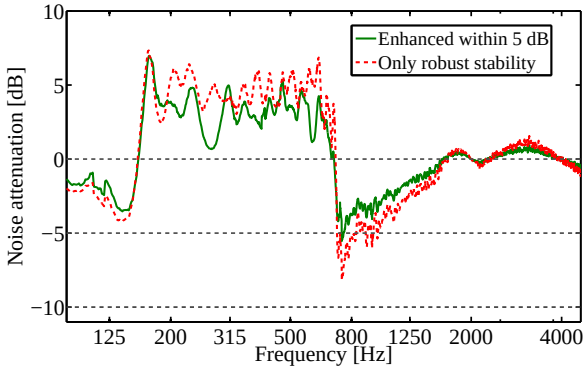

Figure C.1: Noise attenuation for the different noise amplification conditions at the center FB control point

The noise attenuation distributions in control area behind the ANB are shown in Fig. C.2 and Fig. C.3. The results at 250 Hz and 500 Hz 1/3 octave band as the representatives of the FB control bandwidth, and the results at 800 Hz and 1 kHz 1/3 octave band as the representatives of the waterbed effect bandwidth are depicted in the figures. In the control area, the primary noise is reduced within the FB control bandwidth, whereas the noise amplification exists at other frequencies. It can be confirmed that the noise amplification reduces in the control area if the noise amplification constraint is considered in the FB controller design. However, the noise attenuation in the control area also decreases. The waterbed effect cancellation strategy proposed in Section 3.2.2 can be an effective solution to this problem. Therefore, in order to guarantee the robustness and the noise attenuation performance of the HB-ANC system simultaneously, one can design the FB controller by only considering the robust stability condition and exploit the waterbed effect cancellation strategy to suppress the noise amplification in the control area.

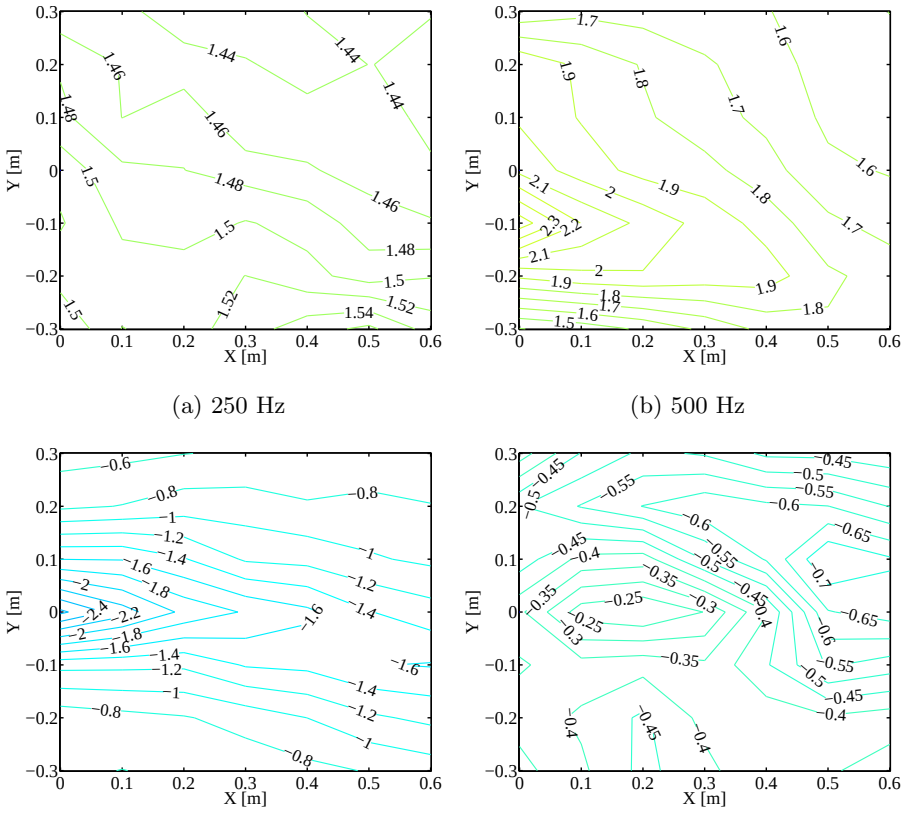

(a) 250 Hz

(b) 500 Hz

(c) 800 Hz

(d) 1 kHz

Figure C.2: Noise attenuation [dB] in the measurement area on the condition that the maximum noise enhancement is set to be 5 dB

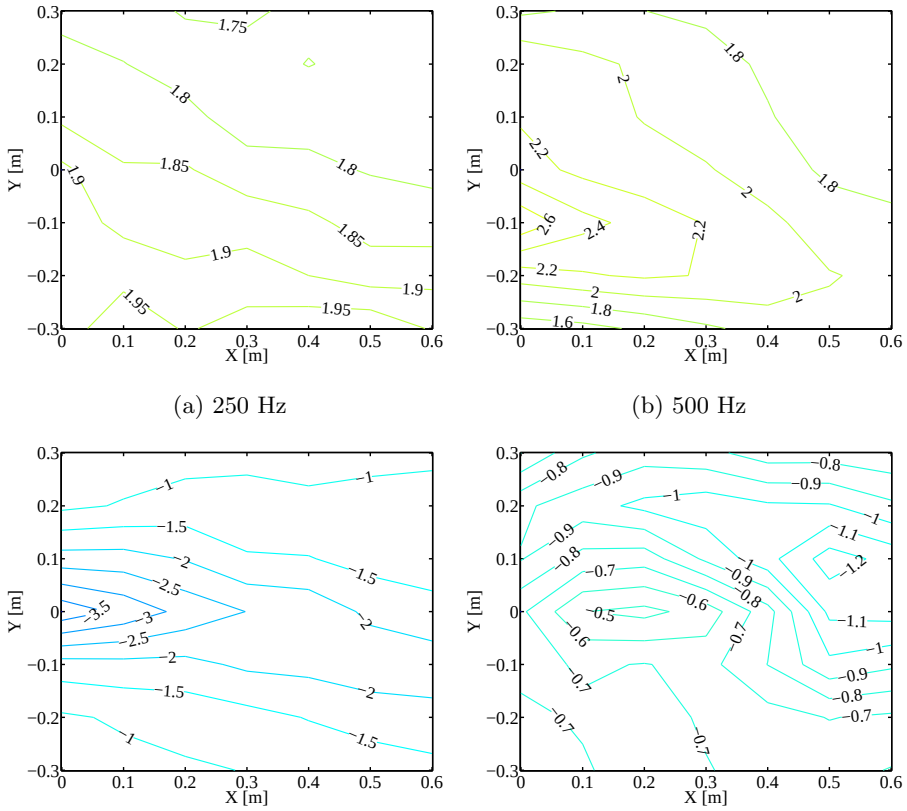

(a) 250 Hz

(b) 500 Hz

(c) 800 Hz

(d) 1 kHz

Figure C.3: Noise attenuation [dB] in the measurement area on the condition that only the robust stability is verified online

Appendix D

Drawing an Active Quiet Zone of Arbitrary Shape

In practical ANC applications, as the "undesired sound" is based on the subjective judgment of each person, the ANC systems should reduce the undesired sound for the target person and not change the acoustics at the others, which refers to "personal quiet zone". However, the majority of the works on ANC focus on the issues of improving the noise attenuation in the target area and enlarging the extent of the quiet zone, and only a few works [160–162] investigate the problem of creating a personal quiet zone without changing the acoustics outside the control area.

The personal quiet zone can be realized by using a parametric loudspeaker as the control source [160, 161] or a specified control algorithm for an MIMO ANC system [162]. Parametric loudspeakers take use of the ultrasonic sound as a carrier of the audible sound to realize the super-directional sound wave [66]. Therefore, using a parametric loudspeaker as the control source can project the control sound to a small area so that the noise amplification outside the target area can be suppressed. However, to emit the desired audible sound levels, 30 – 50 dB higher ultrasonic sound levels are needed [66, 163]. In the case where the primary noise is relatively large and so the control sound is, the exposure to ultrasound of high levels will affect the hearing and non-hearing parts of the human body even if the ultrasound is inaudible [164, 165].

In this appendix, two types of control approaches to the personal quiet zone using an array of the ordinary cone loudspeakers with a specified control algorithm are investigated. The first one is based on the direct formulation of the ANC in an area. The second approach is based on the concept of dividing the MIMO ANC system into a loudspeaker array system and a SISO ANC system described in Chapter 6, which aims to minimize the control sound power outside the target area. The second approach can simplify the hardware and control algorithm of such an MIMO ANC system.

The investigations of drawing a personal quiet zone with an arbitrary shape in this appendix are performed according to the geometry shown in Fig. D.1. The quiet zone

$\boldsymbol{V}_Q$ refers to the area where the primary noise should be reduced, and the sound pressure preserved zone $\boldsymbol{V}_P$ refers to the area where the acoustics should not be changed.

D.1 Direct solution

ANC is an optimization process to minimize the interfered sound pressures of the primary noise and the control sound at the control points, of which the cost function can be described by

$$J = \boldsymbol{e}^{\mathrm{H}}\boldsymbol{e} = (\boldsymbol{p}_N + \boldsymbol{p}_C)^{\mathrm{H}}(\boldsymbol{p}_N + \boldsymbol{p}_C), \tag{D.1}$$

where

$$\boldsymbol{p}_N = \boldsymbol{W} q_N, \tag{D.2}$$

$$\boldsymbol{p}_C = \boldsymbol{G}\boldsymbol{q}_C, \tag{D.3}$$

$$\boldsymbol{W} = [W(\boldsymbol{r}_1|\boldsymbol{r}_N),\ W(\boldsymbol{r}_2|\boldsymbol{r}_N),\ \ldots,\ W(\boldsymbol{r}_l|\boldsymbol{r}_N)]^{\mathrm{T}}, \tag{D.4}$$

$$\boldsymbol{G} = \begin{bmatrix} G(\boldsymbol{r}_1|\boldsymbol{r}_{C,1}) & G(\boldsymbol{r}_1|\boldsymbol{r}_{C,2}) & \ldots & G(\boldsymbol{r}_1|\boldsymbol{r}_{C,m}) \\ G(\boldsymbol{r}_2|\boldsymbol{r}_{C,1}) & G(\boldsymbol{r}_2|\boldsymbol{r}_{C,2}) & \ldots & G(\boldsymbol{r}_2|\boldsymbol{r}_{C,m}) \\ \vdots & \vdots & \ddots & \vdots \\ G(\boldsymbol{r}_l|\boldsymbol{r}_{C,1}) & G(\boldsymbol{r}_l|\boldsymbol{r}_{C,2}) & \ldots & G(\boldsymbol{r}_l|\boldsymbol{r}_{C,m}) \end{bmatrix}, \tag{D.5}$$

$\boldsymbol{r}$ is the position of a point in the target area, $\boldsymbol{q}_N$ and $\boldsymbol{p}_N$ is the source strength and the sound pressure distribution of the primary noise source, $\boldsymbol{q}_C$ and $\boldsymbol{p}_C$ is the source strength and the sound pressure distribution of the control source, $\boldsymbol{W}$ is a vector of the transfer functions from the noise source to points in the target area, and $\boldsymbol{G}$ is a matrix of the transfer functions from the control sources to points in the target area. Accordingly, the control source strength $\boldsymbol{q}_C$ given by the LS method can be written as

$$\boldsymbol{q}_C = -(\boldsymbol{G}^{\mathrm{H}}\boldsymbol{G})^{-1}\boldsymbol{G}^{\mathrm{H}}\boldsymbol{p}_N = -(\boldsymbol{G}^{\mathrm{H}}\boldsymbol{G})^{-1}(\boldsymbol{G}^{\mathrm{H}}\boldsymbol{W})q_N. \tag{D.6}$$

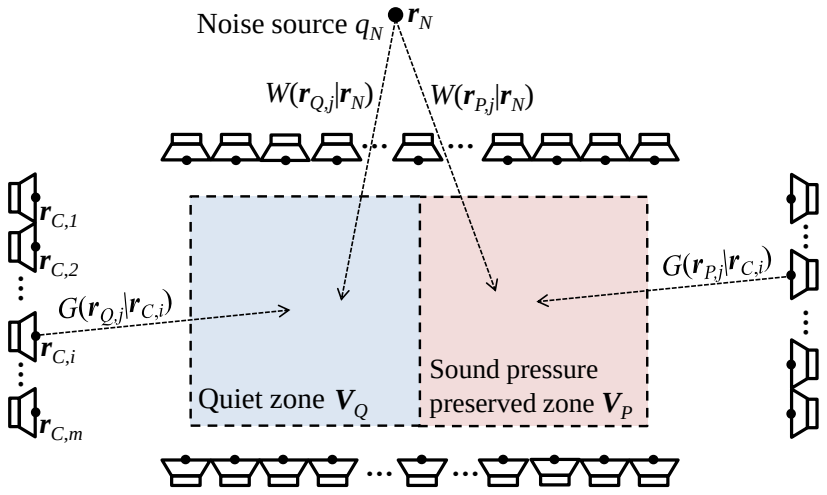

Figure D.1: Diagrammatic sketch of the problem of drawing a personal quiet zone

This process can also be interpreted by matching the control sound pressures $\boldsymbol{p}_C$ with the target sound pressures $\boldsymbol{p}_T = -\boldsymbol{p}_N$. In order to create a personal quiet zone, the target sound pressure distribution $\boldsymbol{p}_T$ can be set as

$$\boldsymbol{p}_T = [-\boldsymbol{p}_N(\boldsymbol{r}_Q), \quad \boldsymbol{0}]^{\mathrm{T}}, \tag{D.7}$$

which means the target of the control sound is $-\boldsymbol{p}_N$ in the quiet zone $\boldsymbol{V}_Q$, and 0 in the sound pressure preserved zone $\boldsymbol{V}_P$. A filter $\boldsymbol{H}$ to adjust the target pressure $\boldsymbol{p}_T$ is added into right-hand of Eq. (D.6) to realize this control strategy so that

$$\boldsymbol{q}_C = -(\boldsymbol{G}^{\mathrm{H}}\boldsymbol{G})^{-1}\boldsymbol{G}^{\mathrm{H}}(\boldsymbol{W} - \boldsymbol{H})q_N, \tag{D.8}$$

where

$$\boldsymbol{H} = [\boldsymbol{0}, \quad \hat{\boldsymbol{W}}(\boldsymbol{r}_P|\boldsymbol{r}_N)]^{\mathrm{T}}, \tag{D.9}$$

$\hat{\boldsymbol{W}}(\boldsymbol{r}_P|\boldsymbol{r}_N)$ is the estimate of the transfer functions from the noise source to the points in $\boldsymbol{V}_P$. Equation (D.8) is the solution of the modeling ANC method presented in Ref. [162]. This method can effectively create a personal quiet zone. However, as shown in Eq. (D.9), $\hat{\boldsymbol{W}}(\boldsymbol{r}_P|\boldsymbol{r}_N)$ must be obtained in advance.

To simplify the control process, the aim of setting the target of the control sound pressures as 0 in $\boldsymbol{V}_P$ is implemented by minimizing the following cost function as

$$J_P = \boldsymbol{p}_C(\boldsymbol{r}_P)^{\mathrm{H}}\boldsymbol{p}_C(\boldsymbol{r}_P), \tag{D.10}$$

which stands for the acoustic potential energy of the control sound in $\boldsymbol{V}_P$. Therefore, the ANC to create a personal quiet zone can be expressed as the following optimization problem,

$$\begin{aligned} &\text{Minimize:} \quad J = (\boldsymbol{p}_N(\boldsymbol{r}_Q) + \boldsymbol{p}_C(\boldsymbol{r}_Q))^{\mathrm{H}}(\boldsymbol{p}_N(\boldsymbol{r}_Q) + \boldsymbol{p}_C(\boldsymbol{r}_Q)), \\ &\text{subject to} \quad \boldsymbol{p}_C(\boldsymbol{r}_P)^{\mathrm{H}}\boldsymbol{p}_C(\boldsymbol{r}_P) = \epsilon, \end{aligned} \tag{D.11}$$

in which ϵ is a small positive number to limit the acoustic potential energy of the control sound in $\boldsymbol{V}_P$. By introducing a Lagrange multiplier λ, the above equation can be rewritten as

$$\text{Minimize: } J = (\boldsymbol{p}_N(\boldsymbol{r}_Q) + \boldsymbol{p}_C(\boldsymbol{r}_Q))^{\mathrm{H}}(\boldsymbol{p}_N(\boldsymbol{r}_Q) + \boldsymbol{p}_C(\boldsymbol{r}_Q)) + \lambda(\boldsymbol{p}_C(\boldsymbol{r}_P)^{\mathrm{H}}\boldsymbol{p}_C(\boldsymbol{r}_P) - \epsilon). \tag{D.12}$$

Accordingly, the control source strength given by this optimization can be written as

$$\begin{aligned} &\boldsymbol{q}_C = -[\boldsymbol{G}(\boldsymbol{r}_Q|\boldsymbol{r}_C)^{\mathrm{H}}\boldsymbol{G}(\boldsymbol{r}_Q|\boldsymbol{r}_C) + \lambda\boldsymbol{G}(\boldsymbol{r}_P|\boldsymbol{r}_C)^{\mathrm{H}}\boldsymbol{G}(\boldsymbol{r}_P|\boldsymbol{r}_C)]^{-1}\boldsymbol{G}(\boldsymbol{r}_Q|\boldsymbol{r}_C)^{\mathrm{H}}\boldsymbol{W}(\boldsymbol{r}_Q|\boldsymbol{r}_C)q_N, \\ &\boldsymbol{p}_C(\boldsymbol{r}_P)^{\mathrm{H}}\boldsymbol{p}_C(\boldsymbol{r}_P) = \boldsymbol{q}_C^{\mathrm{H}}\boldsymbol{G}(\boldsymbol{r}_P|\boldsymbol{r}_C)^{\mathrm{H}}\boldsymbol{G}(\boldsymbol{r}_P|\boldsymbol{r}_C)\boldsymbol{q}_C = \epsilon. \end{aligned} \tag{D.13}$$

The trade-off between the noise attenuation in $\boldsymbol{V}_Q$ and the preservation of the sound pressures in $\boldsymbol{V}_P$ can be selected by tuning the Lagrange multiplier λ. In comparison with the modeling ANC method, the solution in Eq. (D.13) does not require the information of the primary noise signals in the area $\boldsymbol{V}_P$ so that this method can be applied in the multiple noise sources or moving noise source occasions

D.2 Approach based on wavefront synthesis

The ANC system to create a personal quiet zone can be further simplified by applying the concept of dividing an MIMO ANC system into a loudspeaker array system and a SISO ANC system that is proposed in Chapter 6. In this case, the design of the loudspeaker array system has two stages. The first stage finds an array input filter to achieve the aim of emitting the control sound only into the quiet zone. In the second stage, the aim is to obtain an input filter to control the loudspeaker array to reproduce the primary noise field in the target area. As the second stage has been investigated in Chapter 6, this appendix focuses on the verification of the first stage.

D.2.1 Description of the method

To evaluate how well the sound can be focused in a certain area, the acoustic contrast (AC) [166] defined by

$$AC = \frac{n_P \boldsymbol{p}(\boldsymbol{r}_Q)^{\mathrm{H}} \boldsymbol{p}(\boldsymbol{r}_Q)}{n_Q \boldsymbol{p}(\boldsymbol{r}_P)^{\mathrm{H}} \boldsymbol{p}(\boldsymbol{r}_P)}, \tag{D.14}$$

which is the ratio of the acoustic potential energy density in $\boldsymbol{V}_Q$ and $\boldsymbol{V}_P$, is often used. n_P and n_Q is the number of the measurement points in $\boldsymbol{V}_Q$ and $\boldsymbol{V}_P$. In order to improve the AC, a number of approaches – a hybrid method combining active sound control, beam forming and passive methods [167], time reversal method [168, 169], acoustic brightness control [166], acoustic contrast control (ACC) [166], acoustic energy difference maximization [170], and pressure matching method [171, 172] have been proposed. In these methods, the ACC has the best sound focusing performance [173–175]. Therefore, in the following investigations, the ACC method is applied.

The ACC method maximizes the acoustic contrast between the areas $\boldsymbol{V}_Q$ and $\boldsymbol{V}_P$, and gives the optimal input filter $\boldsymbol{h}$ as the eigenvector corresponding to the maximum eigenvalue of the matrix $[\boldsymbol{G}(\boldsymbol{r}_P|\boldsymbol{r}_C)^{\mathrm{H}}\boldsymbol{G}(\boldsymbol{r}_P|\boldsymbol{r}_C) + \lambda \boldsymbol{I}]^{-1}\boldsymbol{G}(\boldsymbol{r}_Q|\boldsymbol{r}_C)^{\mathrm{H}}\boldsymbol{G}(\boldsymbol{r}_Q|\boldsymbol{r}_C)$ [166, 174], in which the Lagrange multiplier λ is adjusted to limit the input power to within a certain constraint. Accordingly, the control source strength for ANC can be written as

$$q_C = -(\boldsymbol{G}_E \boldsymbol{h})^{-1} W q_N, \tag{D.15}$$

which is a similar form with Eq. (6.8). $\boldsymbol{G}_E$ denotes the transfer functions from the loudspeaker units to the control point $\boldsymbol{r}_E$, which is defined as

$$\boldsymbol{G}_E = \left[G(\boldsymbol{r}_E|\boldsymbol{r}_{C,1}),\ \ G(\boldsymbol{r}_E|\boldsymbol{r}_{C,2}),\ \ \ldots,\ \ G(\boldsymbol{r}_E|\boldsymbol{r}_{C,m})\right], \tag{D.16}$$

and $W(\boldsymbol{r}_E|\boldsymbol{r}_N)$ is the transfer function from the primary noise source location $\boldsymbol{r}_N$ to the control point $\boldsymbol{r}_E$ where $(\boldsymbol{r}_E|\boldsymbol{r}_N)$ is omitted for convenience.

D.2.2 A numerical case study

In order to verify the effectiveness of the above method to generate a personal quiet zone, several numerical simulations are conducted according to the analysis geometry shown in Fig. D.2. The control objective is to reduce the primary noise in the area $\boldsymbol{V}_Q$ around the listener without resulting noise amplification in the area $\boldsymbol{V}_P$. The primary noise source and the loudspeaker units are point sources, and the acoustic transfer functions use the free field Green's function. Eleven loudspeaker units are used to form a linear array, and the distance between the loudspeaker units is set as 32 mm. A specified input power constraint is not considered in the simulations so that the Lagrange multiplier λ for calculating the input filter $\boldsymbol{h}$ of the loudspeaker array is set as a very small number.

In the first simulation, the sound focusing performances of two types of loudspeaker arrays are compared to verify the effectiveness of the ACC method. Figure D.3 shows the relative SPL distribution generated by the loudspeaker array with the equal input signal of each unit. The relative SPL is defined as the difference between the SPL at the reference point and at the other points. When the distance between the loudspeaker units is much smaller than the wavelength at the frequency of interest, this loudspeaker array can be seen as a line sound source. The array is omni-directional at low frequencies because the length of the line source is much shorter than the wavelength, and as the frequency increases, the directivity of the sound becomes higher. Figure D.4 shows

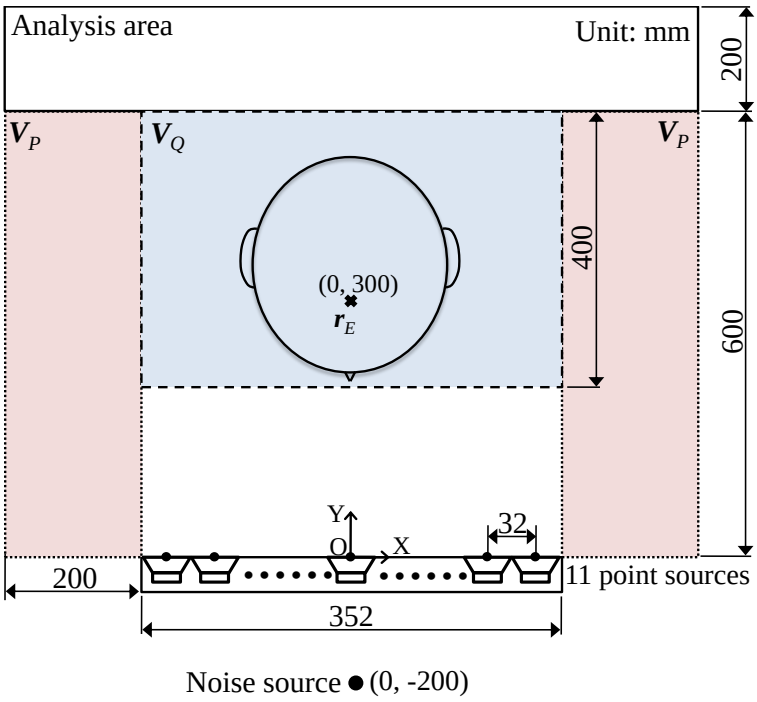

Figure D.2: Analysis geometry of the numerical case study

the relative SPL distribution generated by the loudspeaker array with the input filter obtained by the ACC method. It can be confirmed from the results that the directivity of the loudspeaker array is obviously improved. At low frequencies, the sound focusing performance is relatively low because the distance between loudspeaker units and the length of the array is shorter than the wavelength so that each unit create a similar sound pressure distribution in the target area which makes the sound field control difficult. Using a long enough loudspeaker array comparing with the wavelength can improve the array performance. At higher frequencies, a sharp directivity can be realized.

The second simulation compares the performance of the SISO ANC system using the center loudspeaker unit as the control source and the ANC system using the sound focusing loudspeaker array as the control source to validated the effectiveness of the proposed approach to create personal quiet zone. Figure D.5 shows the changes in the SPL provided by the SISO ANC system. The noise amplification at the positions far from the control point in the sound pressure preserved zone $\boldsymbol{V}_P$ can be found at all of the four frequencies. Figure D.6 shows the changes in the SPL provided by the ANC system using the sound focusing loudspeaker array. The control sound is only emitted to the direction of the target quiet zone $\boldsymbol{V}_Q$ so that the preservation of the sound pressures in $\boldsymbol{V}_P$ can be realized.

The results of the numerical investigations indicate that the approach using a sound focusing loudspeaker array can be effective to create a personal quiet zone. The occasion using a linear loudspeaker array to realize a one-dimensionally controlled personal quiet zone was investigated by numerical simulations in this appendix, and if a loudspeaker array enclosing the target area is used, it is possible to create a personal quiet zone with an arbitrary shape.

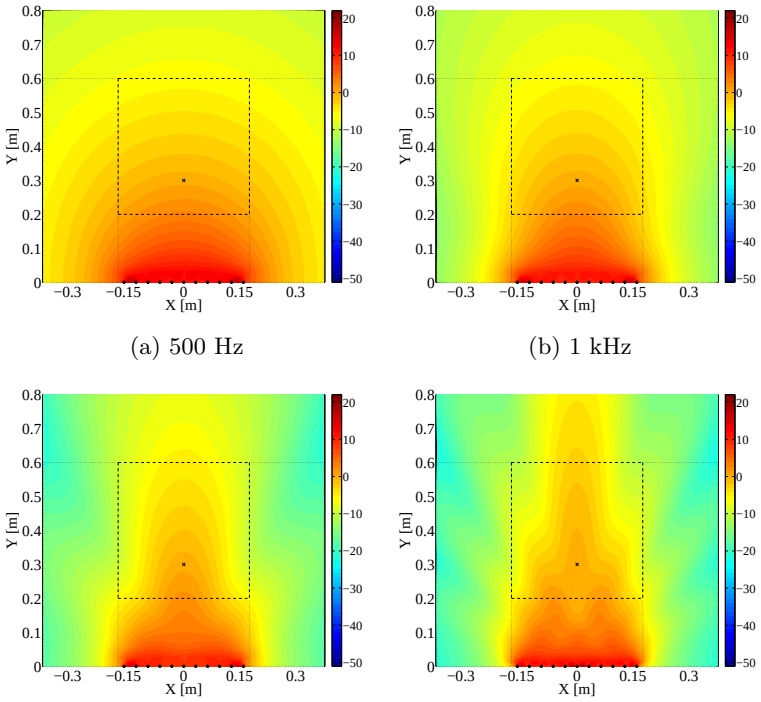

(a) 500 Hz (b) 1 kHz

(c) 2 kHz (d) 4 kHz

Figure D.3: Relative SPL [dB] distribution generated by the equal input loudspeaker array. "•" represents the point control source, and "×" represents the reference point.

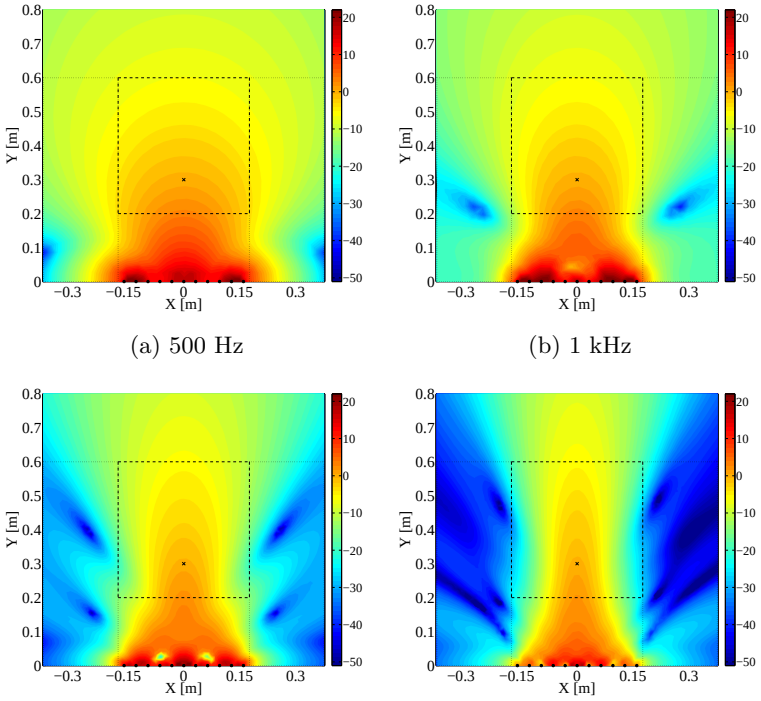

(a) 500 Hz (b) 1 kHz

(c) 2 kHz (d) 4 kHz

Figure D.4: Relative SPL [dB] distribution generated by the ACC loudspeaker array. "•" represents the point control source, and "×" represents the reference point.

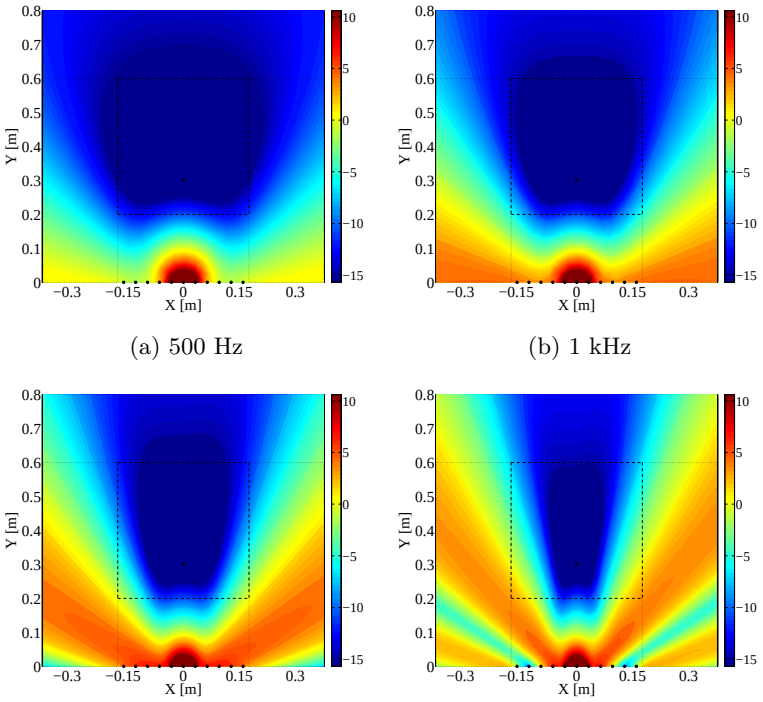

(a) 500 Hz (b) 1 kHz

(c) 2 kHz (d) 4 kHz

Figure D.5: Reduction of the SPL [dB] by only using the center loudspeaker unit as the control source. "×" represents the control point.

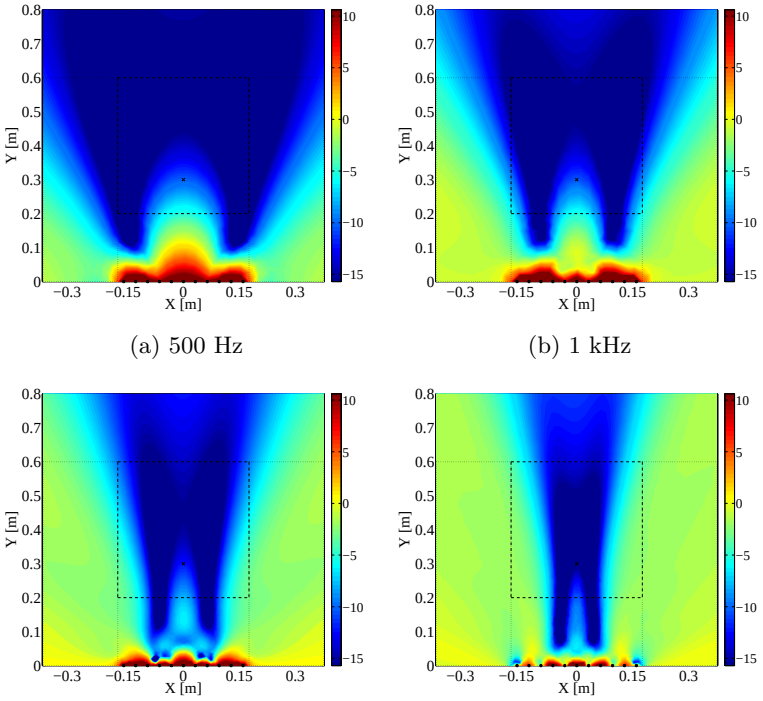

(a) 500 Hz (b) 1 kHz

(c) 2 kHz (d) 4 kHz

Figure D.6: Reduction of the SPL [dB] by using the ACC loudspeaker array as the control source. "×" represents the control point.

D.2.3 Time domain implementation of a loudspeaker array system

In the previous section, a frequency domain numerical simulation shows the effectiveness of the proposed ANC system using a sound focused loudspeaker array. The input filters of the sound focused loudspeaker array system often apply FIR filters. The coefficients of the input filter can be obtained by using IFFT of the frequency responses calculated by the frequency domain AC maximization. However, the frequency domain optimization method cannot ensure the practical time domain performance of the loudspeaker array because it does not guarantee the causality of the FIR filters. Adding time delay can obtain a causal FIR filter. However, when it is supposed to be used in a real-time system such as the ANC system, it is undesirable to increase the time delay of the system. Therefore, time-domain optimization methods to obtain the input filter coefficients to ensure has been proposed [176].

The sound pressure signal at the ith control point in the quiet zone for the ANC (Bright zone for the loudspeaker array system) p_{Bi} generated by a series of unit input signals can be written as

$$p_{Bi}(n) = \boldsymbol{g}_{Bi}^{\mathrm{T}} \boldsymbol{h}, \tag{D.17}$$

where

$$\boldsymbol{g}_{Bi} = [\boldsymbol{g}_{Bi1}^{\mathrm{T}},\ \boldsymbol{g}_{Bi2}^{\mathrm{T}},\ \ldots,\ \boldsymbol{g}_{Bij}^{\mathrm{T}},\ \ldots,\ \boldsymbol{g}_{BiN}^{\mathrm{T}}]^{\mathrm{T}}, \tag{D.18}$$

$$\boldsymbol{h} = [\boldsymbol{h}_1^{\mathrm{T}},\ \boldsymbol{h}_2^{\mathrm{T}},\ \ldots,\ \boldsymbol{h}_j^{\mathrm{T}},\ \ldots,\ \boldsymbol{h}_N^{\mathrm{T}}]^{\mathrm{T}}, \tag{D.19}$$

$$\boldsymbol{g}_{Bij} = [g_{Bij1},\ g_{Bij2},\ \ldots,\ g_{BijL}]^{\mathrm{T}}, \tag{D.20}$$

$$\boldsymbol{h}_j = [h_{j1},\ h_{j2},\ \ldots,\ h_{jL}]^{\mathrm{T}}, \tag{D.21}$$

$\boldsymbol{g}_{Bij}$ is the impulse response of the acoustic path from the jth loudspeaker to the ith control point in the bright zone, $\boldsymbol{h}_j$ is the input filter coefficients for the jth loudspeaker, N is the number of the loudspeakers, and L is the filter length. Similarly, the sound pressure signal at the ith control point in the sound pressure preservation zone (Dark zone for the loudspeaker array system) p_{Di} generated by a series of unit input signals can be written as

$$p_{Di}(n) = \boldsymbol{g}_{Di}^{\mathrm{T}} \boldsymbol{h}. \tag{D.22}$$

Therefore, according to Eq. (D.14), the time domain AC can be expressed as

$$AC = \frac{n_D \boldsymbol{p}_B^{\mathrm{T}} \boldsymbol{p}_B}{n_B \boldsymbol{p}_D^{\mathrm{T}} \boldsymbol{p}_D} = \frac{\boldsymbol{h}^{\mathrm{T}} \boldsymbol{R}_B \boldsymbol{h}}{\boldsymbol{h}^{\mathrm{T}} \boldsymbol{R}_D \boldsymbol{h}}, \tag{D.23}$$

where

$$\boldsymbol{p}_B = [p_{B1}(n),\ p_{B2}(n),\ \ldots,\ p_{Bi}(n),\ \ldots,\ p_{Bn_B}(n)]^{\mathrm{T}}, \tag{D.24}$$

$$\boldsymbol{p}_D = [p_{D1}(n),\ p_{D2}(n),\ \ldots,\ p_{Di}(n),\ \ldots,\ p_{Dn_D}(n)]^{\mathrm{T}}, \tag{D.25}$$

$$\boldsymbol{R}_B = \sum_{i=1}^{n_B} \boldsymbol{g}_{Bi}\boldsymbol{g}_{Bi}^{\mathrm{T}}/n_B, \tag{D.26}$$

$$\boldsymbol{R}_D = \sum_{i=1}^{n_D} \boldsymbol{g}_{Di}\boldsymbol{g}_{Di}^{\mathrm{T}}/n_D, \tag{D.27}$$

n_B and n_D are the numbers of the control points in the bright zone and dark zone, $\boldsymbol{R}_B$ and $\boldsymbol{R}_D$ are the normalized correlation matrix of the acoustic transfer functions in the bright zone and dark zone, respectively. In order to maximize the AC, the input filter $\boldsymbol{h}$ is given as the eigenvector corresponding to the maximum eigenvalue of the matrix $[\boldsymbol{R}_D + \lambda\boldsymbol{R}_{rr}]^{-1}\boldsymbol{R}_B$, where $\boldsymbol{R}_{rr}$ is the correlation matrix of a filtered input signal that can be used to regularize the ACC performance at different frequencies.

A simulation is conducted to verify the ACC performance of a linear loudspeaker

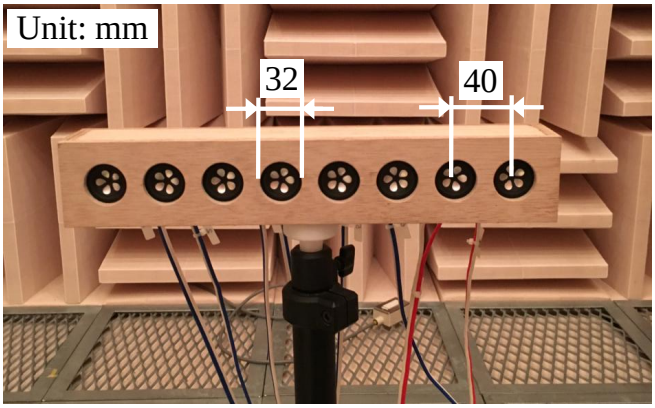

(a) Hardware

(b) Configuration

Figure D.7: Loudspeaker array

array designed by the above method. The loudspeaker array, which is composed of eight sources, is shown in Fig. D.7. The acoustic paths used in the simulation are expressed as FIR filters measured in the anechoic chamber. The configuration of the simulation is shown in Fig. D.8. The measurement points are set at intervals of 0.04 m in the analysis area.

Figure D.9 shows the distribution of the relative SPL for 1 kHz, 2 kHz, 4 kHz 1/3 octave bands and that of the overall SPL in the analysis area generated by one loudspeaker that is the fourth loudspeaker of the array, and Figure D.10 shows the results generated by the ACC loudspeaker array. The results in Fig. D.9 show that the loudspeaker is omni-directional because the small loudspeaker can be seen as a point source at low frequencies where the wavelength is much longer than the diameter of it. On the other hand, by comparing the results in two figures, it can be confirmed that the ACC method can improve the directivity of a loudspeaker array significantly. By using this ACC loudspeaker array as the control source, it is possible to reduce the noise in the target area without increasing the SPL at other positions.

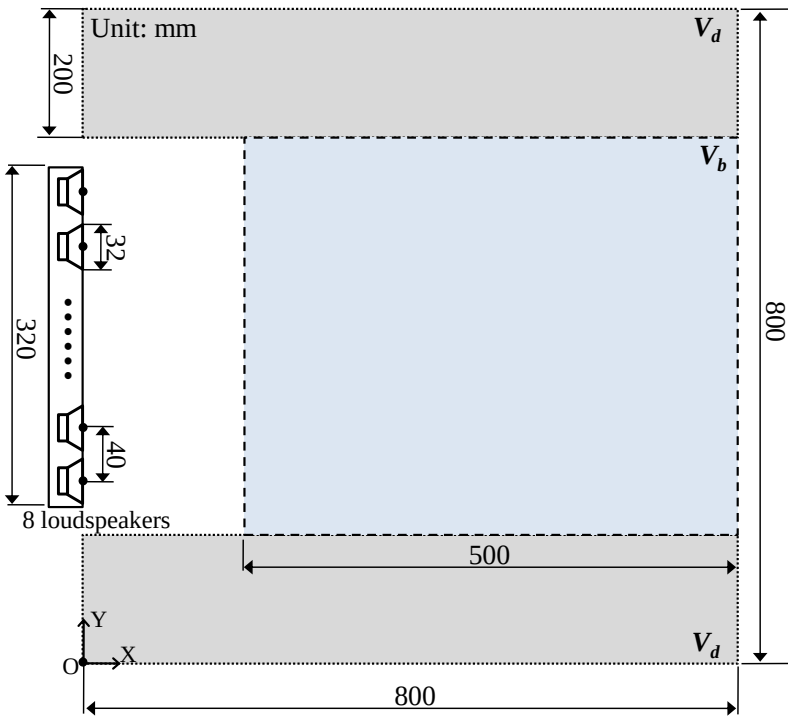

Figure D.8: Measurement configuration for simulation

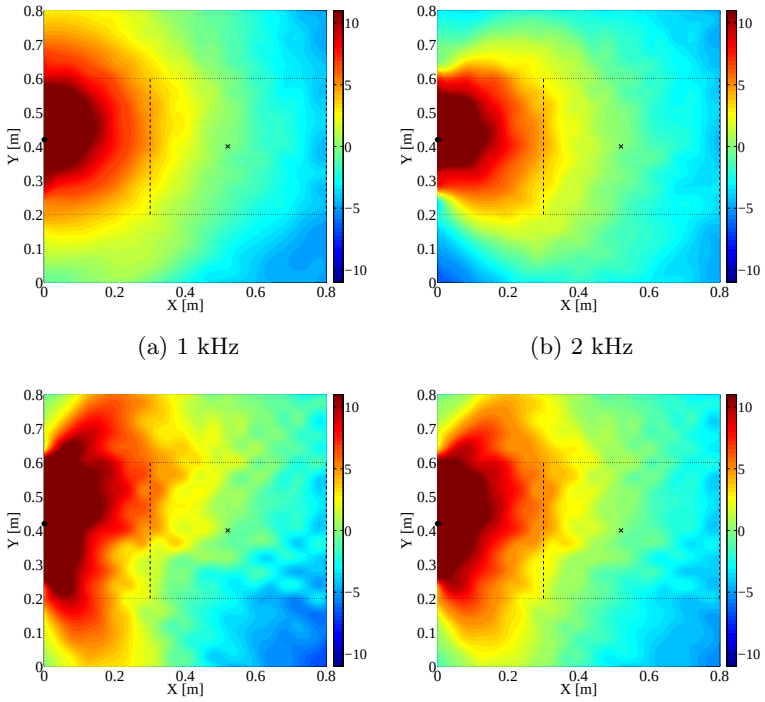

(a) 1 kHz (b) 2 kHz

(c) 4 kHz (d) Overall

Figure D.9: Relative SPL [dB] distribution generated by the fourth loudspeaker in the array. "•" represents the point control source, and "×" represents the reference point.

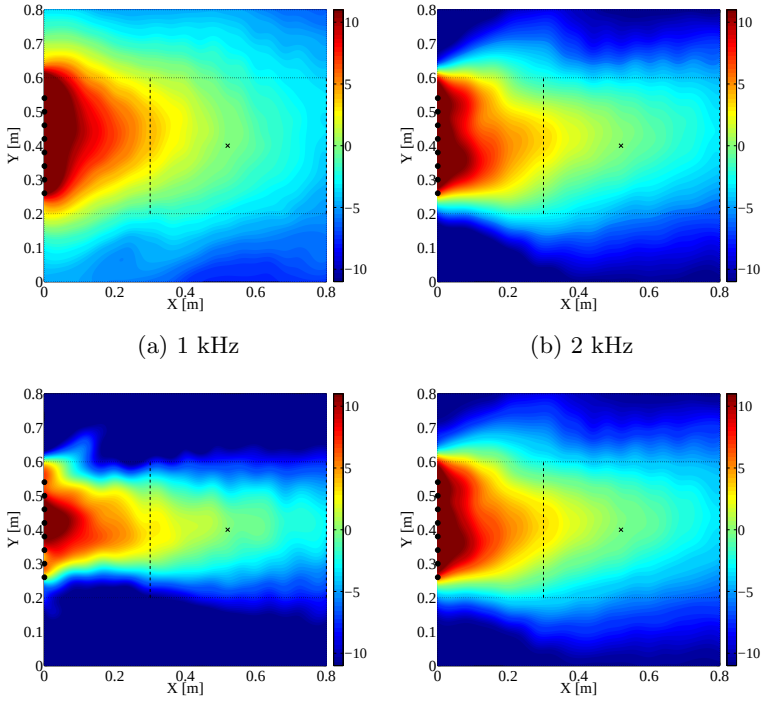

(a) 1 kHz (b) 2 kHz

(c) 4 kHz (d) Overall

Figure D.10: Relative SPL [dB] distribution generated by the ACC loudspeaker array. "•" represents the point control source, and "×" represents the reference point.

Bibliography

[1] A. Hedge, "The open-plan office: A systematic investigation of employee reactions to their work environment," *Environment and Behavior*, vol. 14, pp. 519–542, 1982.

[2] F. Becker, "Improving organisational performance by exploiting workplace flexibility," *Journal of Facilities Management*, vol. 1, no. 2, pp. 154–162, 2002.

[3] J. L. Brand and T. J. Smith, "Effects of reducing enclosure on perceptions of occupancy quality, job satisfaction, and job performance in open-plan offices," in *Proceedings of the Human Factors and Ergonomics Society*, pp. 818–822, 2005.

[4] V. Kupritz, "Accommodating privacy to facilitate new ways of working," *Journal of Architectural and Planning Research*, vol. 20, no. 2, pp. 122–135, 2003.

[5] E. Sundstrom, J. P. Town, R. W. Rice, D. P. Osborn, and M. Brill, "Office noise, satisfaction, and performance," *Environment and Behavior*, vol. 26, no. 2, pp. 195–222, 1994.

[6] A. Brennan, J. S. Chugh, and T. Kline, "Traditional versus open office design: A longitudinal field study," *Environment and Behavior*, vol. 34, no. 3, pp. 279–299, 2002.

[7] M. Navai and J. A. Veitch, "Acoustic satisfaction in open-plan offices: Review and recommendations," tech. rep., National research council Canada, 2003.

[8] J. Kim and R. de Dear, "Workspace satisfaction: The privacy-communication trade-off in open-plan offices," *Journal of Environmental Psychology*, vol. 36, pp. 18–26, 2013.

[9] S. Y. Lee and J. L. Brand, "Effects of control over office workspace on perceptions of the work environment and work outcomes," *Journal of Environmental Psychology*, vol. 25, pp. 323–333, 2005.

[10] T. L. Smith-Jackson and K. W. Klein, "Open-plan offices: Task performance and mental workload," *Journal of Environmental Psychology*, vol. 29, pp. 279–289, 2009.

[11] A. Kaarlela-Tuomaala, R. Helenius, E. Keskinen, and V. O. Hongisto, "Effects of acoustic environment on work in private office rooms and open-plan offices - longitudinal study during relocation," *Ergonomics*, vol. 52, no. 11, pp. 1423–1444, 2009.

[12] H. Jahncke, S. Hygge, N. Halin, A. M. Green, and K. Dimberg, "Open-plan office noise: Cognitive performance and restoration," *Journal of Environmental Psychology*, vol. 31, no. 4, pp. 373–382, 2011.

[13] G. W. Evans and D. Johnson, "Stress and open-office noise," *Journal of Applied Psychology*, vol. 85, no. 5, pp. 779–783, 2000.

[14] A. Haapakangas, R. Helenius, E. Keekinen, and V. O. Hongisto, "Perceived acoustic environment, work performance and well-being - survey results from finnish offices," in *Proceedings of the 9th International Congress on Noise as a Public Health Problem*, 2008.

[15] S. Klitzman and J. M. Stellman, "The impact of the physical environment on the psychological well-being of office workers," *Social Science & Medicine*, vol. 29, no. 6, pp. 733–742, 1989.

[16] S. P. Banbury and D. C. Berry, "Office noise and employee concentration: identifying causes of disruption and potential improvements.," *Ergonomics*, vol. 48, no. 1, pp. 25–37, 2005.

[17] T. A. Judge, C. J. Thoresen, J. E. Bono, and G. K. Patton, "The job satisfaction-job performance relationship: a qualitative and quantitative review.," *Psychological bulletin*, vol. 127, no. 3, pp. 376–407, 2001.

[18] R. Pirn, "Acoustical variables in open planning.," *The Journal of the Acoustical Society of America*, vol. 49, no. 5, pp. 1339–1345, 1971.

[19] M. West, "The sound attenuation in an open-plan office," *Applied Acoustics*, vol. 6, pp. 35–56, 1973.

[20] P. Virjonen, J. Keränen, and V. O. Hongisto, "Determination of acoustical conditions in open-plan offices: Proposal for new measurement method and target values," *Acta Acustica united with Acustica*, vol. 95, pp. 279–290, 2009.

[21] E. Nilsson and B. Hellström, "Room acoustic design in open-plan offices," in *10ème Congrès Français d'Acoustique*, 2010.

[22] J. S. Bradley and B. Gover, "Describing levels of speech privacy in open-plan offices," tech. rep., National Research Council Canada, 2003.

[23] V. O. Hongisto, J. Keränen, and P. Larm, "Simple model for the acoustical design of open-plan offices," *Acta Acustica united with Acustica*, vol. 90, pp. 481–495, 2004.

[24] C. Wang and J. S. Bradley, "A mathematical model for a single screen barrier in open-plan offices," *Applied Acoustics*, vol. 63, pp. 849–866, 2002.

[25] R. A. Waller, "Office acoustics - effect of background noise," *Applied Acoustics*, vol. 2, pp. 121–130, 1969.

[26] R. C. Chanaud, "Progress in sound masking," *Acoustics Today*, vol. 3, pp. 21–26, oct 2007.

[27] A. C. C. Warnock, "Acoustical privacy in the landscaped office," *The Journal of the Acoustical Society of America*, vol. 53, no. 6, pp. 1535–1543, 1973.

[28] P. Virjonen, J. Keränen, R. Helenius, J. Hakala, and V. O. Hongisto, "Speech privacy between neighboring workstations in an open office - a laboratory study," *Acta Acustica united with Acustica*, vol. 93, pp. 771–782, 2007.

[29] S. J. Elliott and P. A. Nelson, "Active noise control," *IEEE Signal Processing Magazine*, pp. 12–35, oct 1993.

[30] W. J. Cavanaugh, W. R. Farrell, P. W. Hirtle, and B. G. Watters, "Speech privacy in buildings," *The Journal of the Acoustical Society of America*, vol. 34, no. 4, pp. 475–492, 1962.

[31] R. Drullman, "Temporal envelope and fine structure cues for speech intelligibility.," vol. 97, pp. 585–592, 1995.

[32] H. G. Latham, "The signal-to-noise ratio for speech intelligibility - an auditorium acoustics design index," *Applied Acoustics*, vol. 12, pp. 253–320, 1979.

[33] J. S. Bradley, "Predictors of speech intelligibility in rooms.," *The Journal of the Acoustical Society of America*, vol. 80, no. 3, pp. 837–845, 1986.

[34] S. M. Kuo and D. R. Morgan, *Active Noise Control System: Algorithm and DSP Implementations*. New York: John Wiley&Sons, Inc., 1996.

[35] S. J. Elliott, *Signal processing for active control*. London: Academic Press, 2001.

[36] C. H. Hansen, S. D. Snyder, X. Qiu, L. Brooks, and D. J. Moreau, *Active Control of Noise and Vibration*. Boca Raton, FL: CRC Press, 2012.

[37] S. J. Elliott and J. Cheer, "Modelling local active sound control with remote sensors in spatially random pressure fields," *The Journal of the Acoustical Society of America*, vol. 137, no. 4, pp. 1936–1946, 2015.

[38] A. J. Bullmore, P. A. Nelson, A. R. D. Curtis, and S. J. Elliott, "The active minimization of harmonic enclosed sound fields, part ii: A computer simulation," *Journal of Sound and Vibration*, vol. 117, no. 1, pp. 15–33, 1987.

[39] S. J. Elliott, A. R. D. Curtis, A. J. Bullmore, and P. A. Nelson, "The active minimization of harmonic enclosed sound fields, part iii: Experimental verification," *Journal of Sound and Vibration*, vol. 117, no. 1, pp. 35–58, 1987.

[40] M. R. Schroeder and K. H. Kuttruff, "On frequency response curves in rooms. comparison of experimental, theoretical, and monte carlo results for the average frequency spacing between maxima," *The Journal of the Acoustical Society of America*, vol. 34, no. 1, pp. 76–80, 1962.

[41] M. R. Schroeder, "The "Schroeder frequency" revisited," *The Journal of the Acoustical Society of America*, vol. 99, no. 5, pp. 3240–3241, 1996.

[42] P. A. Nelson, A. R. D. Curtis, S. J. Elliott, and A. J. Bullmore, "The active minimization of harmonic enclosed sound fields, part i : Theory," *Journal of Sound and Vibration*, vol. 117, no. 1, pp. 1–13, 1987.

[43] P. A. Nelson and S. J. Elliott, "The minimum power output of a pair of free field monopole sources," *Journal of sound and vibration*, vol. 105, no. 1, pp. 173–178, 1986.

[44] P. A. Nelson, A. R. D. Curtis, S. J. Elliott, and A. J. Bullmore, "The minimum power output of free field point sources and the active control of sound," *Journal of Sound and Vibration*, vol. 116, pp. 397–414, 1987.

[45] S. J. Elliott, P. Joseph, P. A. Nelson, and M. E. Johnson, "Power output minimization and power absorption in the active control of sound," *The Journal of the Acoustical Society of America*, vol. 90, no. 5, pp. 2501–2512, 1991.

[46] S. J. Elliott, P. Joseph, A. J. Bullmore, and P. A. Nelson, "Active cancellation at a point in a pure tone diffuse sound field," *Journal of Sound and Vibration*, vol. 120, no. 1, pp. 183–189, 1988.

[47] B. Rafaely, "Zones of quiet in a broadband diffuse sound field," *The Journal of the Acoustical Society of America*, vol. 110, no. 1, pp. 296–302, 2001.

[48] P. Joseph, S. J. Elliott, and P. A. Nelson, "Near field zones of quiet," *Journal of Sound and Vibration*, vol. 172, no. 5, pp. 605–627, 1994.

[49] S.-H. Yu and J.-S. Hu, "Controller design for active noise cancellation headphones using experimental raw data," *IEEE/ASME Transactions on Mechatronics*, vol. 6, no. 4, pp. 483–490, 2001.

[50] Y. Song, Y. Gong, and S. M. Kuo, "A robust hybrid feedback active noise cancellation headset.," *IEEE Transactions on Speech and Audio Processing*, vol. 13, no. 4, pp. 607–617, 2005.

[51] S. M. Kuo, S. Mitra, and W.-S. Gan, "Active noise control system for headphone applications," *IEEE Transactions on Control Systems Technology*, vol. 14, no. 2, pp. 331–335, 2006.

[52] N. Miyazaki and Y. Kajikawa, "Head-mounted active noise control system with virtual sensing technique," *Journal of Sound and Vibration*, vol. 339, pp. 65–83, 2015.

[53] B. Rafaely and S. J. Elliott, "H_2/H_∞ active control of sound in a headrest: Design and implementation," *IEEE Transactions on Control Systems Technology*, vol. 7, no. 1, pp. 79–84, 1999.

[54] B. Rafaely, S. J. Elliott, and J. J. Garcia-Bonito *The Journal of the Acoustical Society of America*, vol. 106, no. 2, pp. 787–793, 1999.

[55] M. Pawelczyk, "Adaptive noise control algorithms for active headrest system," *Control Engineering Practice*, vol. 12, pp. 1101–1112, 2004.

[56] J. Guo, J. Pan, and C. Bao, "Actively created quiet zones by multiple control sources in free space," *The Journal of the Acoustical Society of America*, vol. 101, no. 3, pp. 1492–1501, 1997.

[57] J. Guo and J. Pan, "Actively created quiet zones for broadband noise using multiple control sources and error microphones," *The Journal of the Acoustical Society of America*, vol. 105, no. 4, pp. 2294–2303, 1999.

[58] Y. C. Park and S. D. Sommerfeldt, "Global attenuation of broadband noise fields using energy density control," *The Journal of the Acoustical Society of America*, vol. 101, no. 1, pp. 350–359, 1997.

[59] J. W. Parkins, S. D. Sommerfeldt, and J. Tichy, "Narrowband and broadband active control in an enclosure using the acoustic energy density," *The Journal of the Acoustical Society of America*, vol. 108, no. 1, pp. 192–203, 2000.

[60] D. J. Moreau, B. S. Cazzolato, and A. C. Zander, "Active noise control at a virtual acoustic energy density sensor in a three-dimensional sound field," in *International Congress on Acoustics*, 2010.

[61] B. Xu and S. D. Sommerfeldt, "Generalized acoustic energy density based active noise control in single frequency diffuse sound fields," *The Journal of the Acoustical Society of America*, vol. 136, no. May, pp. 1112–1119, 2014.

[62] B. Xu, S. D. Sommerfeldt, and T. W. Leishman, "Generalized acoustic energy density," *The Journal of the Acoustical Society of America*, vol. 130, no. 3, pp. 1370–1380, 2011.

[63] D. Li and M. Hodgson, "Optimal active noise control in large rooms using a "locally global" control strategy," *The Journal of the Acoustical Society of America*, vol. 118, no. 6, pp. 3653–3661, 2005.

[64] W.-K. Tseng, "Local active noise control using a novel method of designing quiet zones," *Control Engineering Practice*, vol. 19, pp. 1450–1458, 2011.

[65] N. Tanaka and M. Tanaka, "Mathematically trivial control of sound using a parametric beam focusing source.," *The Journal of the Acoustical Society of America*, vol. 129, no. 1, pp. 165–172, 2011.

[66] W.-S. Gan, J. Yang, and T. Kamakura, "A review of parametric acoustic array in air," *Applied Acoustics*, vol. 73, pp. 1211–1219, 2012.

[67] D. J. Moreau, B. S. Cazzolato, A. C. Zander, and C. Petersen, "A review of virtual sensing algorithms for active noise control," *Algorithms*, vol. 1, pp. 69–99, 2008.

[68] S. Elliott and A. David, "A virtual microphone arrangement for local active sound control," in *Proceedings of the 1st International Conference on Motion and Vibration Control*, pp. 1027–1031, 1992.

[69] J. J. Garcia-Bonito, S. J. Elliott, and C. C. Boucher, "Generation of zones of quiet using a virtual microphone arrangement," *The Journal of the Acoustical Society of America*, vol. 101, no. 6, pp. 3498–3561, 1997.

[70] C. D. Kestell, B. S. Cazzolato, and C. H. Hansen, "Active noise control in a free field with virtual sensors.," *The Journal of the Acoustical Society of America*, vol. 109, no. September 2000, pp. 232–243, 2001.

[71] D. J. Moreau, J. Ghan, B. S. Cazzolato, and A. C. Zander, "Active noise control in a pure tone diffuse sound field using virtual sensing.," *The Journal of the Acoustical Society of America*, vol. 125, no. 6, pp. 3742–3755, 2009.

[72] S. Ise, "A principle of sound field control based on the kirchhoff-helmholtz integral equation and the theory of inverse systems," *Acta Acustica united with Acustica*, vol. 85, pp. 78–87, 1999.

[73] S. Ise, "Application of the boundary surface control principle to the active noise control," *The Journal of the Institute of Noise Control Engineering of Japan (in Japanese)*, vol. 27, no. 4, pp. 263–266, 2003.

[74] S. Ise, "The boundary surface control principle and its applications," *IEICE Transactions on Fundamentals of Electronics, Communications and Computer Sciences*, vol. E88-A, no. 7, pp. 1656–1664, 2005.

[75] T. Murao and M. Nishimura, "Basic study on active acoustic shielding," *Journal of Environment and Engineering*, vol. 7, no. 1, pp. 76–91, 2012.

[76] T. Murao, M. Nishimura, K. Sakurama, and S. Nishida, "Basic study on active acoustic shielding (improving noise-reducing performance in low-frequency range)," *Mechanical Engineering Journal*, vol. 1, no. 6, pp. 1–12, 2014.

[77] T. Murao, M. Nishimura, K. Sakurama, and S. Nishida, "Basic study on active acoustic shielding (Improving the method to enlarge the AAS window)," *Mechanical Engineering Journal*, vol. 3, no. 1, pp. 1–12, 2016.

[78] D. N. May and M. M. Osman, "Highway noise barriers: New shapes.," *Journal of Sound and Vibration*, vol. 71, no. 1, pp. 73–101, 1980.

[79] S. Samuels and E. Ancich, "Recent developments in the design and performance of road traffic noise barriers," *Acoustics Australia*, vol. 29, no. 2, pp. 73–78, 2001.

[80] T. Ishizuka and K. Fujiwara, "Performance of noise barriers with various edge shapes and acoustical conditions," *Applied Acoustics*, vol. 65, pp. 125–141, 2004.

[81] S. Ise, H. Yano, and H. Tachibana, "Basic study on active noise barrier," *Journal of the Acoustical Society of Japan (E)*, vol. 12, no. 6, pp. 299–306, 1991.

[82] A. Omoto and K. Fujiwara, "A study of an actively controlled noise barrier," *The Journal of the Acoustical Society of America*, vol. 94, no. 4, pp. 2173–2180, 1993.

[83] W. Chen, H. Min, and X. Qiu, "Noise reduction mechanisms of active noise barriers," *Noise Control Engineering Journal*, vol. 61, no. 2, pp. 120–126, 2013.

[84] A. Omoto, K. Takashima, and K. Fujiwara, "Active suppression of sound diffracted by barrier - cancellation of reflected sound from the ground," *Journal of the Acoustical Society of Japan (in Japanese)*, vol. 51, pp. 375–383, may 1995.

[85] J. Guo and J. Pan, "Increasing the insertion loss of noise barriers using an active-control system," *The Journal of the Acoustical Society of America*, vol. 104, no. 6, pp. 3408–3416, 1998.

[86] J. Guo, J. Pan, and M. Hodgson, "Active control of a moving noise source–effect of off-axis source position," *Journal of Sound and Vibration*, vol. 251, pp. 457–475, 2002.

[87] A. Omoto, K. Takashima, K. Fujiwara, M. Aoki, and Y. Shimizu, "Active suppression of sound diffracted by a barrier: An outdoor experiment," *Journal of the Acoustical Society of America*, vol. 102, no. 3, pp. 1671–1679, 1997.

[88] K. Ohnishi, S. Teranishi, M. Nishimura, K. Uesaka, and H. Ohnishi, "Development of the noise barrier with active controlled acoustical soft edge, basic concept and noise reduction measurement using a 2m length prototype," *Journal of the Acoustical Society of Japan (in Japanese)*, vol. 57, no. 2, pp. 129–138, 2001.

[89] K. Ohnishi, T. Saito, S. Teranishi, Y. Namikawa, T. Mori, K. Kimura, and K. Uesaka, "Development of the product-type active soft edge noise barrier," *International Congress on Acoustics*, pp. 1041–1044, 2004.

[90] Ministry of Land, Infrastructure, Tansport and Tourism of Japan, "Installation of a new-type noise barrier to reduce road noise." `http://www.mlit.go.jp/chosahokoku/h16giken/pdf/0217.pdf`. Accessed: 2015-12-26.

[91] A. P. Berkhoff, "Control strategies for active noise barriers using near-field error sensing," *The Journal of the Acoustical Society of America*, vol. 118, no. 3, pp. 1469–1479, 2005.

[92] T. Nakashima and S. Ise, "Active noise barrier aiming at the noise reduction in far field," *Journal of the Acoustical Society of Japan (in Japanese)*, vol. 63, no. 10, pp. 577–584, 2007.

[93] C. R. Hart and S.-K. Lau, "Active noise control with linear control source and sensor arrays for a noise barrier," *Journal of Sound and Vibration*, vol. 331, no. 1, pp. 15–26, 2012.

[94] N. Han and X. Qiu, "A study of sound intensity control for active noise barriers," *Applied Acoustics*, vol. 68, pp. 1297–1306, 2007.

[95] F. Niu, H. Zou, X. Qiu, and M. Wu, "Error sensor location optimization for active soft edge noise barrier," *Journal of Sound and Vibration*, vol. 299, pp. 409–417, 2007.

[96] J. C. C. Liu and F. Niu, "Study on the analogy feedback active soft edge noise barrier," *Applied Acoustics*, vol. 69, pp. 728–732, 2008.

[97] W. Chen, W. Rao, H. Min, and X. Qiu, "An active noise barrier with unidirectional secondary sources," *Applied Acoustics*, vol. 72, no. 12, pp. 969–974, 2011.

[98] X. Wang, S. Kijimoto, Y. Koba, and K. Matsuda, "Noise barrier using feedback active noise control," in *Inter-Noise 2011*, 2011.

[99] X. Huang, H. Zou, and X. Qiu, "A study of a single screen active noise barrier in open-plan offices," in *The 21st International Congress on Sound and Vibration*, 2014.

[100] D. S. Brungart, B. D. Simpson, M. A. Ericson, and K. R. Scott, "Informational and energetic masking effects in the perception of multiple simultaneous talkers.," *The Journal of the Acoustical Society of America*, vol. 110, no. 5, pp. 2527–2538, 2001.

[101] T. L. Arbogast, C. R. Mason, and G. Kidd, "The effect of spatial separation on informational and energetic masking of speech," *The Journal of the Acoustical Society of America*, vol. 112, no. 5, pp. 2086–2098, 2002.

[102] D. S. Brungart and B. D. Simpson, "The effects of spatial separation in distance on the informational and energetic masking of a nearby speech signal.," *The Journal of the Acoustical Society of America*, vol. 112, no. 5, pp. 664–676, 2002.

[103] N. I. Durlach, C. R. Mason, G. Kidd, T. L. Arbogast, H. S. Colburn, and B. G. Shinn-Cunningham, "Note on informational masking.," *The Journal of the Acoustical Society of America*, vol. 113, no. 6, pp. 2984–2987, 2003.

[104] V. Best, E. Ozmeral, F. J. Gallun, K. Sen, and B. G. Shinn-Cunningham, "Spatial unmasking of birdsong in human listeners: energetic and informational factors.," *The Journal of the Acoustical Society of America*, vol. 118, no. 6, pp. 3766–3773, 2005.

[105] N. I. Durlach, "Auditory masking: need for improved conceptual structure.," *The Journal of the Acoustical Society of America*, vol. 120, no. 4, pp. 1787–1790, 2006.

[106] N. I. Durlach, C. R. Mason, B. G. Shinn-Cunningham, T. L. Arbogast, H. S. Colburn, and G. Kidd, "Informational masking: counteracting the effects of stimulus uncertainty by decreasing target-masker similarity.," *The Journal of the Acoustical Society of America*, vol. 114, no. 1, pp. 368–379, 2003.

[107] E. L. Oh and R. a. Lutfi, "Informational masking by everyday sounds.," *The Journal of the Acoustical Society of America*, vol. 106, no. 6, pp. 3521–3528, 1999.

[108] J. Chen, H. Li, L. Li, X. Wu, and B. C. J. Moore, "Informational masking of speech produced by speech-like sounds without linguistic content," *The Journal of the Acoustical Society of America*, vol. 131, no. 4, pp. 2914–2926, 2012.

[109] R. A. Lutfi, "How much masking is informational masking?," *The Journal of the Acoustical Society of America*, vol. 88, no. 6, pp. 2607–2610, 1990.

[110] T. Saeki, T. Tamesue, S. Yamaguchi, and K. Sunada, "Selection of meaningless steady noise for masking of speech," *Applied Acoustics*, vol. 65, pp. 203–210, 2004.

[111] T. Tamesue, S. Yamaguchi, and T. Saeki, "Study on achieving speech privacy using masking noise," *Journal of Sound and Vibration*, vol. 297, pp. 1088–1096, 2006.

[112] T. Arai, "Masking speech with its time-reversed signal," *Acoustical Science and Technology*, vol. 31, pp. 188–190, 2010.

[113] B. Jiang, A. Liebl, P. Leistner, and J. Yang, "Sound masking performance of time-reversed masker processed from the target speech," *Acta Acustica united with Acustica*, vol. 98, pp. 135–141, 2012.

[114] M. Akagi and Y. Irie, "Privacy protection for speech based on concepts of auditory scene analysis," in *Inter-Noise 2012*, 2012.

[115] A. Haapakangas, E. Kankkunen, V. O. Hongisto, P. Virjonen, D. Oliva, and E. Keskinen, "Effects of five speech masking sounds on performance and acoustic satisfaction. implications for open-plan offices," *Acta Acustica united with Acustica*, vol. 97, pp. 641–655, 2011.

[116] A. Ebissou, E. Parizet, and P. Chevret, "Use of the speech transmission index for the assessment of sound annoyance in open-plan offices," *Applied Acoustics*, vol. 88, pp. 90–95, 2015.

[117] V. O. Hongisto, "Effect of sound masking on workers in an open office," in *Acoustics 08*, (Paris), pp. 537–542, 2008.

[118] Y. Lei and M. Hodgson, "Prediction of the effectiveness of a sound-masking system in an open-plan office including the lombard effect," *Acta Acustica united with Acustica*, vol. 99, pp. 729–736, 2013.

[119] A. Haapakangas, V. O. Hongisto, J. Hyönä, J. Kokko, and J. Keränen, "Effects of unattended speech on performance and subjective distraction: The role of acoustic design in open-plan offices," *Applied Acoustics*, vol. 86, pp. 1–16, 2014.

[120] H. Sano, T. Inoue, A. Takahashi, K. Terai, and Y. Nakamura, "Active control system for low-frequency road noise combined with an audio system," *IEEE Transactions on Speech and Audio Processing*, vol. 9, no. 7, pp. 755–763, 2001.

[121] S. J. Elliott and T. J. Sutton, "Performance of feedforward and feedback systems for active control," *IEEE Transactions on Speech and Audio Processing*, vol. 4, no. 3, pp. 214–223, 1996.

[122] M. Morari and E. Zafiriou, *Robust Process Control*. Englewood Cliffs, London: Prentice Hall, 1989.

[123] D. R. Morgan, "Analysis of multiple correlation cancellation loop with a filter in the auxiliary path," *IEEE Transactions on Acoustic, Speech and Signal Processing*, vol. 5, pp. 454–467, 1980.

[124] J. C. Burgess, "Active adaptive sound control in a duct: A computer simulation.," *The Journal of the Acoustical Society of America*, vol. 70, no. 3, pp. 715–726, 1981.

[125] J. S. Freudenberg and D. Looze, "Right half plane poles and zeros and design tradeoffs in feedback systems," *IEEE Transactions on Automatic Control*, vol. 30, no. 6, pp. 555–565, 1985.

[126] S. Skogestad and I. Postlethwaite, *Multivariable Feedback Control Analysis and design*. New York: John Wiley&Sons, Inc., 2001.

[127] H. Sakai and S. Miyagi, "Analysis of the adaptive filter algorithm for feedback-type active noise control," *Signal Processing*, vol. 83, pp. 1291–1298, 2003.

[128] S. D. Snyder and C. H. Hansen, "The influence of transducer transfer functions and acoustic time delays on the implementation of the LMS algorithm in active noise control systems," *Journal of Sound and Vibration*, vol. 141, no. 3, pp. 409–424, 1990.

[129] S. D. Snyder and C. H. Hansen, "The effect of transfer function estimation errors on the filtered-x LMS algorithm," *IEEE Transactions on Signal Processing*, vol. 42, no. 4, pp. 950–953, 1994.

[130] L. V. Wang, W.-S. Gan, A. W. H. Khong, and S. M. Kuo, "Convergence analysis of narrowband feedback active noise control system with imperfect secondary path estimation," *IEEE Transactions on Audio, Speech, and Language Processing*, vol. 21, no. 11, pp. 2403–2411, 2013.

[131] T. Wang and W.-S. Gan, "Stochastic analysis of FXLMS-based internal model control feedback active noise control systems," *Signal Processing*, vol. 101, pp. 121–133, 2014.

[132] L. Wu, X. Qiu, and Y. Guo, "A simplified adaptive feedback active noise control system," *Applied Acoustics*, vol. 81, pp. 40–46, 2014.

[133] O. J. Tobias and R. Seara, "Leaky-FXLMS algorithm: Stochastic analysis for gaussian data and secondary path modeling error," *IEEE Transactions on Speech and Audio Processing*, vol. 13, no. 6, pp. 1217–1230, 2005.

[134] H. Kwakernaak, "Robust control and H_∞ optimization – Tutorial paper," *Automatica*, vol. 29, no. 2, pp. 255–273, 1993.

[135] M. R. Bai and H. H. Lin, "Comparison of active noise control structures in the presence of acoustical feedback by using the H_∞ synthesis technique," *Journal of Sound and Vibration*, vol. 206, no. 4, pp. 453–471, 1997.

[136] J. C. Carmona and V. M. Alvarado, "Active noise control of a duct using robust control theory," *IEEE Transactions on Control Systems Technology*, vol. 8, no. 6, pp. 930–938, 2000.

[137] M. O'Brien and P. Pratt, "Active noise control using robust feedback techniques," in *IEEE International Conference on Acoustics, Speech, and Signal Processing.*, pp. 3209–3212, 2001.

[138] R. S. Sánchez Peña, M. A. Cugueró, A. Masip, J. Quevedo, and V. Puig, "Robust identification and feedback design: An active noise control case study," *Control Engineering Practice*, vol. 16, pp. 1265–1274, 2008.

[139] L. Zhang, L. Wu, and X. Qiu, "An intuitive approach for feedback active noise controller design," *Applied Acoustics*, vol. 74, no. 1, pp. 160–168, 2013.

[140] J. J. Shynk, "Frequency-domain and multirate adaptive filtering," *IEEE Signal Processing Magazine*, pp. 14–37, jan 1992.

[141] E. R. Ferrara, "Fast implementation of LMS adaptive filters," *IEEE Transactions on Acoustics, Speech, and Signal Processing*, vol. 28, pp. 474–475, 1980.

[142] S. J. Elliott and B. Rafaely, "Frequency-domain adaptation of causal digital filters," *IEEE Transactions on Signal Processing*, vol. 48, no. 5, pp. 1354–1364, 2000.

[143] L. Pelkowitz, "Frequency domain analysis of wrap-around error in fast convolution algorithms," *IEEE Transactions on Acoustics, Speech, and Signal Processing*, vol. 29, pp. 413–422, 1981.

[144] B. Farhang-Boroujeny and K. S. Chan, "Analysis of the frequency-domain block LMS algorithm," *IEEE Transactions on Signal Processing*, vol. 48, no. 8, pp. 2332–2342, 2000.

[145] T. Kailath, *Lectures on Wiener and Kalman filtering.* Vienna: Springer, 1981.

[146] J. Lu, X. Qiu, and H. Zou, "A modified frequency-domain block LMS algorithm with guaranteed optimal steady-state performance," *Signal Processing*, vol. 104, pp. 27–32, 2014.

[147] Y. Kajikawa, K. Ashitaka, and Y. Nomura, "Frequency-domain active noise control system using optimal step sizes," *The IEICE Transactions (Japanese Edition)*, vol. J84-A, no. 7, pp. 883–892, 2001.

[148] J. Xue, X. Huang, J. Lu, S. Wang, J. Tao, and K. Chen, "Evaluation of a large scale active control system for transformer noise control," in *Inter-Noise 2015*, 2015.

[149] Y. Koba, D. Kondo, and S. Kijimoto, "Active noise control using a virtual sensing algorithm with incident direction information of noise," *Transactions of The Japan Society of Mechanical Engineers Series B (in Japanese)*, vol. 78, no. 789, pp. 954–958, 2012.

[150] JIS A 1417 : 2000, "AcousticsField measurement of airborne sound insulation of buildings."

[151] J. L. Flanagan, "A difference limen for vowel formant frequency," *The Journal of the Acoustical Society of America*, vol. 27, pp. 613–617, 1955.

[152] D. Kewley-Port and C. S. Watson, "Formant-frequency discrimination for isolated english vowels.," *The Journal of the Acoustical Society of America*, vol. 95, no. 1, pp. 485–496, 1994.

[153] N. I. Durlach, C. R. Mason, F. J. Gallun, B. G. Shinn-Cunningham, H. S. Colburn, and G. Kidd, "Informational masking for simultaneous nonspeech stimuli: psychometric functions for fixed and randomly mixed maskers.," *The Journal of the Acoustical Society of America*, vol. 118, pp. 2482–2497, 2005.

[154] S. Amano, S. Sakamoto, T. Kondo, and Y. Suzuki, "Development of familiarity-controlled word lists 2003 (FW03) to assess spoken-word intelligibility in japanese," *Speech Communication*, vol. 51, pp. 76–82, 2009.

[155] J. Fields, R. De Jong, T. Gjestland, I. Flindell, R. Job, S. Kurra, P. Lercher, M. Vallet, T. Yano, R. Guski, U. Felscher-Suhr, and R. Schumer, "Standardized general-purpose noise reaction questions for community noise surveys: Research and a recommendation," *Journal of Sound and Vibration*, vol. 242, no. 4, pp. 641–679, 2001.

[156] A. J. Berkhout, D. D. Vries, and P. Vogel, "Acoustic control by wave field synthesis," *The Journal of the Acoustical Society of America*, vol. 93, no. 5, pp. 2764–2778, 1993.

[157] J. Ahrens and S. Spors, "Sound field reproduction using planar and linear arrays of loudspeakers," *IEEE Transactions on Audio, Speech, and Language Processing*, vol. 18, no. 8, pp. 2038–2050, 2010.

[158] O. Kirkeby and P. A. Nelson, "Reproduction of plane wave sound fields," *The Journal of the Acoustical Society of America*, vol. 94, no. 5, pp. 2992–3000, 1993.

[159] C. Liu, B. C. Wheeler, W. D. O'Brien, R. C. Bilger, C. R. Lansing, and A. S. Feng, "Localization of multiple sound sources with two microphones.," *The Journal of the Acoustical Society of America*, vol. 108, no. 4, pp. 1888–1905, 2000.

[160] N. Tanaka and M. Tanaka, "Active noise control using a steerable parametric array loudspeaker.," *The Journal of the Acoustical Society of America*, vol. 127, pp. 3526–3537, 2010.

[161] N. Tanaka and R. Tachi, "Active noise control using acoustic wave reflection of a parametric loudspeaker," *Transactions of The Japan Society of Mechanical Engineers Series C (in Japanese)*, vol. 77, no. 775, pp. 764–773, 2011.

[162] N. Mori and A. Omoto, "Application of active control system -Towards realization of global-local control considering the movement of control points-," *IEICE Technical Report (in Japanese)*, vol. 108, no. 333, pp. 43–47, 2008.

[163] C. H. Hansen, "Current and future industrial applications of active noise control," *Noise Control Engineering Journal*, vol. 53, no. 5, pp. 181–196, 2005.

[164] T. Kamakura, K. Ito, and H. Nomura, "Survey of ultrasound exposure: Through topic of parametric loudspeaker," *Journal of the Acoustical Society of Japan (in Japanese)*, vol. 67, no. 5, pp. 200–203, 2011.

[165] B. Smagowska, "Effects of ultrasonic noise on the human body – a bibliographic review," *International Journal of Occupational Safety and Ergonomics*, vol. 19, no. 2, pp. 195–202, 2013.

[166] J.-W. Choi and Y.-H. Kim, "Generation of an acoustically bright zone with an illuminated region using multiple sources.," *The Journal of the Acoustical Society of America*, vol. 111, no. 4, pp. 1695–1700, 2002.

[167] W. F. Druyvesteyn and J. Garas, "Personal Sound," *Journal of the Audio Engineering Society*, vol. 45, no. 9, pp. 685–701, 1997.

[168] S. Yon, M. Tanter, and M. Fink, "Sound focusing in rooms: The time-reversal approach.," *The Journal of the Acoustical Society of America*, vol. 113, no. 3, pp. 1533–1543, 2003.

[169] S. Yon, M. Tanter, and M. Fink, "Sound focusing in rooms. II. The spatio-temporal inverse filter.," *The Journal of the Acoustical Society of America*, vol. 114, no. 6, pp. 3044–3052, 2003.

[170] M. Shin, S. Q. Lee, F. M. Fazi, P. A. Nelson, D. Kim, S. Wang, K. H. Park, and J. Seo, "Maximization of acoustic energy difference between two spaces.," *The Journal of the Acoustical Society of America*, vol. 128, no. 1, pp. 121–131, 2010.

[171] N. Radmanesh and I. S. Burnett, "Generation of isolated wideband sound fields using a combined two-stage lasso-LS algorithm," *IEEE Transactions on Audio, Speech and Language Processing*, vol. 21, no. 2, pp. 378–387, 2013.

[172] Y. Cai, M. Wu, and J. Yang, "Sound reproduction in personal audio systems using the least-squares approach with acoustic contrast control constraint," *The Journal of the Acoustical Society of America*, vol. 135, no. 2, pp. 734–741, 2014.

[173] S. J. Elliott and M. Jones, "An active headrest for personal audio," *The Journal of the Acoustical Society of America*, vol. 119, no. 5, pp. 2702–2709, 2006.

[174] S. J. Elliott, J. Cheer, J.-W. Choi, and Y. Kim, "Robustness and regularization of personal audio systems," *IEEE Transactions on Audio, Speech, and Language Processing*, vol. 20, no. 7, pp. 2123–2133, 2012.

[175] P. Coleman, P. J. B. Jackson, M. Olik, M. Moller, M. Olsen, and J. Abildgaard Pedersen, "Acoustic contrast, planarity and robustness of sound zone methods using a circular loudspeaker array," *The Journal of the Acoustical Society of America*, vol. 135, no. 4, pp. 1929–1940, 2014.

[176] Y. Cai, M. Wu, L. Liu, and J. Yang, "Time-domain acoustic contrast control design with response differential constraint in personal audio systems," *The Journal of the Acoustical Society of America*, vol. 135, no. 6, pp. EL252–EL257, 2014.